



2009

ANALYTICAL STRIP METHOD TO ANTISYMMETRIC LAMINATED PLATES

Liecheng Sun

University of Kentucky, charlie.sun@uky.edu

Recommended Citation

Sun, Liecheng, "ANALYTICAL STRIP METHOD TO ANTISYMMETRIC LAMINATED PLATES" (2009). *University of Kentucky Doctoral Dissertations*. 715.

http://uknowledge.uky.edu/gradschool_diss/715

This Dissertation is brought to you for free and open access by the Graduate School at UKnowledge. It has been accepted for inclusion in University of Kentucky Doctoral Dissertations by an authorized administrator of UKnowledge. For more information, please contact UKnowledge@lsv.uky.edu.

ABSTRACT OF DISSERTATION

Liecheng Sun

The Graduate School
University of Kentucky

2009

ANALYTICAL STRIP METHOD TO
ANTISYMMETRIC LAMINATED PLATES

ABSTRACT OF DISSERTATION

A dissertation submitted in partial fulfillment of the
requirements for the degree of Doctor of Philosophy
at the University of Kentucky

By
Liecheng Sun
Lexington, KY

Director: Dr. Issam E. Harik, Professor of Civil Engineering
University of Kentucky
Lexington, KY

2009

Copyright © Liecheng Sun 2009

ABSTRACT OF DISSERTATION

ANALYTICAL STRIP METHOD TO ANTISYMMETRIC LAMINATED PLATES

An Analytical Strip Method (ASM) for the analysis of stiffened and non-stiffened antisymmetric laminated composite plates is derived by considering the bending-extension coupling effect for bending, free vibration and buckling. A system of three equations of equilibrium, governing the general response of arbitrarily laminated composite plates, is reduced to a single eighth order partial differential equation in terms of a displacement function. The displacement function is solved in a single series form to determine the displacement, fundamental frequency, and buckling load of antisymmetric cross-ply and angle-ply laminated composite plates. The solution is applicable to rectangular plates with two opposite edges simply supported, while the other edges are simply supported, clamped, free, beam supported, or any combinations of these boundary conditions.

This method overcomes the limitations of other analytical methods (Navier's and Lévy's), and provides an alternative to numerical, semi-numerical, and approximate methods of analysis. Numerical examples of bending, free vibration, and buckling of antisymmetric laminated composite plates are presented in tabular and graphical form. Whenever possible, the results of the present study are compared with those published in the literature and/or ANSYS solutions. The comparison firmly establishes that this method could be used for the analysis of antisymmetric laminated composite plates. Future research needs are identified for the aspects that have not been reached by the present study and others.

KEYWORDS: Analytical solution; stiffened laminated plates; bending-extension coupling; fundamental frequency; buckling

(Liecheng Sun)

(Date)

ANALYTICAL STRIP METHOD TO
ANTISYMMETRIC LAMINATED PLATES

By

Liecheng Sun

Director of Dissertation

Director of Graduate Studies

Date

RULES FOR THE USE OF THESES

Unpublished theses submitted for the Master's and Doctor's degrees and deposited in the University of Kentucky Library are as a rule open for inspection, but are to be used only with due regard to the authors. Bibliographical references may be noted, but quotations or summaries of parts may be published only with the permission of the author, and with the usual scholarly acknowledgments.

Extensive copying or publication of the thesis in whole or in part requires also the consent of the Dean of The Graduate School of the University of Kentucky.

A library which borrows this thesis for use by its patrons is expected to secure the signature of each user.

Name

Date

DISSERTATION

Liecheng Sun

The Graduate School
University of Kentucky

2009

ANALYTICAL STRIP METHOD TO
ANTISYMMETRIC LAMINATED PLATES

DISSERTATION

A dissertation submitted in partial fulfillment of the
requirements for the degree of Doctor of Philosophy
at the University of Kentucky

By
Liecheng Sun
Lexington, KY

Director: Dr. Issam E. Harik, Professor of Civil Engineering
University of Kentucky
Lexington, KY

2009

Copyright © Liecheng Sun 2009

ACKNOWLEDGEMENT

There are many people I would like to acknowledge toward the completion of my Ph.D. program. Foremost, I am indebted to my primary advisor Dr. Issam E. Harik for his inspiration and encouragement to take on this challenging topic as my dissertation research. It was his valuable instruction during the entire research process that made the investigation smooth and fruitful. My professional capacity and experience were greatly increased during the period working under his guidance. I express my deepest gratitude to him.

Many sincere thanks to Dr. Hans Gesund, Dr. Kamyar C. Mahboub, and Dr. Tingwen Wu for serving as my committee members. Their valuable input and scientific guidance have been critical for my research. Appreciation is also extended to the University of Kentucky, for a tuition waiver through the Employee Education Program.

Finally, I thank my wife, Lu, for her love, patience, and care; I thank my son for his stimulating and humorous conversations; I thank my parents for believing in their son; I thank my friends for their moral support; and I also thank my teachers in China, for their dedication to their students, and for providing me with a strong educational background.

It is impossible to end my acknowledgements without mentioning the graduate program in the Department of Civil Engineering and the many faculty and staff I have interacted with during my *long* time pursuing Ph.D., at the University of Kentucky. I appreciate very much all of their support and help.

TABLE OF CONTENTS

Acknowledgement	iii
List of Tables	viii
List of Figures.....	xi
List of Files	xiv
Nomenclature.....	xv
Chapter 1 INTRODUCTION	1
1.1 Background.....	1
1.2 Literature Review	2
1.2.1 Analytical solution.....	3
1.2.2 Numerical solution.....	4
1.2.3 Semi-numerical solution.....	5
1.3 Scope of Work	5
1.4 Dissertation Outline	6
Chapter 2 BASIC EQUATIONS FOR ANTISYMMETRIC LAMINATED PLATES.....	9
2.1 Introduction.....	9
2.2 Governing Differential Equations for Antisymmetric Laminated Plates ..	10
2.2.1 Antisymmetric cross-ply laminated plate	13
2.2.2 Antisymmetric angle-ply laminated plate.....	16
Chapter 3 BENDING-EXTENSION COUPLING OF ANTISYMMETRIC LAMINATED PLATES	21
3.1 Introduction.....	21
3.2 Governing Differential Equation	21
3.3 Analytical Strip Method.....	21
3.3.1 Homogeneous solution, $\Phi_H(x, y) = \sum_m^{\infty} \phi_{Hm}(x) \sin(\beta_m y)$	23
3.3.2 Particular solution, $\Phi_P(x, y) = \sum_m^{\infty} \phi_{Pm}(x) \sin(\beta_m y)$	26
3.3.3 Edge loading function.....	26

	3.3.4	Boundary conditions	27
	3.3.5	Continuity conditions.....	27
3.4		Applications	28
	3.4.1	Example 1: Effect of ply angle and number of layers on deflection and stresses	28
	3.4.2	Example 2: Effect of in-plane orthotropy ratio (E_1/E_2) on deflection and stresses	30
	3.4.3	Example 3: Effect of aspect ratio (a/b)	31
	3.4.4	Example 4: Square plate subjected to a patch load	31
	3.4.5	Example 5: Square plate subjected to a point load	32
3.5		Summary and Conclusions	32
Chapter 4		BENDING-EXTENSION COUPLING OF STIFFENED AND CONTINUOUS ANTISYMMETRIC LAMINATED PLATES	45
	4.1	Introduction	45
	4.2	Governing Differential Equation	45
	4.3	Beam Elements	46
	4.4	Applications	47
	4.4.1	Example 1: Edge beam effect for a square antisymmetric angle-ply plate	47
	4.4.2	Example 2: Two interior beams for rectangular antisymmetric angle-ply plate	48
	4.4.3	Example 3: Two points supported rectangular antisymmetric angle-ply plate	50
	4.4.4	Example 4: Two beam supported antisymmetric angle-ply 6-layer square laminated plate subjected to a patch load and a concentrated load P	52
	4.5	Summary and Conclusions	52
Chapter 5		FREE VIBRATION OF STIFFENED ANTISYMMETRIC LAMINATED PLATES	66
	5.1	Introduction	66
	5.2	Free Vibration Analysis	66

5.3	Method of Solution	68
5.4	Application	69
5.4.1	Example 1: Effects of aspect ratio (a/b), beam rigidity (KI) and number of layers (n) on the dimensionless fundamental frequency $\left[\bar{\omega} = \left(\frac{b^2}{h} \sqrt{\frac{\rho}{E_2}} \right) \omega \right]$	69
5.4.2	Example 2 : Effects of orthotropicity ratio (E_1/E_2), beam rigidity (KI) and number of layers (n) on the dimensionless fundamental frequency $\left[\bar{\omega} = \left(\frac{a^2}{h} \sqrt{\frac{\rho}{E_2}} \right) \omega \right]$	71
5.4.3	Example 3: Effects of ply angle (θ) and number of layers (n) on the dimensionless fundamental frequency $\left[\bar{\omega} = \left(\frac{b^2}{h} \sqrt{\frac{\rho}{E_2}} \right) \omega \right]$	72
5.4.4	Example 4: Maximizing fundamental frequency $\left[\bar{\omega} = \left(\frac{b^2}{h} \sqrt{\frac{\rho}{E_2}} \right) \omega \right]$ by varying inside beam position for cross-ply (0/90/0/90/...) and angle-ply ($\theta/-\theta/\theta/-\theta/...$) laminated plates with varied boundary conditions	73
5.5	Summary and Conclusions	74
Chapter 6	BUCKLING OF STIFFENED ANTISYMMETRIC LAMINATED PLATES	83
6.1	Introduction	83
6.2	Buckling Analysis	83
6.3	Method of Solution	84
6.4	Application	86
6.4.1	Example 1: Effects of aspect ratio (a/b), beam rigidity (KI) and number of layers (n) on the dimensionless uniaxial	

buckling load $\left[\bar{N}_y = \left(\frac{b^2}{E_2 h^3} \right) N_y \right]$ and bi-axial buckling loads $\left[\bar{N}_y = \bar{N}_x = \left(\frac{b^2}{E_2 h^3} \right) N_x \right]$ 86

6.4.2 Example 2: Effects of orthotropy ratio (E_1/E_2), beam rigidity (KI) and number of layers (n) on the dimensionless uniaxial buckling load $\left[\bar{N}_y = \left(\frac{b^2}{E_2 h^3} \right) N_y \right]$ 88

6.4.3 Example 3: Effects of ply angle (θ) and number of layers (n) on the dimensionless uniaxial buckling load $\left[\bar{N}_y = \left(\frac{b^2}{E_2 h^3} \right) N_y \right]$ 89

6.4.4 Maximizing dimensionless uniaxial buckling load $\left[\bar{N}_y = \left(\frac{b^2}{E_2 h^3} \right) N_y \right]$ by varying inside beam position for cross-ply ($0^\circ/90^\circ/0^\circ/90^\circ/\dots$) and angle-ply ($\theta/-\theta/\theta/-\theta/\dots$) laminated plates with varied boundary conditions89

6.5 Summary and Conclusions91

Chapter 7 CONCLUSIONS AND FURTHER RESEARCH NEEDS101

7.1 General Summary101

7.2 Bending of Laminated Plate101

7.3 Free Vibration and Buckling of Laminated Plate102

7.4 Recommendation for Future Research102

Appendix A HOMOGENOUS SOLUTIONS, $\Phi_H(x, y)$, OF GDE FOR ANTISYMMETRIC LAMINATED PLATES104

BIBLIOGRAPHY.....109

VITA.....112

LIST OF TABLES

Table 3.1	Particular solution $\Phi_{PI}(x, y)$ for strip I	33
Table 3.2	Edge loading function $\psi_i(y)$ at $x = x_i$	34
Table 3.3	Effect of ply angle (θ°) and number of layers (n) on the center of an antisymmetric square laminated plate (θ° /- θ° / θ° /- θ° /...) $a/h = 1000$, $E_1 = 132.38$ GPa, $E_2 = 10.76$ GPa, $G_{12} = G_{13} = 5.65$ GPa, $G_{23} = 3.61$ GPa, $\nu_{12} = 0.24$	35
Table 3.4	Effect of ply angle (θ°) and number of layers (n) on the center stresses $\Sigma(a/2, a/2) = \frac{h^2}{a^2 q} \sigma$ at bottom surface of a square plate (θ° /- θ° / θ° /.../- θ°) $a/h = 1000$, $E_1 = 132.38$ GPa, $E_2 = 10.76$ GPa, $G_{12} = G_{13} = 5.65$ GPa, $G_{23} = 3.61$ GPa, $\nu_{12} = 0.24$	36
Table 3.5	Convergence study for ASM on the center deflection and stresses of an antisymmetric angle-ply square plates (30° /- 30° / 30° /- 30° /...) $a/h = 1000$, $E_1 = 132.38$ GPa, $E_2 = 10.76$ GPa, $G_{12} = G_{13} = 5.65$ GPa, $G_{23} = 3.61$ GPa, $\nu_{12} = 0.24$	37
Table 3.6	Effect of in-plane orthotropy ratio, E_1/E_2 on the dimensionless center deflection, \hat{w} , and stress, Σ_x , of a four layer square laminated plate (45° /- 45° / 45° /- 45°) $a/h = 1000$, $E_1/E_2 = 2, 10, 20, 30$ and 40 , $G_{12}/E_2 = G_{13}/E_2 = 0.6$, $G_{23}/E_2 = 0.5$, $\nu_{12} = 0.25$	38
Table 4.1	Convergence study for ASM on the center deflection, $\hat{w}(a/2, a/2)$ of an antisymmetric angle-ply square plate (30° /- 30° / 30° /- 30° /...) having three edges simply supported and the fourth edge ($x = a$) with varied beam supported, $a/h = 1000$, $E_1 = 132.38$ GPa, $E_2 = 10.76$ GPa, $G_{12} = G_{13} = 5.65$ GPa, $G_{23} = 3.61$ GPa, $\nu_{12} = 0.24$	54
Table 4.2	Convergence study for ASM on the center stresses $\Sigma(a/2, a/2)$ of an antisymmetric angle-ply square plate (30° /- 30° / 30° /- 30° /...) having three edges simply supported and the fourth edge ($x = a$) with varied beam supported, $a/h = 1000$, $E_1 = 132.38$ GPa, $E_2 = 10.76$ GPa, $G_{12} = G_{13} = 5.65$ GPa, $G_{23} = 3.61$ GPa, $\nu_{12} = 0.24$	55

Table 4.3	Effect of ply angle (θ°) and number of layers (n) on deflection \hat{w} of a uniformly loaded rectangular antisymmetric angle-ply plate ($a/b = 2, \theta^\circ/-\theta^\circ/\theta^\circ/.../-\theta^\circ$) with two beams supported inside, $b/h = 1000, E_1 = 132.38$ GPa, $E_2 = 10.76$ GPa, $G_{12} = G_{13} = 5.65$ GPa, $G_{23} = 3.61$ GPa, $\nu_{12} = 0.24$	56
Table 4.4	Effect of ply angle (θ°) and number of layers (n) on stress Σ at center plate and middle beams of a uniformly loaded rectangular antisymmetric angle-ply plate ($a/b = 2, \theta^\circ/-\theta^\circ/\theta^\circ/.../-\theta^\circ$) with two beams supported inside plate, $b/h = 1000, E_1 = 132.38$ GPa, $E_2 = 10.76$ GPa, $G_{12} = G_{13} = 5.65$ GPa, $G_{23} = 3.61$ GPa, $\nu_{12} = 0.24$	57
Table 5.1	Effects of aspect ratio (a/b), beam rigidity (KI) and number of layers (n) on the dimensionless fundamental frequency (ϖ) of a rectangular cross-ply laminated plate ($0^\circ/90^\circ/0^\circ/90^\circ/...$, $b/h = 1000, E_1/E_2=20, G_{12} = G_{13} = 0.6E_2, G_{23} = 0.5E_2, \nu_{12} = 0.25$)	76
Table 5.2	Effects of in-plane orthotropy ratio ($E1/E2$), beam rigidity (KI) and number of layers (n) on the dimensionless fundamental frequency (ϖ) of a square angle-ply laminated plate ($45^\circ/-45^\circ/45^\circ/-45^\circ/...$, $b/h = 1000, G_{12} = G_{13} = 0.6E_2, G_{23} = 0.5E_2, \nu_{12} = 0.25$)	77
Table 5.3	Effects of ply angle (θ) and number of layers (n) on the dimensionless fundamental frequency (ϖ) of a rectangular angle-ply laminated plate ($a/b = 2, b/h = 1000, E_1/E_2=20, G_{12} = G_{13} = 0.6E_2, G_{23} = 0.5E_2, \nu_{12} = 0.25$) with beams at $x = 0, x = a/2$ and $x = a$ respectively, $KI = 1$ for all 3 beams	78
Table 5.4	Effect of boundary condition and positions of two inside beams on maximized dimensionless fundamental frequency for a rectangular cross-ply laminated plate ($0^\circ/90^\circ/0^\circ/90^\circ/...$, $b/h = 1000, E_1/E_2=40, G_{12} = G_{13} = 0.6E_2, G_{23} = 0.5E_2, \nu_{12} = 0.25$)	79
Table 5.5	Effect of ply angle and positions of two inside beams on maximized dimensionless fundamental frequency for a rectangular angle-ply laminated plate ($\theta/-\theta/\theta/-\theta/...$, $b/h = 1000, E_1/E_2=20, G_{12}$	

	= $G_{13} = 0.6E_2$, $G_{23} = 0.5E_2$, $\nu_{12} = 0.25$) with two boundary beams at $x = 0$ and $x = a$	80
Table 6.1	Effects of aspect Ratio (a/b), beam rigidity (KI) and number of layers (n) on the dimensionless uniaxial buckling load (\bar{N}_y) of a rectangular cross-ply laminated plate ($0^\circ/90^\circ/0^\circ/90^\circ/...$, $b/h = 1000$, $E_1/E_2=20$, $G_{12} = G_{13} = 0.6E_2$, $G_{23} = 0.5E_2$, $\nu_{12} = 0.25$	93
Table 6.2	Effects of aspect ratio (a/b), beam rigidity (KI) and number of layers (n) on the dimensionless bi-axial buckling loads ($\bar{N}_x = \bar{N}_y$) of a rectangular cross-ply laminated plate ($0^\circ/90^\circ/0^\circ/90^\circ/...$, $b/h = 1000$, $E_1/E_2=20$, $G_{12} = G_{13} = 0.6E_2$, $G_{23} = 0.5E_2$, $\nu_{12} = 0.25$	94
Table 6.3	Effects of in-plane orthotropy ratio (E_1/E_2), beam rigidity (KI) and number of layers (n) on the dimensionless uniaxial buckling load (\bar{N}_y) of a square angle-ply laminated plate ($45^\circ/-45^\circ/45^\circ/-45^\circ/...$, $b/h = 1000$, $G_{12} = G_{13} = 0.6E_2$, $G_{23} = 0.5E_2$, $\nu_{12} = 0.25$)	95
Table 6.4	Effects of ply angle (θ) and number of layers (n) on the dimensionless uniaxial buckling load (\bar{N}_y) of a rectangular angle-ply laminated plate ($a/b = 2$, $b/h = 1000$, $E_1/E_2=20$, $G_{12} = G_{13} = 0.6E_2$, $G_{23} = 0.5E_2$, $\nu_{12} = 0.25$) with beams at $x = 0$, $x = a/2$ and $x = a$ respectively, $KI = 1$ for all 3 beams	96
Table 6.5	Effect of boundary condition and positions of two inside beams on maximized dimensionless uniaxial buckling load for a rectangular cross-ply laminated plate ($0^\circ/90^\circ/0^\circ/90^\circ/...$, $b/h = 1000$, $E_1/E_2=20$, $G_{12} = G_{13} = 0.6E_2$, $G_{23} = 0.5E_2$, $\nu_{12} = 0.25$)	97
Table 6.6	Effect of ply angle and positions of two inside beams on maximized dimensionless uniaxial buckling load for a rectangular angle-ply laminated plate ($\theta/-\theta/\theta/-\theta/...$, $b/h = 1000$, $E_1/E_2=20$, $G_{12} = G_{13} = 0.6E_2$, $G_{23} = 0.5E_2$, $\nu_{12} = 0.25$) with two boundary beams at $x = 0$ and $x = a$	98

LIST OF FIGURES

Figure 1.1	Plate strips with strip and edge loadings	8
Figure 2.1	An antisymmetric cross-ply laminate	19
Figure 2.2	An antisymmetric angle-ply laminate.....	20
Figure 3.1	Deflection at the center of a uniformly loaded antisymmetric angle-ply square plate, $\hat{w}\left(\frac{a}{2}, \frac{a}{2}\right) = \left(\frac{100E_2h^3}{a^4q}\right)w$, versus ply orientation angle, θ , for different boundary conditions	39
Figure 3.2a	Stress in the x -direction at the center of bottom surface on a uniformly loaded antisymmetric angle-ply square plate, $\Sigma_x\left(\frac{a}{2}, \frac{a}{2}\right) = \left(\frac{h^2}{a^2q}\right)\sigma_x$ versus ply orientation angle, θ	40
Figure 3.2b	Stress in the y -direction at the center of bottom surface on a uniformly loaded antisymmetric angle-ply square plate, $\Sigma_y\left(\frac{a}{2}, \frac{a}{2}\right) = \left(\frac{h^2}{a^2q}\right)\sigma_y$ versus ply orientation angle, θ	41
Figure 3.3	Deflection at the center of a uniformly loaded antisymmetric angle-ply rectangular plate with all sides simply supported, $\hat{w}\left(\frac{a}{2}, \frac{b}{2}\right) = \left(\frac{100E_2h^3}{b^4q}\right)w$ versus ply orientation angle, θ	42
Figure 3.4	Contour of the dimensionless deflection, $\hat{w} = \left(\frac{100E_2h^3}{a^4q}\right)w$ for an antisymmetric angle-ply 6-layer $(-15^\circ/-45^\circ/-75^\circ/75^\circ/45^\circ/15^\circ)$ square laminated plate subjected to a patch load	43
Figure 3.5	Contour of the dimensionless deflection, $\hat{w} = \left(\frac{100E_2h^3}{a^2P}\right)w$ for an antisymmetric angle-ply 8-layer $(-30^\circ/-40^\circ/-50^\circ/-60^\circ/60^\circ/50^\circ/40^\circ/30^\circ)$ square laminated plate subjected to a concentrated load, P	44
Figure 4.1	Stiffed plate strips with strip and edge loadings (beams are concentric and only half beams on bottom are shown for clarity)	58

Figure 4.2	Deflection $\hat{w}\left(\frac{a}{2}, \frac{a}{2}\right) = \left(\frac{100E_2h^3}{a^4q}\right)w$ at the center of a uniformly loaded antisymmetric angle-ply square plate having three edges simply supported and the fourth edge ($x = a$) with varied beam supported, versus fiber orientation angle, θ 59
Figure 4.3	Stress $\Sigma_x\left(0.975a, \frac{a}{2}\right) = \left(\frac{h^2}{qa^2}\right)\sigma_x$ close to beam edge of a uniformly loaded antisymmetric angle-ply square plate having three edges simply supported and fourth edge ($x = a$) with varied beam supported, versus fiber orientation angle, θ 60
Figure 4.4	Contour of dimensionless deflection, $\hat{w} = \left(\frac{100E_2h^3}{b^4q}\right)w$ for a uniformly loaded antisymmetric angle-ply 10-layer $(-45/45)_5$ rectangular laminated plate having $a/b = 2$, simply supported at $y = 0$ and $y = b$, beams supported at $x = 0.5b$ and $x = 1.85b$, free at $x = 0$ and $x = 2b$ 61
Figure 4.5	Contour of dimensionless deflection, $\hat{w} = \left(\frac{100E_2h^3}{b^4q}\right)w$ for a uniformly loaded antisymmetric angle-ply 2-layer $(-45/45)$ rectangular laminated plate ($a/b = 2$) having simply supported on $y = 0$ and $y = b$, two point supports at $x = 0.4b, y = b/2$ and $x = 1.7b, y = b/2$, free at $x = 0$ and $x = 2b$ 62
Figure 4.6	Dimensionless deflections at middle edges of left and right plate, and the center of plate of a uniformly loaded antisymmetric angle-ply rectangular laminated plate, having $a/b = 2$, simply supported at $y = 0$ and $y = a$, two points supported at $x = 0.4b, y = b/2$ and $x = 1.7b, y = b/2$, free at $x = 0$ and $x = 2b$, $\hat{w} = \left(\frac{100E_2h^3}{b^4q}\right)w$ versus ply orientation angle, θ 63
Figure 4.7	Dimensionless stresses at the center of plates of a uniformly loaded

antisymmetric angle-ply rectangular laminated plate, having $a/b = 2$, simply supported at $y = 0$ and $y = a$, two points supported at $x = 0.4b, y = b/2$ and $x = 1.7b, y = b/2$, free at $x = 0$ and $x = 2b$,

$$\Sigma\left(\frac{a}{2}, \frac{b}{2}\right) = \left(\frac{h^2}{b^2 q}\right) \sigma \text{ versus ply orientation angle, } \theta \dots\dots\dots 64$$

Figure 4.8	Contour of dimensionless deflection for an antisymmetric angle-ply 6-layer (-15/-45/-75/75/45/15) square laminated plate with simply supported on $y = 0$ and $y = a$, one beam at $x = 0$, and another beam at $x = 7a/8$ having a patch load and concentrated load	65
Figure 5.1	Stiffened plate with stiffeners parallel to y -axis	81
Figure 5.2	Maximizing dimensionless fundamental frequency by varying inside beam position for a square cross-ply laminated plate ($0^\circ/90^\circ/0^\circ/90^\circ/\dots$, $b/h = 1000$) with two boundary beams at $x = 0$ and $x = a$	82
Figure 6.1	Stiffened plate subject to in-plane loads	99
Figure 6.2	Maximizing dimensionless uniaxial buckling load (\bar{N}_y) by varying inside beam position for a square cross-ply laminated plate ($0^\circ/90^\circ/0^\circ/90^\circ/\dots$, $b/h = 1000$) with two boundary beams at $x = 0$ and $x = a$	100

LIST OF FILE

SunDissertation.pdf, 2.6 MB

NOMENCLATURE

- a, b = plate dimensions in x direction and y direction, respectively
 a_i = coefficients for displacements, force, and moment results for antisymmetric cross-ply laminated plates
 A_i = coefficients for governing differential equation of laminated plate
 A_i^* = modified coefficients for governing differential equation of laminated plate under free vibration or buckling study
 A_{ij} = extensional stiffness coefficients
 b_i = coefficients for displacements, force, and moment results for antisymmetric angle-ply laminated plates
 B_{ij} = bending-extension coupling stiffness coefficients
 C_{dm} = constants of the general expression of the homogeneous solution for ordinary differential equation associated with the m^{th} eigenmode ($d = 1, 2, \dots, 8$)
 d = d^{th} index if used as subscript
 D_E = equivalent flexural rigidity of orthotropic plate
 D_{ij} = bending stiffness coefficients
 E_1, E_2 = elastic moduli in fiber direction and the direction perpendicular to the fibers
 $E_b C_w$ = warping rigidity of the beam
 $E_b I_b$ = flexural rigidity of the beam
 $f(x)$ = load distribution function in the x direction
 $g(y)$ = load distribution function in the y direction
 $g_{1m} = \frac{2}{b} \int_0^b g(y) \sin(\beta_m y) dy$, the constant for the m^{th} mode of deflection
 G_{12}, G_{23}, G_{31} = elastic moduli with respect to fiber principle directions: G_{23} is the shear modulus with respect to the shear strain γ_{23} in the 2-3 plane of the fiber coordinate, and so forth
 $G_b J_b$ = torsional rigidity of the beam
 H = total laminate thickness
 I = strip number if used as subscript
 I_0 = mass inertia

- I_2 = rotary inertia
 J = J^{th} beam if used as subscript
 k = layer number if used as subscript or superscript
 k_N = in-plane force ratio between N_x and N_y , $k_N = \frac{N_y}{N_x}$
 $K1, K2, \text{ and } K3$ = dimensionless flexural rigidity, torsional rigidity, and warping rigidity of the beam, respectively
 L = total layers of laminated plate
 L_{ij} = differential operators
 m, n = m^{th} or n^{th} series if used as subscript
 M_x, M_y, M_{xy} = membrane moments
 N_x, N_y, N_{xy} = membrane forces
 \bar{N}_x = dimensionless buckling load in x -direction
 \bar{N}_y = dimensionless buckling load in y -direction
 $q(x,y)$ = transverse load on plate
 Q_{bl} = lateral load per unit length applied to the beam element at the line $x = x_l$
 \bar{Q}_{ij} = reduced stiffness coefficients
 r = total number of loads applied on strip I
 T_{bl} = twisting moment per unit length applied to the beam element at the line $x = x_l$
 u, v, w = translational displacements in global axis x, y and z directions
 u_0, v_0 = mid-plane values of in-plane displacements in global axis x and y directions
 V = lateral load per unit length on boundary
 w = lateral displacement in global axis z direction
 \hat{w} = dimensionless deflection
 W_b = deflection of the beam
 x, y, z = global Cartesian coordinates
 z_k = distance between midplane of plate and the k^{th} orthotropic lamina surface

- $\beta_m = \frac{m\pi}{b}$, the eigenfrequency associated with the m^{th} eigenmode
 $\gamma_n \beta_n =$ characteristic root for function $\phi_n(x)$ for the n^{th} mode
 $\varepsilon_{xx}^{(0)}, \varepsilon_{yy}^{(0)}, \gamma_{xy}^{(0)} =$ membrane strains in global coordinates
 $\varepsilon_{xx}^{(1)}, \varepsilon_{yy}^{(1)}, \gamma_{xy}^{(1)} =$ flexural strains in global coordinates
 $\left\{ \begin{array}{c} \varepsilon_{xx} \\ \varepsilon_{yy} \\ \gamma_{xy} \end{array} \right\}^k =$ strains in the k^{th} layer of plate
 $\varepsilon_{xz}, \varepsilon_{yz}, \varepsilon_{zz} =$ transverse strains
 $\theta =$ ply orientation angle, from global x -axis to fiber direction
 $\kappa = \varepsilon_{xx}^{(1)}, \varepsilon_{yy}^{(1)}, \gamma_{xy}^{(1)}$, the flexural strains in global coordinates
 $\rho^k =$ volumetric mass density of material for the k^{th} layer
 $\nu_{ij} =$ Poisson's ratio of the transverse strain in j -direction to strain in i -direction, when stressed in i -direction
 $\sigma_x, \sigma_y =$ stresses in global coordinates
 $\omega =$ fundamental frequency of laminated plate
 $\bar{\omega} =$ dimensionless fundamental frequency of laminated plate
 $\Sigma_x, \Sigma_y, \Sigma_{xy} =$ dimensionless stresses
 $\phi_b =$ twist angle of the beam
 $\phi_m(x)$ or $\phi_n(x) =$ displacement function in x -direction associated with the m^{th} or n^{th} eigenmode
 $\phi_{Hn}(x) =$ general expression of the homogeneous solution for ordinary differential equation associated with the n^{th} eigenmode
 $\phi_{Pn}(x) =$ general expression of the particular solution for differential equation associated with the n^{th} eigenmode
 $\Phi(x, y) =$ displacement function
 $\Phi_H(x, y) =$ general expression of the homogeneous solution for differential equation
 $\Phi_P(x, y) =$ general expression of the particular solution for differential equation

$\psi_i(y)$ = edge loading function

CHAPTER 1

INTRODUCTION

1.1 Background

Composite materials consist of two or more materials which together produce desirable properties that cannot be achieved with any of the constituents alone. They have a long history of usage. Their beginnings are unknown, but all recorded history contains references to some form of composite material. For example, plywood was used by ancient Egyptians to achieve superior strength and high resistance to thermal expansion and swelling, due to the presence of moisture; and Medieval swords and armor were constructed with layers of different materials (Jones, 1975). Currently, composite materials are extensively used in engineering applications, due to their high strength to weight ratio, stiffness to weight ratio, high thermal stability, excellent resistance to environmental and corrosion attack, magnetic transparency, and high fatigue strength.

More specifically, composite laminated plates are formed by stacking layers of different composite materials and/or ply orientation. Lamination is used to combine the best aspects of the constituent layers, in order to achieve a more useful material. The properties that can be emphasized by lamination are strength, stiffness, low weight, corrosion resistance, wear resistance, beauty or attractiveness, thermal insulation, acoustical insulation, etc.

By construction, laminated plates have planar dimensions one to two orders of magnitude larger than their thickness. Regularly laminated plates are used in applications that require membrane and bending strengths. When ply stacking sequence, material, and geometry (*i.e.*, ply thicknesses) are symmetric to the midplane of the laminated plate, it is called a symmetric laminated plate. An antisymmetric laminated plate is one whose lamination scheme is antisymmetric, and material and thicknesses are symmetric to the midplane. Unlike symmetric laminated plate, bending is coupled with extension (in-plane) or twisting in antisymmetric laminated plate. This coupling makes analytical solutions difficult, and creates pronounced differences in plate response. Due to the complexity of the analysis of antisymmetric laminated plate, better understanding of this plate's behavior and performance, as well as more efficient analysis approaches, are desirable.

1.2 Literature Review

A variety of laminated plate theories have been developed and reported in much of the literature concerning the analysis of multi-layered composite plates.

An extensive review of various equivalent single layer and layerwise laminated plate theories was presented by Reddy and Robbins (1994). An overall comparison of laminated theories, based on displacement hypothesis, was presented by Liu and Li (1996), which compared theories including shear deformation, layerwise, generalized Zigzag, and the proposed global-local double-superposition. A detail review of theories for laminated and sandwich plates was given by Altenbach (1998). A review of displacement and stress based refined theories, for isotropic and anisotropic laminated plates, was presented by Ghugal and Shimpi (2002). In this specific review, Ghugal and Shimpi discussed various equivalent single layer and layerwise theories for laminated plates, together with their merits and demerits. A historical review of the Zig-Zag theories for multilayered plates and shells, up to 2003, was given by Carrera (2003). A piecewise, continuous displacement field in the plate thickness direction is described and interlaminar continuity of transverse stresses at each layer interface is fulfilled in Zig-Zag theories. A review of shear deformation plate and shell theories was presented by Reddy and Arciniega (2004). The discussion of plate and shell theories from Stavsky up to 2004 was a review of various theories for modeling laminated shells, including shear effects and some analytical studies. A review on the different methods used for the estimation of transverse/interlaminar stresses in laminated composite plates and shells was reported by Kant and Swaminathan (2000). A selective literature survey on the free-edge effect since 1967 up to 2004 was given by Mittelstedk and Becker (2004).

Generally, the laminated plate theories can be broadly divided into two categories: equivalent single layer theories (ESL) and layerwise or layer-by-layer theories. The ESL theories are derived from the 3-D elasticity theory, making suitable assumptions concerning the kinematics of deformation or the stress state through the thickness of the laminate. These assumptions reduce a 3-D problem to a 2-D problem. Layerwise theories provide an intermediate discretization level between a complete 3D representation and an equivalent single layer 2D model. They predict highly accurate

responses at the ply level, where material discontinuities take place but the complexity involved makes research a major concern. Among the ESL theories, the classical laminated plate theory (CLPT) (Whitney and Leissa, 1969) is established through small deformation assumptions, as well as the well-known Kirchhoff-Love hypothesis, which indicates that a straight line, normal to the middle surface before deformation, remains straight and normal to the deformed middle surface. Transverse deformations, including transverse normal and transverse shear deformations, are neglected. The CLPT is broadly applied to obtain analytical, numerical, and semi- numerical solutions.

1.2.1 Analytical solution

An analytical, or exact, solution (Timoshenko, 1961) of a problem is one that satisfies the governing equations at every point of the domain, the boundary, and initial conditions of the problem. It is general and valid for all parameter values. We get the specific solution by simple substitution, without the need for solving the problem from the beginning. An analytical solution can be either closed-form or an infinite series. The solutions found with any method, such as Navier, Lévy, and Ritz methods (Ugural , 1999; Reddy, 2004), are termed analytical solutions.

The Navier solutions can be developed for a rectangular laminate when all four edges of the laminate are simply supported. The limitation of these solutions is that only laminated plates with four edges simply supported can be solved. The Lévy solutions can be developed for plates with two opposite edges simply supported and remaining two edges having any possible combination of boundary conditions: free, simple support, or clamped support. Compared with Navier solutions, Lévy solutions can solve problems with more complicated boundary conditions, but Lévy solutions are limited to plates that have supports on edges. The Ritz method can be used to determine approximate solutions for more general boundary conditions, as long as suitable approximation functions can be found for the problem. The limitation of the Ritz method is that the solution converges slowly, unless the complexity of approximation functions is increased.

The basic procedure of deriving analytical solutions can be described by the following steps: (1) find a function with unknown coefficients that satisfies the primary

boundary conditions; (2) substitute its derivatives into the governing differential equation or energy expression; (3) derive a group of algebraic equations according to the equilibrium or energy principle; and (4) determine the unknown coefficients in the function by solving the derived algebraic equations (Timoshenko, 1961).

If applicable, an analytical solution is often used as a benchmark to check solutions attained by other methods. Analytical methods have been used to demonstrate various plate theories, especially for illustrative purposes.

1.2.2 Numerical solution

A numerical solution (Szilard, 1974) is one that is obtained by satisfying the governing equations and boundary conditions of the problem in an approximate sense. Since most real world problems are defined on domains, which are geometrically complex and may have different types of boundary conditions on different portions of the boundary of the domain, it is difficult to generate the functions required in traditional analytical methods. The use of numerical approaches enables the engineer to expand his or her ability to solve such problems of practical significance.

The solutions obtained with any of the numerical methods, such as finite difference method and finite element method, are termed numerical solutions. Both finite difference and finite element techniques eventually require the solution of a system of linear algebraic equations. Such calculations are commonly performed by means of a digital computer, employing matrix methods. The finite difference method is simple, versatile, and suitable for computer and programmable desk calculator use. The results from finite difference method have acceptable accuracy for most technical purposes, provided that a relatively fine mesh is used. While the finite element methods have proved to be extremely powerful and versatile tools for static and dynamic analysis of a wide variety of beam, plate, and shell problems; they, however, require the use of a computer with considerable speed and storage capacity. Numerical methods cannot give a continuous solution.

1.2.3 Semi-numerical solution

A semi-numerical, or semi-analytical, solution of a problem is one that satisfies the governing equations analytically, in one or two directions, and numerically, in remaining directions. A typical semi-numerical solution is achieved by the finite strip method (Cheung *et al.*, 1982). In comparison with the numerical method, the main advantage is that the effort and expense for data preparation and input are minimized because the finite strip method reduces the high dimensional model to a low dimensional model. However, the limitations that exist in both analytical and numerical solutions are not fully overcome.

1.3 Scope of Work

The objective of this research is to extend Analytical Strip Method (ASM) to antisymmetric stiffened cross-ply and angle-ply laminated plates with various boundary and/or internal supports and loading conditions.

The ASM, as an analytical solution, was introduced by Harik and Salamoun (1986) for the analysis of thin orthotropic and stiffened rectangular plates subjected to uniform, partial uniform, patch, line, partial line, point loads, and to any combination of these loads (Figure 1.1). The method requires that the plate be divided into strips whose number depends on the geometrical discontinuities and the type and location of the loads. The solution to the governing differential equation of each strip employs the classical method of separation of variables. Unlike the numerical and semi-numerical methods, the accuracy of the analytic strip method does not depend on the number of strips, but on the number of modes considered in the series. The number of algebraic equations and the computational difficulties are reduced considerably.

In order to achieve the objective of this research, the following tasks will be conducted:

1. Derive analytical bending-extension coupling solutions for stiffened and non-stiffened antisymmetric cross-ply laminated and angle-ply laminated plates, simply supported along two parallel edges, and any combination of boundary conditions along the other edges under varied loading conditions.

2. Apply the method to continuous antisymmetric cross-ply and angle-ply laminated plates with internal support.
3. Determine fundamental frequencies for the laminated plates mentioned in Task 1.
4. Determine critical buckling loads for the laminated plates mentioned in Task 1.

The significance of this study lies in the derivation of an analytical solution to antisymmetric cross-ply and angle-ply laminated plates comprising bending-extension coupling with various support and loading conditions. This proposed work overcomes some limitations of the Navier, Lévy, and Ritz analytical solutions mentioned in Section 1.2.

1.4 Dissertation Outline

The dissertation consists of seven chapters organized in the following manner:

- Chapter 2 presents the procedure for the solution of the governing differential equation for bending-extension coupling of antisymmetric cross-ply and angle-ply laminated plates, with two opposite edges simply supported, and any boundary conditions along other two edges. Assumptions, relations, and mathematical operations that are necessary to the formulas are presented. The detailed expressions of coefficients A_i , for governing differential equation of antisymmetric laminated plates; coefficients a_i and b_i , for displacements, force, and moment results of antisymmetric cross-ply and angle-ply laminated plates are provided respectively in this chapter.
- Chapter 3 presents the solution of the deflection and stresses for antisymmetric cross-ply and angle-ply laminated plates with different types of supports on edges only. The procedure of an analytical solution for quartic equation is detailed in this chapter. The numerical examples are presented for special features from an ASM approach.
- Chapter 4 presents the solution of the deflection and stresses for continuous antisymmetric cross-ply and angle-ply laminated plates with beam on boundary, beam, and point supports inside plates.

- Chapters 5 and 6 present the solutions for the governing differential equation for free vibration and buckling of antisymmetric stiffened cross-ply and angle-ply laminated plates, with two opposite edges simply supported, and any boundary conditions along other two edges, respectively. Comparisons with ANSYS results are presented for typical situations. The numerical examples are indicated to demonstrate the advantages from an ASM approach.
- In Chapter 7, there is a summary of the significant findings from this research. Conclusions are drawn with regards to its relevance. Future research needs are identified and discussed according to the present research and the related areas.

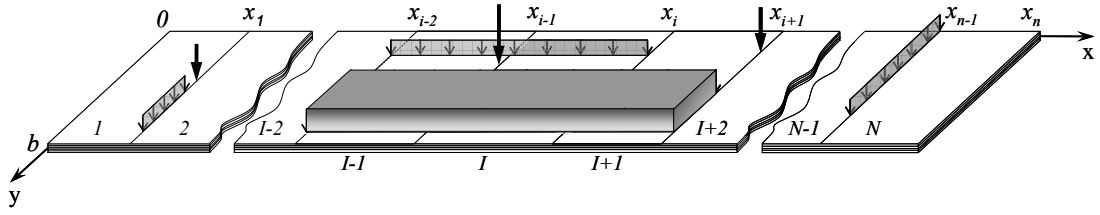


Figure 1.1. Plate strips with strip and edge loadings

CHAPTER 2
BASIC EQUATIONS FOR ANTISYMMETRIC
LAMINATED PLATES

2.1 Introduction

This chapter presents the formulation for the bending-extension coupling on deflection, free vibration, and buckling of laminated plates. In this dissertation, the term “layer”, or “lamina” refers to a single layer. A laminated plate, or laminate, is composed of several layers (laminae).

There are two classes of antisymmetric laminated plates: antisymmetric cross-ply and antisymmetric angle-ply laminated plates. An antisymmetric cross-ply laminated plate consists of an even number of orthotropic laminae laid on each other with principal material directions, alternating at 0° and 90° to the laminate axes as in the simple example of Figure 2.1. An antisymmetric angle-ply laminated plate has laminae oriented at $+\alpha$ degrees to the laminate coordinate axes on one side of the middle surface, and corresponding equal thickness laminae oriented at $-\alpha$ degrees on the other side (Figure 2.2).

The derivation of ASM solution is based on the following assumptions:

1. The materials from which the laminated plate is made are linear and elastic; The laminae are composed of homogeneous orthotropic materials.
2. The laminated plate is built by a number of laminae perfectly bonded together; No delamination appears at the lamina interfaces.
3. The deformations in a layer follow the Kirchhoff hypothesis; That is, a straight line perpendicular to the middle plane before deformation remains straight and normal to the mid-surface after deformation.
4. The effect of transverse normal stress is neglected.
5. The transverse normal strain is assumed negligible as well. As a result, the transverse deflections along a normal line are identical.
6. Displacements are assumed to be small compared with the laminated plate thickness.

2.2 Governing Differential Equations for Antisymmetric Laminated Plates

The system of three equations of equilibrium governing the general response of arbitrarily laminated composite plates can be written as (Whitney and Leissa, 1969):

$$\begin{bmatrix} L_{11} & L_{12} & L_{13} \\ L_{12} & L_{22} & L_{23} \\ L_{13} & L_{23} & L_{33} \end{bmatrix} \begin{Bmatrix} u_0 \\ v_0 \\ w \end{Bmatrix} = \begin{Bmatrix} 0 \\ 0 \\ q \end{Bmatrix} \quad (2.1)$$

in which, the displacements in the x , y , and z directions, u_0 , v_0 , and w , respectively, are presented in terms of the displacement function $\Phi(x, y)$ (Sharma *et al.*, 1980):

$$u_0 = (L_{12}L_{23} - L_{13}L_{22})\Phi(x, y) \quad (2.2)$$

$$v_0 = (L_{13}L_{21} - L_{23}L_{11})\Phi(x, y) \quad (2.3)$$

$$w = (L_{11}L_{22} - L_{12}L_{21})\Phi(x, y) \quad (2.4)$$

The differential operators L_{ij} are defined as follows:

$$L_{11} = A_{11} \frac{\partial^2}{\partial x^2} + A_{66} \frac{\partial^2}{\partial y^2} \quad (2.5a)$$

$$L_{12} = (A_{12} + A_{66}) \frac{\partial^2}{\partial x \partial y} \quad (2.5b)$$

$$L_{13} = - \left[B_{11} \frac{\partial^3}{\partial x^3} + 3B_{16} \frac{\partial^3}{\partial x^2 \partial y} + B_{12} \frac{\partial^3}{\partial x \partial y^2} + B_{26} \frac{\partial^3}{\partial y^3} \right] \quad (2.5c)$$

$$L_{22} = A_{66} \frac{\partial^2}{\partial x^2} + A_{22} \frac{\partial^2}{\partial y^2} \quad (2.5d)$$

$$L_{23} = - \left[B_{16} \frac{\partial^3}{\partial x^3} + B_{12} \frac{\partial^3}{\partial x^2 \partial y} + 3B_{26} \frac{\partial^3}{\partial x \partial y^2} + B_{22} \frac{\partial^3}{\partial y^3} \right] \quad (2.5e)$$

$$L_{33} = D_{11} \frac{\partial^4}{\partial x^4} + 2(D_{12} + 2D_{66}) \frac{\partial^4}{\partial x^2 \partial y^2} + D_{22} \frac{\partial^4}{\partial y^4} \quad (2.5f)$$

in which A_{ij} are the extensional stiffness coefficients, B_{ij} are the bending-extensional coupling stiffness coefficients, and D_{ij} are the bending stiffness coefficients. The stiffness coefficients are given by Reddy (2004) and are defined as follows:

$$\{A_{ij}, B_{ij}, D_{ij}\} = \int_{-\frac{h}{2}}^{\frac{h}{2}} \bar{Q}_{ij} \left\{ 1, z, z^2 \right\} dz; \quad (i, j = 1, 2, 6) \quad (2.6)$$

where, h is the thickness of the plate, and \bar{Q}_{ij} are reduced stiffness coefficients, given by Reddy (2004):

$$\bar{Q}_{11} = Q_{11} \cos^4 \theta + 2(Q_{12} + 2Q_{66}) \sin^2 \theta \cos^2 \theta + Q_{22} \sin^4 \theta \quad (2.7a)$$

$$\bar{Q}_{12} = (Q_{11} + Q_{22} - 4Q_{66}) \sin^2 \theta \cos^2 \theta + Q_{12} (\sin^4 \theta + \cos^4 \theta) \quad (2.7b)$$

$$\bar{Q}_{22} = Q_{11} \sin^4 \theta + 2(Q_{12} + 2Q_{66}) \sin^2 \theta \cos^2 \theta + Q_{22} \cos^4 \theta \quad (2.7c)$$

$$\bar{Q}_{16} = (Q_{11} - Q_{12} - 2Q_{66}) \sin \theta \cos^3 \theta + (Q_{12} - Q_{22} + 2Q_{66}) \sin^3 \theta \cos \theta \quad (2.7d)$$

$$\bar{Q}_{26} = (Q_{11} - Q_{12} - 2Q_{66}) \sin^3 \theta \cos \theta + (Q_{12} - Q_{22} + 2Q_{66}) \sin \theta \cos^3 \theta \quad (2.7e)$$

$$\bar{Q}_{66} = (Q_{11} + Q_{22} - 2Q_{12} - 2Q_{66}) \sin^2 \theta \cos^2 \theta + Q_{66} (\sin^4 \theta + \cos^4 \theta) \quad (2.7f)$$

in which θ is the angle measured counterclockwise from the x -coordinate to the fiber direction of the lamina, and the coefficients Q_{ij} are known in terms of the engineering constants:

$$Q_{11} = \frac{E_1}{1 - \nu_{12}\nu_{21}} \quad (2.8a)$$

$$Q_{12} = \frac{\nu_{12}E_2}{1 - \nu_{12}\nu_{21}} = \frac{\nu_{21}E_1}{1 - \nu_{12}\nu_{21}} \quad (2.8b)$$

$$Q_{22} = \frac{E_2}{1 - \nu_{12}\nu_{21}} \quad (2.8c)$$

$$Q_{66} = G_{12} \quad (2.8d)$$

The membrane strain $\{\varepsilon_0\} = \{\varepsilon_{xx}^{(0)}, \varepsilon_{yy}^{(0)}, \gamma_{xy}^{(0)}\}^T$ and flexural strain $\{\kappa\} = \{\varepsilon_{xx}^{(1)}, \varepsilon_{yy}^{(1)}, \gamma_{xy}^{(1)}\}^T$ can be presented in terms of the membrane forces, $\{N\} = \{N_x, N_y, N_{xy}\}^T$, and moments, $\{M\} = \{M_x, M_y, M_{xy}\}^T$, as follows:

$$\begin{Bmatrix} \{\varepsilon_0\} \\ \{\kappa\} \end{Bmatrix} = \begin{bmatrix} [A] & [B] \\ [B] & [D] \end{bmatrix}^{-1} \begin{Bmatrix} \{N\} \\ \{M\} \end{Bmatrix} \quad (2.9)$$

where $[A]$, $[B]$, and $[D]$ are the matrices containing A_{ij} , B_{ij} , and D_{ij} ($i, j = 1, 2, 6$), respectively. It should be noted that the transverse strains $\{\varepsilon_{xz}, \varepsilon_{yz}, \varepsilon_{zz}\}$ are identically zero in the classical plate theory.

Based on von Kármán's plate theory, the strains in the k^{th} layer can be presented in the following form (Reddy, 2004):

$$\begin{Bmatrix} \varepsilon_{xx} \\ \varepsilon_{yy} \\ \gamma_{xy} \end{Bmatrix}^k = \begin{Bmatrix} \varepsilon_{xx}^{(0)} \\ \varepsilon_{yy}^{(0)} \\ \gamma_{xy}^{(0)} \end{Bmatrix}^k + z_k \begin{Bmatrix} \varepsilon_{xx}^{(1)} \\ \varepsilon_{yy}^{(1)} \\ \gamma_{xy}^{(1)} \end{Bmatrix}^k \quad (2.10)$$

in which z_k is the distance between the midplane of the plate and a point in the k^{th} orthotropic lamina.

The linear constitutive relations for the k^{th} orthotropic lamina in the principal material coordinates of the lamina are:

$$\begin{Bmatrix} \sigma_{xx} \\ \sigma_{yy} \\ \tau_{xy} \end{Bmatrix}^k = \begin{bmatrix} \bar{Q}_{11} & \bar{Q}_{12} & \bar{Q}_{16} \\ \bar{Q}_{12} & \bar{Q}_{22} & \bar{Q}_{26} \\ \bar{Q}_{16} & \bar{Q}_{26} & \bar{Q}_{66} \end{bmatrix}^k \begin{Bmatrix} \varepsilon_{xx} \\ \varepsilon_{yy} \\ \gamma_{xy} \end{Bmatrix}^k \quad (2.11)$$

Based on the derivation by Sharma *et al.* (1980), Equation 2.1 can be written as

$$\begin{aligned} (L_{11}L_{22}L_{33} - L_{21}L_{12}L_{33} - L_{32}L_{23}L_{11} + L_{31}L_{12}L_{23} \\ + L_{32}L_{13}L_{21} - L_{31}L_{13}L_{22})\Phi(x, y) = q(x, y) \end{aligned} \quad (2.12)$$

The governing differential equation for antisymmetric laminated plates can be derived from Equation 2.12 by expanding the differential operators L_{ij} :

$$A_1 \frac{\partial^8 \Phi}{\partial x^8} + A_3 \frac{\partial^8 \Phi}{\partial x^6 \partial y^2} + A_5 \frac{\partial^8 \Phi}{\partial x^4 \partial y^4} + A_7 \frac{\partial^8 \Phi}{\partial x^2 \partial y^6} + A_9 \frac{\partial^8 \Phi}{\partial y^8} = q(x, y) \quad (2.13)$$

in which A_i ($i = 1, 3, \dots, 9$) are (Sharma *et al.*, 1980):

$$A_1 = B_{11}(2A_{16}B_{16} - A_{66}B_{11}) - A_{11}B_{16}^2 + D_{11}(A_{11}A_{66} + A_{16}^2) \quad (2.14a)$$

$$\begin{aligned} A_3 = 2B_{11}(3A_{16}B_{26} + A_{12}B_{12} + 2A_{12}B_{66} - 5A_{26}B_{16}) + 2B_{16}(2A_{16}B_{12} + 4A_{16}B_{66} \\ + 3A_{12}B_{16} - 2A_{66}B_{16} - 3A_{11}B_{26}) + D_{11}(2A_{16}A_{66} + A_{11}A_{22} - A_{12}^2 - 2A_{12}A_{66}) \\ + 8D_{16}(A_{11}A_{26} - A_{16}A_{12}) - A_{22}B_{11}^2 - A_{11}(B_{12}^2 + 4B_{12}B_{66} + 4B_{66}^2) \\ + 2(A_{12} + A_{66})(A_{11}A_{66} - A_{16}^2) \end{aligned} \quad (2.14b)$$

$$\begin{aligned}
A_5 = & 2B_{11}(A_{12}B_{22} + A_{66}B_{22} + A_{26}B_{26} - A_{22}B_{12} - 2A_{22}B_{66}) + 2B_{22}(A_{16}B_{16} - A_{11}B_{12} \\
& - 2A_{11}B_{66}) - 4B_{16}A_{26}(B_{12} + 2B_{66}) - 4B_{26}A_{16}(B_{12} + 2B_{66}) - 9(A_{22}B_{16}^2 + A_{11}B_{26}^2) \\
& + 4B_{16}B_{26}(5A_{12} + 2A_{66}) + D_{11}(A_{22}A_{66} - A_{26}^2) + D_{22}(A_{11}A_{66} - A_{16}^2) \\
& + 8D_{16}(A_{22}A_{16} - A_{26}A_{12}) + 8D_{26}(A_{11}A_{66} + A_{11}A_{26} - A_{16}A_{12} - A_{16}A_{66}) \\
& + 2(B_{12} + 2B_{66})(A_{12}^2 + A_{66}^2 + 2A_{12}A_{66} - A_{66}B_{12} - 2A_{66}B_{66}) \\
& + 2(D_{12} + 2D_{66})(A_{11}A_{22} + 2A_{16}A_{26} - A_{12}^2 - 2A_{12}A_{66})
\end{aligned} \tag{2.14c}$$

$$\begin{aligned}
A_7 = & B_{22}(6A_{26}B_{16} + 2A_{12}B_{12} + 4A_{12}B_{66} - 10A_{16}B_{26} - A_{11}B_{22}) - 6B_{16}B_{26}A_{22} \\
& + 2B_{26}^2(3A_{12} - 2A_{66}) + D_{22}(A_{11}A_{22} - A_{12}^2 - 2A_{12}A_{66} + 2A_{16}A_{26}) \\
& + 8D_{26}(A_{22}A_{16} - A_{26}A_{12}) + 2(D_{12} + 2D_{66})(A_{22}A_{66} - A_{26}^2) \\
& + (B_{12} + 2B_{66})(4A_{26}B_{26} - A_{22}B_{12} - 2A_{22}B_{66})
\end{aligned} \tag{2.14d}$$

$$A_9 = B_{22}(2A_{26}B_{26} - A_{66}B_{26}) - A_{22}B_{26}^2 + D_{22}(A_{22}A_{66} - A_{26}^2) \tag{2.14e}$$

Equation 2.13 is the governing differential equation for antisymmetric laminated plates.

2.2.1 Antisymmetric cross-ply laminated plate

Reddy (2004) has shown that for an antisymmetric cross-ply laminate, the stiffness:

$$A_{16} = A_{26} = D_{16} = D_{26} = B_{12} = B_{16} = B_{26} = B_{66} = 0, \text{ and } B_{22} = -B_{11}$$

The coefficients of the governing Equation 2.13 are reduced to

$$A_1 = A_{66}(A_{11}D_{11} - B_{11}^2) \tag{2.15a}$$

$$A_3 = 2A_{11}A_{66}(D_{12} + 2D_{66}) - A_{22}B_{11}^2 + D_{11}(A_{11}A_{22} + A_{66}^2 - E_1^2) \tag{2.15b}$$

$$\begin{aligned}
A_5 = & 2(D_{12} + 2D_{66})(A_{11}A_{22} - A_{12}^2 - 2A_{12}A_{66}) - 2(A_{12} + A_{66})B_{11}^2 \\
& + A_{66}(A_{11}D_{22} + A_{22}D_{11})
\end{aligned} \tag{2.15c}$$

$$A_7 = 2A_{22}A_{66}(D_{12} + 2D_{66}) - A_{11}B_{11}^2 + D_{22}(A_{11}A_{22} - A_{12}^2 - 2A_{12}A_{66}) \tag{2.15d}$$

$$A_9 = A_{66}(A_{22}D_{22} - B_{11}^2) \tag{2.15e}$$

The displacement components in terms of Φ for antisymmetric cross-ply laminate are:

$$u_0 = a_1 \frac{\partial^5 \Phi}{\partial x^5} + a_2 \frac{\partial^5 \Phi}{\partial x^3 \partial y^2} + a_3 \frac{\partial^5 \Phi}{\partial x \partial y^4} \tag{2.16}$$

$$v_0 = a_4 \frac{\partial^5 \Phi}{\partial x^4 \partial y} + a_5 \frac{\partial^5 \Phi}{\partial x^2 \partial y^3} + a_6 \frac{\partial^5 \Phi}{\partial y^5} \quad (2.17)$$

$$w = a_7 \frac{\partial^4 \Phi}{\partial x^4} + a_8 \frac{\partial^4 \Phi}{\partial x^2 \partial y^2} + a_9 \frac{\partial^4 \Phi}{\partial y^4} \quad (2.18)$$

where

$$a_1 = B_{11} A_{66} \quad (2.19a)$$

$$a_2 = B_{11} A_{22} \quad (2.19b)$$

$$a_3 = B_{11} (A_{12} + A_{66}) \quad (2.19c)$$

$$a_4 = -B_{11} (A_{12} + A_{66}) \quad (2.19d)$$

$$a_5 = -B_{11} A_{11} \quad (2.19e)$$

$$a_6 = -B_{11} A_{66} \quad (2.19f)$$

$$a_7 = A_{11} A_{66} \quad (2.19g)$$

$$a_8 = A_{11} A_{22} - A_{12}^2 - 2A_{12} A_{66} \quad (2.19h)$$

$$a_9 = A_{22} A_{66} \quad (2.19i)$$

The force and moment resultants, in terms of Φ , can be obtained from the constitutive relation:

$$\begin{Bmatrix} \{N\} \\ \{M\} \end{Bmatrix} = \begin{bmatrix} [A] & [B] \\ [B] & [D] \end{bmatrix} \begin{Bmatrix} \{\varepsilon_0\} \\ \{\kappa\} \end{Bmatrix} \quad (2.20)$$

And from Equations 2.16 – 2.18. These are:

$$N_x = a_{10} \frac{\partial^6 \Phi}{\partial x^4 \partial y^2} + a_{11} \frac{\partial^6 \Phi}{\partial x^2 \partial y^4} + a_{12} \frac{\partial^6 \Phi}{\partial y^6} \quad (2.21)$$

$$N_y = a_{13} \frac{\partial^6 \Phi}{\partial x^6} + a_{14} \frac{\partial^6 \Phi}{\partial x^4 \partial y^2} + a_{15} \frac{\partial^6 \Phi}{\partial x^2 \partial y^4} \quad (2.22)$$

$$N_{xy} = a_{16} \frac{\partial^6 \Phi}{\partial x^5 \partial y} + a_{17} \frac{\partial^6 \Phi}{\partial x^3 \partial y^3} + a_{18} \frac{\partial^6 \Phi}{\partial x \partial y^5} \quad (2.23)$$

$$M_x = a_{19} \frac{\partial^6 \Phi}{\partial x^6} + a_{20} \frac{\partial^6 \Phi}{\partial x^4 \partial y^2} + a_{21} \frac{\partial^6 \Phi}{\partial x^2 \partial y^4} + a_{22} \frac{\partial^6 \Phi}{\partial y^6} \quad (2.24)$$

$$M_y = a_{23} \frac{\partial^6 \Phi}{\partial x^6} + a_{24} \frac{\partial^6 \Phi}{\partial x^4 \partial y^2} + a_{25} \frac{\partial^6 \Phi}{\partial x^2 \partial y^4} + a_{26} \frac{\partial^6 \Phi}{\partial y^6} \quad (2.25)$$

$$M_{xy} = a_{27} \frac{\partial^6 \Phi}{\partial x^5 \partial y} + a_{28} \frac{\partial^6 \Phi}{\partial x^3 \partial y^3} + a_{29} \frac{\partial^6 \Phi}{\partial x \partial y^5} \quad (2.26)$$

$$V_x = a_{19} \frac{\partial^7 \Phi}{\partial x^7} + a_{30} \frac{\partial^7 \Phi}{\partial x^5 \partial y^2} + a_{31} \frac{\partial^7 \Phi}{\partial x^3 \partial y^4} + a_{32} \frac{\partial^7 \Phi}{\partial x \partial y^6} \quad (2.27)$$

where:

$$a_{10} = A_{12} A_{66} B_{11} \quad (2.28a)$$

$$a_{11} = A_{66} B_{11} (A_{11} - A_{22}) \quad (2.28b)$$

$$a_{12} = -A_{12} A_{66} B_{11} \quad (2.28c)$$

$$a_{13} = A_{12} A_{66} B_{11} \quad (2.28d)$$

$$a_{14} = B_{11} A_{66} (A_{11} - A_{22}) \quad (2.28e)$$

$$a_{15} = -A_{12} A_{66} B_{11} \quad (2.28f)$$

$$a_{16} = -A_{12} A_{66} B_{11} \quad (2.28g)$$

$$a_{17} = B_{11} A_{66} (A_{22} - A_{11}) \quad (2.28h)$$

$$a_{18} = A_{12} A_{66} B_{11} \quad (2.28i)$$

$$a_{19} = A_{66} (B_{11}^2 - A_{11} D_{11}) \quad (2.28j)$$

$$a_{20} = B_{11}^2 A_{22} - D_{11} (A_{11} A_{22} - A_{12}^2 - 2A_{12} A_{66}) - A_{11} A_{66} D_{12} \quad (2.28k)$$

$$a_{21} = B_{11}^2 (A_{12} + A_{66}) - A_{22} A_{66} D_{11} - D_{12} (A_{11} A_{22} - A_{12}^2 - 2A_{12} A_{66}) \quad (2.28l)$$

$$a_{22} = -A_{22} A_{66} D_{12} \quad (2.28m)$$

$$a_{23} = -A_{11} A_{66} D_{12} \quad (2.28n)$$

$$a_{24} = B_{11}^2 (A_{12} + A_{66}) - D_{12} (A_{11} A_{22} - A_{12}^2 - 2A_{12} A_{66}) - A_{11} A_{66} D_{22} \quad (2.28o)$$

$$a_{25} = B_{11}^2 A_{11} - A_{22} A_{66} D_{12} - D_{22} (A_{11} A_{22} - A_{12}^2 - 2A_{12} A_{66}) \quad (2.28p)$$

$$a_{26} = A_{66} (B_{11}^2 - A_{22} D_{22}) \quad (2.28q)$$

$$a_{27} = -2A_{11} A_{66} D_{66} \quad (2.28r)$$

$$a_{28} = -2D_{66} (A_{11} A_{22} - A_{12}^2 - 2A_{12} A_{66}) \quad (2.28s)$$

$$a_{29} = -2A_{22} A_{66} D_{66} \quad (2.28t)$$

$$a_{30} = a_{20} + 2a_{27} \quad (2.28u)$$

$$a_{31} = a_{21} + 2a_{28} \quad (2.28v)$$

$$a_{32} = a_{22} + 2a_{29} \quad (2.28w)$$

2.2.2 Antisymmetric angle-ply laminated plate

Similarly, Reddy (2004) has shown that for an antisymmetric angle-ply laminate, the stiffness:

$$A_{16} = A_{26} = D_{16} = D_{26} = B_{11} = B_{12} = B_{22} = B_{66} = 0$$

The coefficients of the governing Equation 2.13 for this type of plate are reduced to:

$$A_1 = A_{11}(A_{66}D_{11} - B_{16}^2) \quad (2.29a)$$

$$A_3 = 2B_{16}^2(3A_{12} - 2A_{66}) + 2A_{11}(A_{66}D_{12} + 2A_{66}D_{66} - 3B_{16}B_{26}) \\ + D_{11}(A_{11}A_{22} - A_{12}^2 - 2A_{12}A_{66}) \quad (2.29b)$$

$$A_5 = 4B_{16}B_{26}(5A_{12} + 2A_{66}) + 2(D_{12} + 2D_{66})(A_{11}A_{22} - A_{12}^2 - 2A_{12}A_{66}) \\ - 9(A_{22}B_{16}^2 + A_{11}B_{26}^2) + A_{66}(A_{11}D_{22} + A_{22}D_{11}) \quad (2.29c)$$

$$A_7 = 2B_{26}^2(3A_{12} - 2A_{66}) + 2A_{22}(A_{66}D_{12} + 2A_{66}D_{66} - 3B_{16}B_{26}) \\ + D_{22}(A_{11}A_{22} - A_{12}^2 - 2A_{12}A_{66}) \quad (2.29d)$$

$$A_9 = A_{22}(A_{66}D_{22} - B_{26}^2) \quad (2.29e)$$

The displacement components, force and moment resultants, in terms of Φ for an antisymmetric angle-ply plate are:

$$u_0 = b_1 \frac{\partial^5 \Phi}{\partial x^4 \partial y} + b_2 \frac{\partial^5 \Phi}{\partial x^2 \partial y^3} + b_3 \frac{\partial^5 \Phi}{\partial y^5} \quad (2.30)$$

$$v_0 = b_4 \frac{\partial^5 \Phi}{\partial x^5} + b_5 \frac{\partial^5 \Phi}{\partial x^3 \partial y^2} + b_6 \frac{\partial^5 \Phi}{\partial x \partial y^4} \quad (2.31)$$

$$w = b_7 \frac{\partial^4 \Phi}{\partial x^4} + b_8 \frac{\partial^4 \Phi}{\partial x^2 \partial y^2} + b_9 \frac{\partial^4 \Phi}{\partial y^4} \quad (2.32)$$

$$N_x = b_{10} \frac{\partial^6 \Phi}{\partial x^3 \partial y^3} + b_{11} \frac{\partial^6 \Phi}{\partial x \partial y^5} \quad (2.33)$$

$$N_y = b_{12} \frac{\partial^6 \Phi}{\partial x^5 \partial y} + b_{13} \frac{\partial^6 \Phi}{\partial x^3 \partial y^3} \quad (2.34)$$

$$N_{xy} = b_{14} \frac{\partial^6 \Phi}{\partial x^4 \partial y^2} + b_{15} \frac{\partial^6 \Phi}{\partial x^2 \partial y^4} \quad (2.35)$$

$$M_x = b_{16} \frac{\partial^6 \Phi}{\partial x^6} + b_{17} \frac{\partial^6 \Phi}{\partial x^4 \partial y^2} + b_{18} \frac{\partial^6 \Phi}{\partial x^2 \partial y^4} + b_{19} \frac{\partial^6 \Phi}{\partial y^6} \quad (2.36)$$

$$M_y = b_{20} \frac{\partial^6 \Phi}{\partial x^6} + b_{21} \frac{\partial^6 \Phi}{\partial x^4 \partial y^2} + b_{22} \frac{\partial^6 \Phi}{\partial x^2 \partial y^4} + b_{23} \frac{\partial^6 \Phi}{\partial y^6} \quad (2.37)$$

$$M_{xy} = b_{24} \frac{\partial^6 \Phi}{\partial x^5 \partial y} + b_{25} \frac{\partial^6 \Phi}{\partial x^3 \partial y^3} + b_{26} \frac{\partial^6 \Phi}{\partial x \partial y^5} \quad (2.38)$$

$$V_x = b_{16} \frac{\partial^7 \Phi}{\partial x^7} + b_{27} \frac{\partial^7 \Phi}{\partial x^5 \partial y^2} + b_{28} \frac{\partial^7 \Phi}{\partial x^3 \partial y^4} + b_{29} \frac{\partial^7 \Phi}{\partial x \partial y^6} \quad (2.39)$$

where:

$$b_1 = B_{16}(-A_{12} + 2A_{66}) \quad (2.40a)$$

$$b_2 = -B_{26}(3A_{12} + 2A_{66}) + 3A_{22}B_{16} \quad (2.40b)$$

$$b_3 = A_{22}B_{26} \quad (2.40c)$$

$$b_4 = A_{11}B_{16} \quad (2.40d)$$

$$b_5 = -B_{16}(3A_{12} + 2A_{66}) + 3A_{11}B_{26} \quad (2.40e)$$

$$b_6 = B_{26}(-A_{12} + 2A_{66}) \quad (2.40f)$$

$$b_7 = A_{11}A_{66} \quad (2.40g)$$

$$b_8 = A_{11}A_{22} - A_{12}(A_{12} + 2A_{66}) \quad (2.40h)$$

$$b_9 = A_{22}A_{66} \quad (2.40i)$$

$$b_{10} = A_{11}(A_{22}B_{16} - 2A_{66}B_{26}) + A_{12}B_{16}(-A_{12} + 2A_{66}) \quad (2.40j)$$

$$b_{11} = A_{22}(A_{11}B_{26} - 2A_{66}B_{16}) + A_{12}B_{26}(-A_{12} + 2A_{66}) \quad (2.40k)$$

$$b_{12} = B_{16}(A_{11}A_{22} - A_{12}^2 + 2A_{12}A_{66}) - 2A_{11}A_{66}B_{26} \quad (2.40l)$$

$$b_{13} = B_{26}(A_{11}A_{22} - A_{12}^2 + 2A_{12}A_{66}) - 2A_{22}A_{66}B_{16} \quad (2.40m)$$

$$b_{14} = 2A_{66}(A_{11}B_{26} - A_{12}B_{16}) + B_{16}(A_{12}^2 - A_{11}A_{22}) \quad (2.40n)$$

$$b_{15} = 2A_{66}(A_{22}B_{16} - A_{12}B_{26}) + B_{26}(A_{12}^2 - A_{11}A_{22}) \quad (2.40o)$$

$$b_{16} = A_{11}(B_{16}^2 - A_{66}D_{11}) \quad (2.40p)$$

$$b_{17} = B_{16}(3A_{11}B_{26} - 4A_{12}B_{16}) + D_{11}(-A_{11}A_{22} + A_{12}^2 + 2A_{12}A_{66}) - A_{11}A_{66}D_{12} \quad (2.40q)$$

$$b_{18} = B_{16}(3A_{22}B_{16} - 4A_{12}B_{26}) + D_{12}(-A_{11}A_{22} + A_{12}^2 + 2A_{12}A_{66}) - A_{22}A_{66}D_{11} \quad (2.40r)$$

$$b_{19} = A_{22}(B_{16}B_{26} - A_{66}D_{12}) \quad (2.40s)$$

$$b_{20} = A_{11}(B_{16}B_{26} - A_{66}D_{12}) \quad (2.40t)$$

$$b_{21} = B_{26}(3A_{11}B_{26} - 4A_{12}B_{16}) + D_{12}(-A_{11}A_{22} + A_{12}^2 + 2A_{12}A_{66}) - A_{11}A_{66}D_{22} \quad (2.40u)$$

$$b_{22} = B_{26}(3A_{22}B_{16} - 4A_{12}B_{26}) + D_{22}(-A_{11}A_{22} + A_{12}^2 + 2A_{12}A_{66}) - A_{22}A_{66}D_{12} \quad (2.40v)$$

$$b_{23} = A_{22}(B_{26}^2 - A_{66}D_{22}) \quad (2.40w)$$

$$b_{24} = A_{11}(B_{16}B_{26} - 2A_{66}D_{66}) + B_{16}^2(-A_{12} + 2A_{66}) \quad (2.40x)$$

$$b_{25} = -2B_{16}B_{26}(3A_{12} + 2A_{66}) + 3(A_{11}B_{26}^2 + A_{22}B_{16}^2) \\ + 2D_{66}(-A_{11}A_{22} + A_{12}^2 + 2A_{12}A_{66}) \quad (2.40y)$$

$$b_{26} = A_{22}(B_{16}B_{26} - 2A_{66}D_{66}) + B_{26}^2(-A_{12} + 2A_{66}) \quad (2.40z)$$

$$b_{27} = b_{17} + 2b_{24} \quad (2.40aa)$$

$$b_{28} = b_{18} + 2b_{25} \quad (2.40ab)$$

$$b_{29} = b_{19} + 2b_{26} \quad (2.40ac)$$

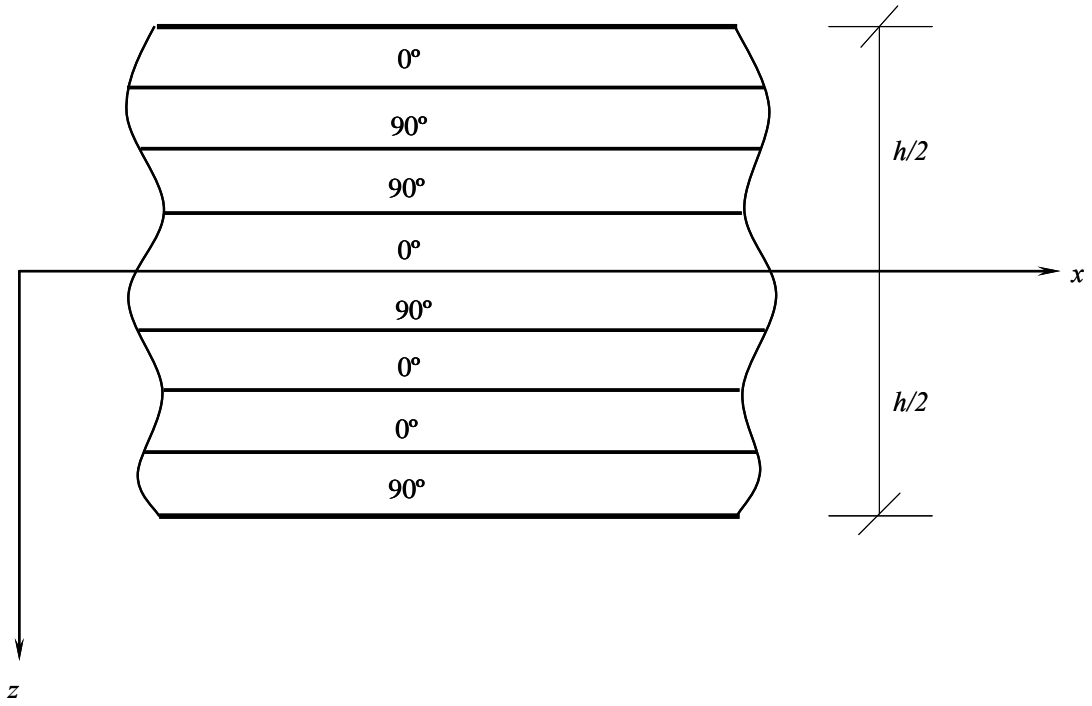


Figure 2.1. An antisymmetric cross-ply laminate.

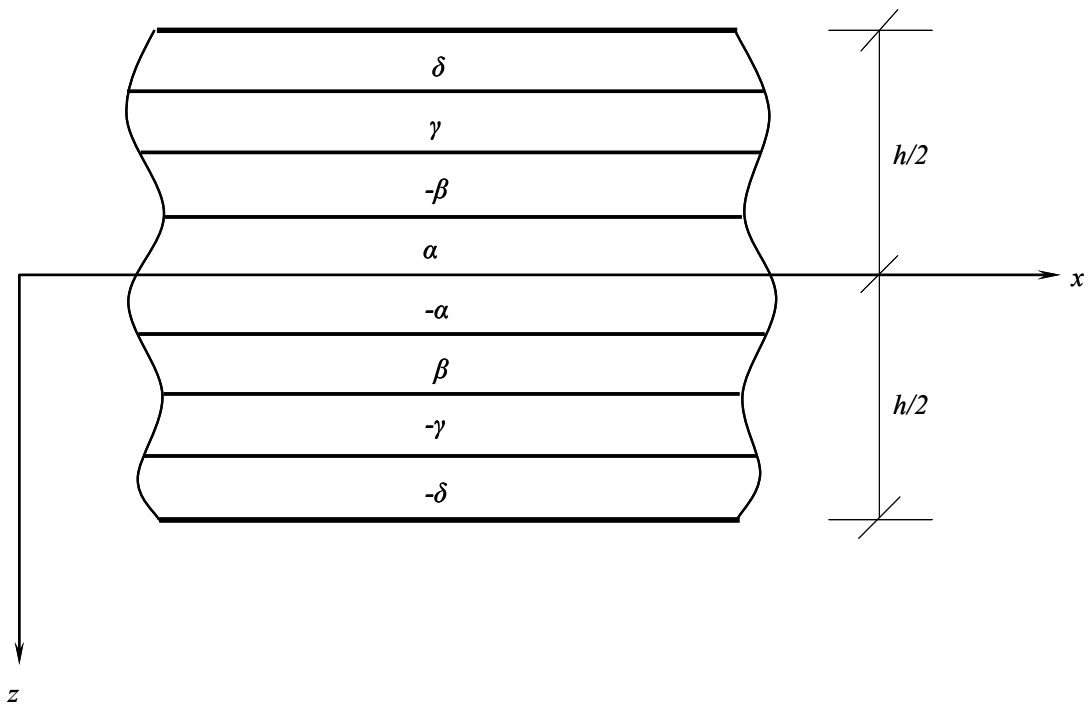


Figure 2.2. An antisymmetric angle-ply laminate.

CHAPTER 3
BENDING-EXTENSION COUPLING OF ANTISYMMETRIC
LAMINATED PLATES

3.1 Introduction

The laminated plate components have wide applications in a variety of structures, such as ships, bridges, aircrafts, pressure vessels, buildings, etc., because of their superior performance. The analysis, however, of laminated plates is more complicated than that of orthotropic ones, due to the bending-extension coupling. During the last two decades, the state-space concept has been used to generate exact solutions for various boundary conditions, in order to address the bending-extension coupling problem of laminated plates (Khdeir, 1989 and 1996; Khdeir and Reddy, 1991). In this chapter, analytical solutions for bending-extension coupling of antisymmetric laminated plates are obtained by using the Analytical Strip Method (ASM).

3.2 Governing Differential Equation

For an antisymmetric laminated plate, subjected to a transverse load $q(x, y)$, the governing differential equation is shown in Equation 2.13:

$$A_1 \frac{\partial^8 \Phi}{\partial x^8} + A_3 \frac{\partial^8 \Phi}{\partial x^6 \partial y^2} + A_5 \frac{\partial^8 \Phi}{\partial x^4 \partial y^4} + A_7 \frac{\partial^8 \Phi}{\partial x^2 \partial y^6} + A_9 \frac{\partial^8 \Phi}{\partial y^8} = q(x, y) \quad (2.13)$$

The Analytical Strip Method (ASM), which was introduced by Harik and Salamoun (1986), will be extended to solve this equation in conjunction with appropriate boundary and continuity conditions.

3.3 Analytical Strip Method

For a rectangular plate strip I , simply supported along two edges parallel to the x -axis (Figure 1.1), the solution to Equation 2.13 can be presented in a single series form:

$$\Phi_I(x, y) = \sum_n^{\infty} \phi_{nl}(x) \cdot \sin(\beta_n y) \quad (3.1)$$

in which,

$$\beta_n = \frac{n\pi}{b} \quad (3.2)$$

and b is the length of the plate along the y -axis. Hereinafter, the subscript I , denoting the I^{th} plate strip, will be excluded in the derivation of the solution to Equation 2.13, for strip I .

Substitution of Equation 3.1 into Equation 2.13, leads to:

$$\begin{aligned}
A_1 \sum_n \frac{d^8 \phi_n(x)}{dx^8} \sin(\beta_n y) - A_3 \sum_n \frac{d^6 \phi_n(x)}{dx^6} \beta_n^2 \sin(\beta_n y) + A_5 \sum_n \frac{d^4 \phi_n(x)}{dx^4} \beta_n^4 \sin(\beta_n y) \\
- A_7 \sum_n \frac{d^2 \phi_n(x)}{dx^2} \beta_n^6 \sin(\beta_n y) + A_9 \sum_n \phi_n(x) \beta_n^8 \sin(\beta_n y) = q(x, y)
\end{aligned} \quad (3.3)$$

Multiplying Equation 3.3 by $\sin(\beta_m y)$, integrating from $y = 0$ to $y = b$, and summing from $m = 1$ to $m = \infty$, Equation 3.3 leads to:

$$\begin{aligned}
\sum_m \left\{ A_1 \left[\int_0^b \sum_n \frac{d^8 \phi_n(x)}{dx^8} \sin(\beta_n y) \sin(\beta_m y) dy \right] \right. \\
- A_3 \left[\int_0^b \sum_n \frac{d^6 \phi_n(x)}{dx^6} \beta_n^2 \sin(\beta_n y) \sin(\beta_m y) dy \right] \\
+ A_5 \left[\int_0^b \sum_n \frac{d^4 \phi_n(x)}{dx^4} \beta_n^4 \sin(\beta_n y) \sin(\beta_m y) dy \right] \\
- A_7 \left[\int_0^b \sum_n \frac{d^2 \phi_n(x)}{dx^2} \beta_n^6 \sin(\beta_n y) \sin(\beta_m y) dy \right] \\
\left. + A_9 \left[\int_0^b \sum_n \phi_n(x) \beta_n^8 \sin(\beta_n y) \sin(\beta_m y) dy \right] \right\} = \sum_m \int_0^b q(x, y) \sin(\beta_m y) dy \quad (3.4)
\end{aligned}$$

Since $\int_0^b \sin(\beta_n y) \sin(\beta_m y) dy = \frac{b}{2}$ for $m = n$, and $\int_0^b \sin(\beta_n y) \sin(\beta_m y) dy = 0$ for

$m \neq n$, Equation 3.4 reduces to:

$$\begin{aligned}
\sum_m \left[A_1 \frac{d^8 \phi_m(x)}{dx^8} - A_3 \beta_m^2 \frac{d^6 \phi_m(x)}{dx^6} + A_5 \beta_m^4 \frac{d^4 \phi_m(x)}{dx^4} - A_7 \beta_m^6 \frac{d^2 \phi_m(x)}{dx^2} + A_9 \beta_m^8 \phi_m(x) \right] \\
= \sum_m \left[\frac{2}{b} \int_0^b q(x, y) \sin(\beta_m y) dy \right] \quad (3.5)
\end{aligned}$$

Equation 3.5 is an infinite set of ordinary differential equations for $\phi_m(x)$ ($m = 1,$

2, 3, ..., ∞). It is a unidirectional and linear 8th order differential equation, which can be solved by the superposition of the homogeneous part, $\Phi_H(x, y)$, and the particular part of the equation, $\Phi_P(x, y)$.

$$\Phi(x, y) = \Phi_H(x, y) + \Phi_P(x, y) \quad (3.6a)$$

or

$$\sum_m^{\infty} \phi_m(x) \sin(\beta_m y) = \sum_m^{\infty} \phi_{Hm}(x) \sin(\beta_m y) + \sum_m^{\infty} \phi_{Pm}(x) \sin(\beta_m y) \quad (3.6b)$$

3.3.1 Homogeneous solution, $\Phi_H(x, y) = \sum_m^{\infty} \phi_{Hm}(x) \sin(\beta_m y)$

The homogeneous solution for mode m , $\phi_{Hm}(x)$, is expressed as follows:

$$\phi_{Hm}(x) = e^{\gamma_m \beta_m x} \quad (3.7)$$

The characteristic equation of the homogeneous part of Equation 3.5 for mode m is:

$$A_1 \gamma_m^8 \beta_m^8 - A_3 \gamma_m^6 \beta_m^8 + A_5 \gamma_m^4 \beta_m^8 - A_7 \gamma_m^2 \beta_m^8 + A_9 \beta_m^8 = 0 \quad (3.8)$$

in which, $\gamma_m \beta_m$ are the characteristic roots for function $\phi_{Hm}(x)$. Since $\beta_m \neq 0$, Equation 3.8 can be simplified as:

$$A_1 \gamma_m^8 - A_3 \gamma_m^6 + A_5 \gamma_m^4 - A_7 \gamma_m^2 + A_9 = 0 \quad (3.9)$$

Dividing Equation 3.9 by A_1 and settling $\gamma_m^2 = \xi_m$, it leads to:

$$\xi_m^4 + b \xi_m^3 + c \xi_m^2 + d \xi_m + e = 0 \quad (3.10)$$

in which,

$$b = -\frac{A_3}{A_1}, \quad c = \frac{A_5}{A_1}, \quad d = -\frac{A_7}{A_1}, \quad e = \frac{A_9}{A_1} \quad (3.11)$$

Equation 3.10 is a quartic equation and can be solved analytically (Editing group of the Manual of Mathematics, 1979). Four roots for Equation 3.10 are same as four roots in following two equations:

$$\xi_n^2 + \left(b + \sqrt{8s + b^2 - 4c} \right) \frac{\xi_n}{2} + \left(s + \frac{bs - d}{\sqrt{8s + b^2 - 4c}} \right) = 0 \quad (3.12a)$$

$$\xi_n^2 + \left(b - \sqrt{8s + b^2 - 4c} \right) \frac{\xi_n}{2} + \left(s - \frac{bs - d}{\sqrt{8s + b^2 - 4c}} \right) = 0 \quad (3.12b)$$

Where, s is any real root for following equation

$$8s^3 - 4cs^2 + (2bd - 8e)s + e(4c - b^2) - d^2 = 0 \quad (3.13)$$

Substituting coefficients in Equation 3.11 to Equation 3.13, it leads to:

$$4c = \frac{4A_5}{A_1} \quad (3.14)$$

$$(2bd - 8e) = \frac{2(A_3A_7 - 4A_1A_9)}{A_1^2} \quad (3.15)$$

$$e(4c - b^2) - d^2 = \frac{4A_1A_5A_9 - (A_3^2A_9 + A_1A_7^2)}{A_1^3} \quad (3.16)$$

Equation 3.13 becomes:

$$s^3 + fs^2 + gs + h = 0 \quad (3.17)$$

where,

$$f = -\frac{A_5}{2A_1} \quad (3.18)$$

$$g = \frac{A_3A_7 - 4A_1A_9}{4A_1^2} \quad (3.19)$$

$$h = \frac{4A_1A_5A_9 - (A_3^2A_9 + A_1A_7^2)}{8A_1^3} \quad (3.20)$$

Let

$$s = t - \frac{f}{3} \quad (3.21)$$

Then, substitute it to Equation 3.17, it leads to:

$$\left(t - \frac{f}{3} \right)^3 + f \left(t - \frac{f}{3} \right)^2 + g \left(t - \frac{f}{3} \right) + h = t^3 + \left(-\frac{f^2}{3} + g \right) t + \left(\frac{2f^3}{27} - \frac{fg}{3} + h \right) \quad (3.22)$$

Equation 3.22 becomes:

$$t^3 + pt + q = 0 \quad (3.23)$$

in which,

$$p = -\frac{f^2}{3} + g \quad (3.24)$$

$$q = \frac{2f^3}{27} - \frac{fg}{3} + h \quad (3.25)$$

$$\text{Let } \Delta = \left(\frac{q}{2}\right)^2 + \left(\frac{p}{3}\right)^3 \quad (3.26)$$

$$\text{If } \Delta > 0 \quad t_1 = \sqrt[3]{-\frac{q}{2} + \sqrt{\Delta}} + \sqrt[3]{-\frac{q}{2} - \sqrt{\Delta}} \quad (3.27)$$

$$\text{If } \Delta < 0 \quad t_1 = 2\sqrt[3]{r} \cos \theta \quad (3.28)$$

where,

$$r = \sqrt{-\left(\frac{p}{3}\right)^3} \quad (3.29)$$

$$\theta = \frac{1}{3} \cos^{-1}\left(-\frac{q}{2r}\right) \quad (3.30)$$

Substituting solution t_1 to Equation 3.21, it gives:

$$s = t_1 - \frac{f}{3} \quad (3.31)$$

Using this result to Equations 3.12a and 3.12b, and solving them, all four roots will suit to Equation 3.10. From relation of $\gamma_m^2 = \xi_m$, γ_m is solved for characteristic Equation 3.8. It leads to the following general expression (all 9 possible expressions are detailed in Appendix A) for the homogeneous solution, $\Phi_H(x, y)$:

$$\Phi_H(x) = \sum_m \left\{ \begin{array}{l} [C_{1m} \cosh(\gamma_{1m}\beta_m x) + C_{2m} \sinh(\gamma_{1m}\beta_m x)] \cos(\gamma_{2m}\beta_m x) \\ + [C_{3m} \cosh(\gamma_{1m}\beta_m x) + C_{4m} \sinh(\gamma_{1m}\beta_m x)] \sin(\gamma_{2m}\beta_m x) \\ + [C_{5m} \cosh(\gamma_{3m}\beta_m x) + C_{6m} \sinh(\gamma_{3m}\beta_m x)] \cos(\gamma_{4m}\beta_m x) \\ + [C_{7m} \cosh(\gamma_{3m}\beta_m x) + C_{8m} \sinh(\gamma_{3m}\beta_m x)] \sin(\gamma_{4m}\beta_m x) \end{array} \right\} \sin(\beta_m y) \quad (3.32)$$

The constants C_{dm} ($d = 1, 2, \dots, 8$) are determined from the boundary conditions at $x = 0$ and $x = x_n = a$, and the continuity conditions at intermediate edges ($x_i, i = 1, 2, 3, \dots, n-1$, Figure 1.1).

3.3.2 Particular solution, $\Phi_p(x, y) = \sum_m^{\infty} \phi_{pm}(x) \sin(\beta_m y)$

The separation of variables can be applied to present the load $q(x, y)$, in Equation 3.5 as follows:

$$q(x, y) = q_0 f(x) g(y) \quad (3.33)$$

in which q_0 is the load amplitude, and $f(x)$ and $g(y)$ are the load distribution functions in the x and y directions, respectively. The right-hand side in Equation 3.5 takes the following form:

$$\frac{2}{b} \int_0^b q(x, y) \sin(\beta_m y) dy = \frac{2}{b} \int_0^b q_0 g(x) f(y) \sin(\beta_m y) dy = q_0 f(x) g_{1m}(y) \quad (3.34)$$

in which,

$$g_{1m} = \frac{2}{b} \int_0^b g(y) \sin(\beta_m y) dy \quad (3.35)$$

The general expression for the particular solution $\Phi_p(x, y)$, for plate strip I when subjected to the load expressed in Equation 3.35, can be presented as follows

$$\Phi_p(x, y) = \sum_m^{\infty} \phi_{pm} \sin(\beta_m y) = \sum_m^{\infty} \frac{q_0 f(x) g_{1m}}{A_9 \beta_m^8} \sin(\beta_m y) \quad (3.36)$$

The particular solutions $\Phi_p(x, y)$ for most common strip loadings are shown in Table 3.1.

When strip I is subjected to more than one loading (Figure 1.1), the method of superposition is employed to determine the particular solution:

$$\Phi_p(x, y) = \sum_{j=1}^r \Phi_p^j(x, y) \quad (3.37)$$

in which r represents the total number of loads applied on strip I .

3.3.3 Edge loading function

When the plate is subjected to line loads in the y direction or to point loads, it is divided into strips in such a way that the loads are applied along the inner or outer edges of the strips (Figure 1.1). These loads are expressed in a Lévy type Fourier series, and incorporated in the solution as discontinuities in the shear force. The edge loading

functions $\psi_i(y)$ for most common loadings are shown Table 3.2.

When the edge x_i is subjected to a combination of loads (Figure 1.1), the method of superposition is employed to determine the edge loading function:

$$\psi_i(y) = \sum_{l=1}^s \psi_i^l(y) \quad (3.38)$$

where s represents the total number of edge loadings applied on edge x_i .

3.3.4 Boundary conditions

The boundary conditions along the edge $x = 0$ and $x = x_n = a$ are:

For simply supported edge: $u = 0, w = 0, N_{xy} = 0, M_x = 0$ (3.39)

clamped edge: $u = 0, v = 0, w = 0, \frac{\partial w}{\partial x} = 0$ (3.40)

free edge: $V_x = \psi, N_x = 0, N_{xy} = 0, M_x = 0$ (3.41)

3.3.5 Continuity conditions

The following continuity conditions are imposed along the common edge, $x = x_i$ between strips I and $I+1$.

$$u_I = u_{(I+1)}, \quad v_I = v_{(I+1)}, \quad w_I = w_{(I+1)}, \quad \frac{\partial w_I}{\partial x} = \frac{\partial w_{(I+1)}}{\partial x} \quad (3.42)$$

and

$$M_{xI} = M_{x(I+1)}, \quad N_{xI} = N_{x(I+1)}, \quad V_{xI} = V_{x(I+1)} + \psi, \quad N_{xyI} = N_{xy(I+1)} \quad (3.43)$$

The solution process is based on dividing a rectangular plate into N -plate strips (Figure 1.1) depending on the number of loading discontinuities. Eight N -simultaneous equations are generated from the boundary and continuity conditions. For the homogeneous solution of strip I ($I = 1, 2, \dots, N$), the constants C_{dmI} ($d = 1, 2, \dots, 8$) are determined for each mode of deflection m ($m = 1, 2, \dots, \infty$). The particular solution is also determined for each strip I and mode m . The deflection for each strip I is derived by summing the homogeneous and particular solutions. The bending and twisting moments, shears and reactions are then determined from the equations for antisymmetric cross-ply or angle-ply respectively.

3.4 Application

The examples presented herein deal with antisymmetric laminated plates, having different loading and boundary conditions. In order to compare the results with ones derived using the classical laminated plate theory (CLPT), all the layers are assumed to be of the same thickness and density.

When comparing the results with ones derived from the finite element program ANSYS (ANSYS, Inc., 2007), an eight-node quadrilateral linear layered structural shell element (Shell99) is used to model the laminated plates. This element has both bending and membrane capabilities, and can accommodate up to 250 layers. It can be subjected to in-plane and normal loads. The element has six degrees of freedom at each node.

3.4.1 Example 1: Effect of ply angle and number of layers on deflection and stresses

Uniformly loaded antisymmetric angle-ply square plates, having a width in the x -direction to plate thickness ratio $a/h = 1000$, are studied in this section. The plates are simply supported along the edges $y = 0$ and $y = b$, and they have varied boundary conditions along the edges $x = 0$ and $x = x_n = a$. The following material properties are considered: $E_1 = 132.38$ GPa (19.2×10^6 psi); $E_2 = 10.76$ GPa (1.56×10^6 psi); $G_{12} = G_{13} = 5.65$ GPa (0.82×10^6 psi); $G_{23} = 3.61$ GPa (0.523×10^6 psi); and $\nu_{12} = 0.24$. The ply orientation angle is varied from $\theta = 0^\circ$ to $\theta = 90^\circ$. Plates with 2 layers and 10 layers are analyzed.

Table 3.3 presents the effect of the ply orientation angle (θ) and number of layers

(n) on the dimensionless deflection $\left[\hat{w} = \left(\frac{100E_2h^3}{a^4q} \right) w \right]$ at the center of plate. The

differences in the results among the ASM, CLPT (Khdeir, 1989), and ANSYS are negligible. Figure 3.1 compares the dimensionless deflection at the center of plate derived from the ASM and ANSYS methods for different boundary conditions, along the x -direction. The differences between the ASM and ANSYS results are negligible for the different ply orientation angles, and the 2-layer and the 10-layer plates. The deflection of the 2-layer plate is larger than deflection of the 10-layer plate, due to the bending-extension coupling effect, *i.e.*, B_{ij} in Equation 2.6 decreases as the number of

layers (n) increases, and it approaches zero as n approaches ∞ . The larger the number of layers in a laminated plate, having a prescribed thickness, the lesser the effect of the bending-extension coupling.

The influence of the boundary conditions at $x = 0$ and $x = a$, on the deflection at the center of the plate, is quite pronounced when the ply orientation angle $\theta = 0^\circ$. This influence diminishes considerably as θ approaches 90° . Consequently, if the interest lies in having stringent limits on the deflection of a laminated plate with two parallel edges, simply supported and various boundary conditions along the other two edges, a ply orientation angle of 90° is the angle of choice, regardless of the number of layers. Figure 3.1 also shows that the bending-extension coupling effect, in the 2 and 10 layer laminates diminishes, as the ply orientation angle θ approaches 0° and 90° ; whereas this effect is quite pronounced as θ approaches 45° .

Table 3.4 presents the effect of ply orientation angle (θ) and number of layers (n), on the dimensionless center stresses $\left[\Sigma_x = \left(\frac{h^2}{a^2 q} \right) \sigma_x, \quad \Sigma_y = \left(\frac{h^2}{a^2 q} \right) \sigma_y, \quad \text{and} \right.$
 $\left. \Sigma_{xy} = \left(\frac{h^2}{a^2 q} \right) \sigma_{xy} \right]$, derived using the ASM and ANSYS. Figures 3.2a and 3.2b present the results for Σ_x and Σ_y . The difference between the results, derived using the two methods, is negligible.

In Figure 3.2a, it is interesting to note that for the 2-layer and 10-layer plates, with a boundary condition combination of free at $x = 0$ and clamped at $x = a$, Σ_x is negative when the ply-orientation angle θ approaches 0° and positive when $\theta > 15^\circ$. This is due to the fact that when $\theta = 0^\circ$, the boundary conditions at $x = 0$ and $x = a$ provide a dominant effect, and a plate strip at the center of the plate, that is parallel to the x -axis, acts like a cantilever beam. As θ increases, the effect from y -direction increases, and Σ_x changes from negative to positive as the “cantilever” effect diminishes. Figure 3.2b shows that the bottom-center stresses Σ_y from the 2-layer plate are always greater than ones from the 10-layer plate for all the boundary condition combinations, due to bending-extension coupling effect.

Table 3.5 shows the convergence study on the dimensionless center deflection

and stresses of 2-layer and 10-layer uniformly loaded square laminated plates (30°/30°/...). Six different boundary conditions along the edges $x = 0$ and $x = a$ are considered. For the plates under consideration in Table 3.5, the deflection converges rapidly and two significant modes ($m = 1, 3$) are sufficient. For the stresses, three significant modes are sufficient.

3.4.2 Example 2: Effect of in-plane orthotropy ratio (E_1/E_2) on deflection and stresses

A uniformly loaded antisymmetric 4-layer angle-ply square plate (45°/45°/45°/45°), having a width in the x -direction to plate thickness ratio $a/h = 1000$, is simply supported along the edges $y = 0$ and $y = b$, and it has varied boundary conditions along the edges $x = 0$ and $x = x_n = a$. The material properties are:

$$\frac{G_{12}}{E_2} = \frac{G_{13}}{E_2} = 0.6, \quad \frac{G_{23}}{E_2} = 0.5, \quad \nu_{12} = 0.25, \quad \text{and the orthotropy ratio } \left(\frac{E_1}{E_2} \right) \text{ is varied from}$$

2 to 40.

Table 3.6 presents the effect of the orthotropy ratio on the dimensionless deflection \hat{w} and stress Σ_x , at the center of the bottom surface of the plate. As expected, the deflections calculated using the ASM and the CLPT (Khdeir, 1989) are identical. The deflections calculated, using the ASM and ANSYS, are very close. The largest difference between the two methods $\left(100 \frac{\hat{w}_{ANSYS} - \hat{w}_{ASM}}{\hat{w}_{ASM}} \right)$ is -4.59%, when

$$\frac{E_1}{E_2} = 40 \text{ and free boundary conditions at } x = 0 \text{ and } x = x_n = a. \text{ For the prescribed}$$

boundary condition and loading, the dimensionless deflection \hat{w} decreases, as the orthotropy ratio $\frac{E_1}{E_2}$ increases.

The in-plane stresses (Σ_x), at the center of the bottom surface of the plate, are listed for the ASM and ANSYS. The maximum difference between the two methods

$$\left(100 \frac{\Sigma_{x,ANSYS} - \Sigma_{x,ASM}}{\Sigma_{x,ASM}} \right) \text{ is } 2.45\%, \text{ when } \frac{E_1}{E_2} = 40 \text{ and all four boundaries are simply}$$

supported.

3.4.3 Example 3: Effect of aspect ratio (a/b)

Uniformly-loaded antisymmetric angle-ply rectangular plates, having a width in the y -direction to plate thickness ratio $b/h = 1000$ and seven different aspect ratios of a/b , are studied in this example. The 2-layer and 10-layer plates are simply supported on all edges and have the following material properties: $E_1 = 132.38$ GPa (19.2×10^6 psi); $E_2 = 10.76$ GPa (1.56×10^6 psi); $G_{12} = G_{13} = 5.65$ GPa (0.82×10^6 psi); $G_{23} = 3.61$ GPa (0.523×10^6 psi); and $\nu_{12} = 0.24$. The ply orientation angle is varied from $\theta = 0^\circ$ to $\theta = 90^\circ$.

Figure 3.3 presents the dimensionless deflections at the center of plate derived, using the ASM and ANSYS. The differences between the results of the two methods are negligible. Figure 3.3 shows that the dimensionless deflection \hat{w} increases as the aspect ratio a/b increases. When the aspect ratio $a/b \geq 1$ and the ply orientation angle, θ , approaches 90° , where the ply length is the shortest and is equal to b , the dimensionless deflection \hat{w} approaches the same value. When the aspect ratio $a/b < 1$, the deflection diminishes considerably, since the shorter edge of length has a dominant effect and the deflections approach the smaller value when $\theta = 0^\circ$.

3.4.4 Example 4: Square plate subjected to a patch load

An antisymmetric 6-layer angle-ply (-15/-45/-75/75/45/15) square plate, with a width to plate thickness ratio $a/h = 1000$, has the following material properties: $E_1 = 132.38$ GPa (19.2×10^6 psi); $E_2 = 10.76$ GPa (1.56×10^6 psi); $G_{12} = G_{13} = 5.65$ GPa (0.82×10^6 psi); $G_{23} = 3.61$ GPa (0.523×10^6 psi); and $\nu_{12} = 0.24$. The plate is subjected to a patch load (Figure 3.4), and it is simply supported along the edges $y = 0$ and $y = b$, clamped at $x = 0$, and simply supported at $x = a$.

The ASM method is used to generate the contour of the dimensionless deflection (\hat{w}) in Figure 3.4. \hat{w} derived from the ASM at the center of the plate, and at the center of patch load are 0.0101 and 0.0155, respectively. The corresponding values from ANSYS are 0.0100 and 0.0157, respectively.

3.4.5 Example 5: Square plate subjected to a point load

An antisymmetric 8-layer angle-ply (-30/-40/-50/-60/60/50/40/30) square plate has a width to plate thickness ratio $a/h = 1000$, and it is subjected to a concentrated load (Figure 3.5). The plate is simply supported along the edges $y = 0$ and $y = b$, clamped at $x = 0$ and free at $x = a$. The material properties are identical to the ones for the plate subjected to the patch load in Example 4.

The ASM method is used to generate the contour of the dimensionless deflection (\hat{w}) in Figure 3.5; \hat{w} derived from the ASM at the center of the plate, at the load point, and the maximum deflection (at $x = 17a/40$ and $y = 3a/10$) are: 1.400, 1.4530, and 1.7410, respectively. The corresponding values from ANSYS are 1.4003, 1.4830, and 1.7412 respectively.

Examples 4 and 5 illustrate the advantage of the ASM over other analytical methods, which are not capable to solve the plate problems in Figures 3.4 and 3.5.

3.5 Summary and Conclusions

An analytical method has been developed for the analysis of antisymmetric laminated composite plates in this chapter. The method is called the analytical strip method (ASM), and it is based on dividing the plate into strips according to loading discontinuities. The plate is limited to two parallel edges being simply supported ($y = 0$ and $y = b$), and varied boundary conditions along the other two edges. In this method, a laminated plate can be subjected to any combination of patch, uniform, line, and concentrated loads. The solution is carried out by deriving an 8th order governing differential equation, and applying the boundary and/or continuity conditions along the edges of each plate strip. The results derived using the ASM are in excellent agreement with ones derived using the finite element program ANSYS, and, where applicable, the results presented in the literature for the classical laminated plate theory. The primary advantage of the ASM over other single series analytic solutions lies in its applicability to different loading and boundary conditions, as illustrated in Examples 4 and 5.

Table 3.1. Particular solution $\Phi_{PI}(x,y)$ for strip I

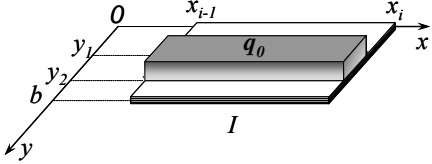
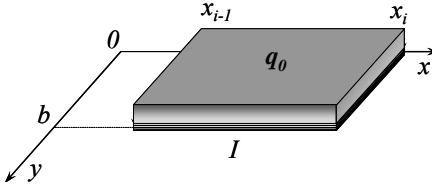
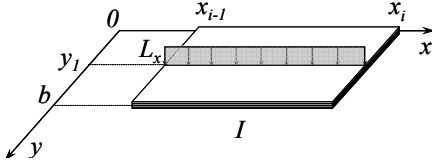
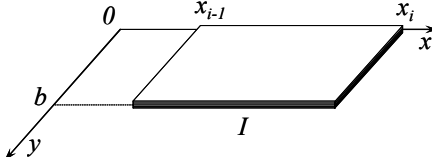
Load Case	$\Phi_{PI}(x,y)$
<p>Case 1 - Partial uniform load q_0</p> 	$\Phi_{PI}(x,y) = \frac{2q_0 b^8}{A_9 \pi^9} \sum_m \frac{1}{m^9} \left[\cos\left(\frac{m\pi}{b} y_1\right) - \cos\left(\frac{m\pi}{b} y_2\right) \right] \sin\left(\frac{m\pi}{b} y\right)$
<p>Case 2 - Uniform load q_0</p> 	$\Phi_{PI}(x,y) = \frac{4q_0 b^8}{A_9 \pi^9} \sum_{m=1,3}^{\infty} \frac{1}{m^9} \sin\left(\frac{m\pi}{b} y\right)$
<p>Case 3 - Line load L_x</p> 	$\Phi_{PI}(x,y) = \frac{2L_x b^7}{A_9 \pi^8} \sum_m \frac{1}{m^8} \sin\left(\frac{m\pi}{b} y_1\right) \cdot \sin\left(\frac{m\pi}{b} y\right)$
<p>Case 4 - Zero load</p> 	$\Phi_{PI}(x,y) = 0$

Table 3.2. Edge loading function $\psi_i(y)$ at $x = x_i$

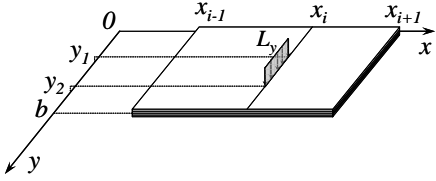
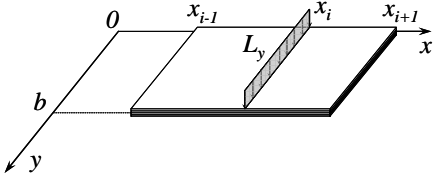
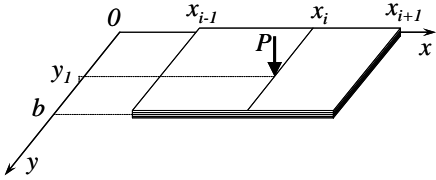
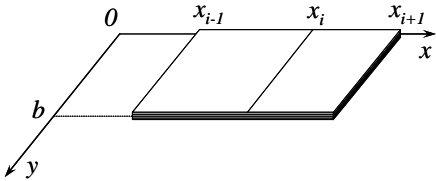
Load Case	$\psi_i(y)$
<p>Case 1 – Partial line load L_y</p> 	$\psi_i(y) = \frac{2L_y}{\pi} \sum_m \frac{1}{m} \left[\cos\left(\frac{m\pi}{b} y_1\right) - \cos\left(\frac{m\pi}{b} y_2\right) \right] \sin\left(\frac{m\pi}{b} y\right)$
<p>Case 2 – Line load L_y in y direction</p> 	$\psi_i(y) = \frac{4L_y}{\pi} \sum_m \frac{1}{m} \sin\left(\frac{m\pi}{b} y\right)$
<p>Case 3. – Concentrated load P</p> 	$\psi_i(y) = \frac{2P}{b} \sum_m \sin\left(\frac{m\pi}{b} y_1\right) \cdot \sin\left(\frac{m\pi}{b} y\right)$
<p>Case 4 – Zero load</p> 	$\psi_i(y) = 0$

Table 3.3. Effect of ply angle (θ°) and number of layers (n) on the center of an antisymmetric square laminated plate (θ° - θ° / θ° - θ° /...) $a/h=1000$, $E_1=132.38$ GPa, $E_2=10.76$ GPa, $G_{12}=G_{13}=5.65$ GPa, $G_{23}=3.61$ GPa, $\nu_{12}=0.24$

θ°	n	Method	\hat{w}^1 at center of plate					
			S at $x=0$	S at $x=0$	C at $x=0$	F at $x=0$	F at $x=0$	F at $x=0$
			S at $x=a^2$	C at $x=a^2$	C at $x=a^2$	F at $x=a^2$	S at $x=a^2$	C at $x=a^2$
0°	2	CLPT ³	N/A ⁶	N/A	N/A	N/A	N/A	N/A
		ASM ⁴	1.1953	0.5264	0.2630	15.5133	7.4793	2.5973
		ANSYS ⁵	1.1960	0.5272	0.2628	15.5555	7.4873	2.6026
	10	CLPT	N/A	N/A	N/A	N/A	N/A	N/A
		ASM	1.1953	0.5264	0.2630	15.5133	7.4793	2.5973
		ANSYS	1.1960	0.5272	0.2628	15.5555	7.4873	2.6026
30°	2	CLPT	1.6184	1.0218	0.6657	12.3713	4.7491	2.8627
		ASM	1.6190	1.0222	0.6660	12.3756	4.7505	2.8636
		ANSYS	1.6220	1.0231	0.6662	12.6235	4.7280	2.8680
	10	CLPT	0.8187	0.5188	0.3364	10.3035	2.7365	1.6391
		ASM	0.8191	0.5190	0.3366	10.3084	2.7376	1.6398
		ANSYS	0.8225	0.5199	0.3369	10.6311	2.7500	1.6440
45°	2	CLPT	1.5807	1.1675	0.8628	7.8765	3.5696	2.6432
		ASM	1.5810	1.1677	0.8634	7.8805	3.5707	2.6445
		ANSYS	1.5870	1.1709	0.8641	8.0484	3.4540	2.6480
	10	CLPT	0.7391	0.5590	0.4229	4.7291	1.8069	1.3554
		ASM	0.7398	0.5590	0.4232	4.7308	1.8074	1.3550
		ANSYS	0.7435	0.5608	0.4238	4.8106	1.8150	1.3600
60°	2	CLPT	1.6185	1.2996	1.0352	4.3732	2.6983	2.2162
		ASM	1.6203	1.3011	1.0357	4.3758	2.6993	2.2173
		ANSYS	1.6220	1.3035	1.0370	4.4457	2.6010	2.2190
	10	CLPT	0.8187	0.6898	0.5786	2.2621	1.3936	1.1913
		ASM	0.8191	0.6902	0.5782	2.2632	1.3943	1.1919
		ANSYS	0.8225	0.6915	0.5799	2.2540	1.3970	1.1940
90°	2	CLPT	N/A	N/A	N/A	N/A	N/A	N/A
		ASM	1.1949	1.0723	0.9524	1.2497	1.2227	1.1082
		ANSYS	1.1960	1.0730	0.9529	1.2625	1.2216	1.1077
	10	CLPT	N/A	N/A	N/A	N/A	N/A	N/A
		ASM	1.1949	1.0723	0.9524	1.2497	1.2227	1.1082
		ANSYS	1.1960	1.0730	0.9529	1.2625	1.2216	1.1077

$$^1 \hat{w} = \left(\frac{100 E_2 h^3}{a^4 q} \right) w$$

² C = Clamped, F = Free, S = Simply supported

³ CLPT - Classical Laminated Plate Theory by Khdeir (Khdeir, 1989)

⁴ ASM - Analytical Strip Method (present method)

⁵ ANSYS - Finite Element Analysis Program (ANSYS Inc., 2007)

⁶ N/A = Results are not available

Table 3.4. Effect of ply angle (θ°) and number of layers (n) on the center stresses $\Sigma(a/2, a/2) = (h^2/a^2 q)\sigma$ at bottom surface of a square plate (θ° - θ° / θ° - θ° ...) $a/h = 1000$, $E_1 = 132.38$ GPa, $E_2 = 10.76$ GPa, $G_{12} = G_{13} = 5.65$ GPa, $G_{23} = 3.61$ GPa, $\nu_{12} = 0.24$

θ°	n	Method	S at $x = 0$ and S at $x = a^1$			S at $x = 0$ and C at $x = a^1$			C at $x = 0$ and C at $x = a^1$			F at $x = 0$ and F at $x = a^1$			F at $x = 0$ and S at $x = a^1$			F at $x = 0$ and C at $x = a^1$		
			Σ_x	Σ_y	Σ_{xy}	Σ_x	Σ_y	Σ_{xy}	Σ_x	Σ_y	Σ_{xy}	Σ_x	Σ_y	Σ_{xy}	Σ_x	Σ_y	Σ_{xy}	Σ_x	Σ_y	Σ_{xy}
0°	2	ASM ²	0.7182	0.0560	0.0000	0.3939	0.0195	0.0000	0.2620	0.0029	0.0000	0.0310	0.7459	0.0000	0.4186	0.3586	0.0000	-0.2140	0.1086	0.0000
		ANSYS ³	0.7184	0.0559	0.0000	0.3943	0.0198	0.0000	0.2657	0.0029	0.0000	0.0314	0.7457	0.0000	0.4192	0.3582	0.0000	-0.2133	0.1082	0.0000
		% Diff. ⁴	0.027	-0.302	0.106	0.099	1.711	-0.044	1.385	-0.158	1.171	1.274	-0.021	1.325	0.146	-0.105	0.232	-0.336	-0.374	-0.217
	10	ASM	0.7182	0.0560	0.0000	0.3939	0.0195	0.0000	0.2620	0.0029	0.0000	0.0310	0.7459	0.0000	0.4186	0.3586	0.0000	-0.2140	0.1086	0.0000
		ANSYS	0.7184	0.0559	0.0000	0.3943	0.0198	0.0000	0.2657	0.0029	0.0000	0.0314	0.7457	0.0000	0.4192	0.3582	0.0000	-0.2133	0.1082	0.0000
		% Diff.	0.027	-0.302	0.018	0.099	1.711	0.019	1.385	-0.158	1.406	1.274	-0.021	1.185	0.146	-0.105	0.204	-0.336	-0.374	-0.491
30°	2	ASM	0.5049	0.2193	0.2116	0.3657	0.1469	0.1479	0.2868	0.1056	0.1125	0.5717	0.8270	0.3015	0.4862	0.3795	0.2039	0.2427	0.2079	0.0960
		ANSYS	0.5058	0.2193	0.2121	0.3661	0.1467	0.1481	0.2868	0.1052	0.1125	0.5780	0.8278	0.3042	0.4878	0.3809	0.2048	0.2441	0.2088	0.0966
		% Diff.	0.186	0.022	0.232	0.118	-0.169	0.145	0.006	-0.354	-0.025	1.094	0.098	0.890	0.325	0.360	0.458	0.589	0.456	0.640
	10	ASM	0.3388	0.1396	0.1659	0.2530	0.0978	0.1225	0.2014	0.0727	0.0965	0.7003	0.7734	0.4222	0.4025	0.2627	0.2112	0.2178	0.1470	0.1144
		ANSYS	0.3397	0.1397	0.1663	0.2533	0.0976	0.1226	0.2013	0.0724	0.0964	0.6989	0.7740	0.4219	0.4037	0.2638	0.2119	0.2174	0.1470	0.1143
		% Diff.	0.270	0.066	0.271	0.109	-0.177	0.094	-0.036	-0.410	-0.091	-0.205	0.075	-0.063	0.288	0.428	0.324	-0.179	0.025	-0.128
45°	2	ASM	0.3182	0.3190	0.2081	0.2677	0.2530	0.1697	0.2305	0.2044	0.1415	0.5635	0.9915	0.4994	0.3946	0.5298	0.2988	0.3065	0.3981	0.2279
		ANSYS	0.3186	0.3186	0.2085	0.2674	0.2518	0.1695	0.2298	0.2028	0.1408	0.5668	0.9934	0.5027	0.3944	0.5295	0.2989	0.3056	0.3968	0.2273
		% Diff.	0.118	-0.124	0.183	-0.106	-0.459	-0.126	-0.295	-0.796	-0.473	0.578	0.190	0.666	-0.049	-0.052	0.026	-0.302	-0.331	-0.272
	10	ASM	0.2104	0.2108	0.1678	0.1796	0.1728	0.1403	0.1563	0.1442	0.1196	0.5277	0.7888	0.5237	0.2915	0.3601	0.2593	0.2282	0.2746	0.2001
		ANSYS	0.2104	0.2104	0.1676	0.1791	0.1719	0.1398	0.1556	0.1431	0.1185	0.5316	0.7951	0.5280	0.2956	0.3659	0.2634	0.2316	0.2795	0.2034
		% Diff.	0.002	-0.193	-0.104	-0.252	-0.526	-0.379	-0.439	-0.750	-0.958	0.733	0.805	0.823	1.392	1.615	1.562	1.496	1.789	1.642
60°	2	ASM	0.2171	0.4983	0.2091	0.1910	0.4056	0.1696	0.1717	0.3375	0.1402	0.2575	1.0005	0.3638	0.2342	0.7024	0.2754	0.2026	0.5789	0.2268
		ANSYS	0.2193	0.5058	0.2121	0.1931	0.4129	0.1725	0.1716	0.3362	0.1399	0.2591	1.0070	0.3662	0.2362	0.7099	0.2783	0.2045	0.5861	0.2295
		% Diff.	0.999	1.512	1.419	1.106	1.800	1.693	-0.085	-0.387	-0.221	0.608	0.653	0.667	0.845	1.065	1.056	0.940	1.244	1.193
	10	ASM	0.1379	0.3340	0.1636	0.1264	0.2908	0.1433	0.1165	0.2537	0.1258	0.2106	0.7377	0.3429	0.1672	0.4957	0.2357	0.1508	0.4307	0.2056
		ANSYS	0.1397	0.3397	0.1663	0.1281	0.2961	0.1458	0.1181	0.2586	0.1282	0.2119	0.7427	0.3452	0.1689	0.5015	0.2384	0.1523	0.4359	0.2080
		% Diff.	1.270	1.709	1.668	1.324	1.807	1.750	1.371	1.942	1.882	0.614	0.680	0.677	1.008	1.175	1.164	0.996	1.219	1.192
90°	2	ASM	0.0556	0.7134	0.0000	0.0637	0.6409	0.0000	0.0716	0.5700	0.0000	0.0138	0.7367	0.0000	0.0344	0.7252	0.0000	0.0426	0.6830	0.0000
		ANSYS	0.0559	0.7184	0.0000	0.0640	0.6457	0.0000	0.0718	0.5747	0.0000	0.0140	0.7418	0.0000	0.0347	0.7302	0.0000	0.0423	0.6792	0.0000
		% Diff.	0.517	0.689	0.651	0.458	0.742	0.300	0.401	0.819	-0.925	1.336	0.692	-1.463	0.840	0.688	0.089	-0.600	-0.565	0.179
	10	ASM	0.0556	0.7134	0.0000	0.0637	0.6409	0.0000	0.0716	0.5700	0.0000	0.0138	0.7367	0.0000	0.0344	0.7252	0.0000	0.0426	0.6830	0.0000
		ANSYS	0.0559	0.7184	0.0000	0.0640	0.6457	0.0000	0.0718	0.5747	0.0000	0.0140	0.7418	0.0000	0.0347	0.7302	0.0000	0.0423	0.6792	0.0000
		% Diff.	0.517	0.689	0.646	0.458	0.742	0.632	0.401	0.819	0.802	1.336	0.692	-0.312	0.840	0.688	-1.195	-0.600	-0.565	-0.399

¹ C = Clamped, F = Free, S = Simply supported

² ASM - Analytical Strip Method

³ ANSYS - Finite Element Analysis program (ANSYS Inc., 2007)

⁴ % Diff. = percent difference: $\left(100 \frac{\Sigma_{ANSYS} - \Sigma_{ASM}}{\Sigma_{ASM}} \right)$

Table 3.5. Convergence study for ASM on the center deflection and stresses of an antisymmetric angle-ply square plates (30°/30°/30°/30°/...) $a/h = 1000$, $E_1 = 132.38$ GPa, $E_2 = 10.76$ GPa, $G_{12} = G_{13} = 5.65$ GPa, $G_{23} = 3.61$ GPa, $\nu_{12} = 0.24$

θ°	n^2	m^3	S at $x = 0$ and S at $x = a^1$				S at $x = 0$ and C at $x = a^1$				C at $x = 0$ and C at $x = a^1$			
			\hat{w}^4	Σ_x^4	Σ_y^4	Σ_{xy}^4	\hat{w}	Σ_x	Σ_y	Σ_{xy}	\hat{w}	Σ_x	Σ_y	Σ_{xy}
30°	2	1	1.6525	0.5257	0.2392	0.2206	1.0535	0.3869	0.1660	0.1572	0.6952	0.3086	0.1238	0.1222
		3	-0.0366	-0.0256	-0.0251	-0.0112	-0.0343	-0.0260	-0.0242	-0.0115	-0.0322	-0.0265	-0.0233	-0.0118
		5	0.0035	0.0059	0.0065	0.0028	0.0035	0.0059	0.0065	0.0028	0.0035	0.0059	0.0064	0.0028
		7	-0.0007	-0.0023	-0.0025	-0.0011	-0.0007	-0.0023	-0.0025	-0.0011	-0.0007	-0.0022	-0.0025	-0.0011
		9	0.0002	0.0011	0.0012	0.0005	0.0002	0.0011	0.0012	0.0005	0.0002	0.0011	0.0012	0.0005
	Sum ⁵	1.6190	0.5049	0.2193	0.2116	1.0222	0.3657	0.1469	0.1479	0.6660	0.2868	0.1056	0.1125	
	10	1	0.8395	0.3595	0.1544	0.1769	0.5378	0.2730	0.1116	0.1331	0.3539	0.2206	0.0856	0.1067
		3	-0.0225	-0.0260	-0.0191	-0.0140	-0.0209	-0.0252	-0.0180	-0.0135	-0.0193	-0.0245	-0.0170	-0.0131
		5	0.0024	0.0066	0.0054	0.0037	0.0024	0.0066	0.0053	0.0036	0.0024	0.0065	0.0052	0.0036
		7	-0.0005	-0.0025	-0.0021	-0.0014	-0.0005	-0.0025	-0.0021	-0.0014	-0.0005	-0.0025	-0.0021	-0.0014
9		0.0001	0.0012	0.0010	0.0007	0.0001	0.0012	0.0010	0.0007	0.0002	0.0012	0.0010	0.0007	
Sum	0.8191	0.3388	0.1396	0.1659	0.5190	0.2530	0.0978	0.1225	0.3366	0.2014	0.0727	0.0965		
30°	2	1	12.4209	0.5972	0.8546	0.3139	4.7898	0.5097	0.4036	0.2147	2.9006	0.2676	0.2313	0.1075
		3	-0.0485	-0.0295	-0.0324	-0.0143	-0.0424	-0.0275	-0.0287	-0.0127	-0.0400	-0.0278	-0.0276	-0.0130
		5	0.0038	0.0063	0.0070	0.0030	0.0037	0.0061	0.0067	0.0029	0.0036	0.0061	0.0067	0.0029
		7	-0.0007	-0.0023	-0.0025	-0.0011	-0.0007	-0.0023	-0.0025	-0.0011	-0.0007	-0.0023	-0.0025	-0.0011
		9	0.0002	0.0011	0.0012	0.0005	0.0002	0.0011	0.0012	0.0005	0.0002	0.0011	0.0012	0.0005
	Sum	12.3756	0.5717	0.8270	0.3015	4.7505	0.4862	0.3795	0.2039	2.8636	0.2427	0.2079	0.0960	
	10	1	10.3429	0.7288	0.7976	0.4381	2.7646	0.4272	0.2822	0.2248	1.6649	0.2414	0.1651	0.1274
		3	-0.0369	-0.0336	-0.0287	-0.0189	-0.0292	-0.0296	-0.0236	-0.0163	-0.0273	-0.0286	-0.0223	-0.0157
		5	0.0028	0.0072	0.0061	0.0040	0.0026	0.0069	0.0057	0.0038	0.0026	0.0068	0.0057	0.0038
		7	-0.0005	-0.0026	-0.0022	-0.0015	-0.0005	-0.0026	-0.0022	-0.0014	-0.0005	-0.0026	-0.0022	-0.0014
9		0.0001	0.0012	0.0010	0.0007	0.0002	0.0012	0.0010	0.0007	0.0001	0.0012	0.0010	0.0007	
Sum	10.3084	0.7003	0.7734	0.4222	2.7376	0.4025	0.2627	0.2112	1.6398	0.2178	0.1470	0.1144		

¹ C = Clamped; F = Free; S = Simply supported

² n = number of layers

³ m = mode of deflection

$$^4 \hat{w} = \left(\frac{100E_2 h^3}{a^4 q} \right) w ; \Sigma = \left(\frac{h^2}{a^2 q} \right) \sigma$$

$$^5 \text{Sum} = \sum_{m=1,3}^9$$

Table 3.6. Effect of in-plane orthotropy ratio, E_1/E_2 on the dimensionless center deflection, \hat{w}^1 , and stress, Σ_x^2 , of a four layer square laminated plate (45°/-45°/45°/-45°) $a/h = 1000$, $E_1/E_2 = 2, 10, 20, 30$ and 40 , $G_{12}/E_2 = G_{13}/E_2 = 0.6$, $G_{23}/E_2 = 0.5$, $\nu_{12} = 0.25$

$\frac{E_1}{E_2}$	Method	S at $x=0$		S at $x=0$		C at $x=0$		F at $x=0$		F at $x=0$		F at $x=0$	
		S at $x=a^3$		C at $x=a^3$		C at $x=a^3$		F at $x=a^3$		S at $x=a^3$		C at $x=a^3$	
		\hat{w}	Σ_x	\hat{w}	Σ_x	\hat{w}	Σ_x	\hat{w}	Σ_x	\hat{w}	Σ_x	\hat{w}	Σ_x
2	CLPT ⁴	3.214	N/A ⁷	2.214	N/A	1.531	N/A	10.47	N/A	6.234	N/A	4.446	N/A
	ASM ⁵	3.214	0.257	2.214	0.215	1.531	0.186	10.47	0.106	6.234	0.195	4.446	0.144
	ANSYS ⁶	3.209	0.257	2.212	0.215	1.529	0.186	10.40	0.106	6.207	0.195	4.430	0.144
10	CLPT	1.000	N/A	0.747	N/A	0.558	N/A	5.571	N/A	2.345	N/A	1.747	N/A
	ASM	1.000	0.216	0.747	0.184	0.558	0.160	5.571	0.415	2.345	0.274	1.748	0.215
	ANSYS	0.994	0.215	0.741	0.184	0.553	0.160	5.347	0.416	2.299	0.274	1.710	0.214
20	CLPT	0.542	N/A	0.412	N/A	0.313	N/A	3.657	N/A	1.343	N/A	1.010	N/A
	ASM	0.542	0.202	0.412	0.176	0.313	0.153	3.658	0.569	1.343	0.298	1.011	0.235
	ANSYS	0.541	0.206	0.409	0.176	0.310	0.153	3.505	0.571	1.320	0.299	0.986	0.234
30	CLPT	0.372	N/A	0.285	N/A	0.218	N/A	2.738	N/A	0.943	N/A	0.712	N/A
	ASM	0.372	0.198	0.285	0.173	0.218	0.151	2.738	0.647	0.943	0.309	0.712	0.243
	ANSYS	0.372	0.202	0.283	0.173	0.216	0.150	2.621	0.651	0.931	0.309	0.695	0.243
40	CLPT	N/A	N/A	N/A	N/A	N/A	N/A	N/A	N/A	N/A	N/A	N/A	N/A
	ASM	0.283	0.196	0.218	0.172	0.167	0.150	2.191	0.696	0.727	0.315	0.550	0.248
	ANSYS	0.284	0.201	0.217	0.172	0.166	0.149	2.090	0.700	0.720	0.315	0.537	0.248

$$^1 \hat{w} = \left(\frac{100 E_2 h^3}{a^4 q} \right) w$$

$$^2 \Sigma_x = \left(\frac{h^2}{a^2 q} \right) \sigma_x$$

³ C = Clamped, F = Free, S = Simply supported

⁴ CLPT - Classical Laminated Plate Theory by Khdeir (Khdeir, 1989)

⁵ ASM - Analytical Strip Method (present method)

⁶ ANSYS - Finite Element Analysis program (ANSYS Inc., 2007)

⁷ N/A = Result is not available

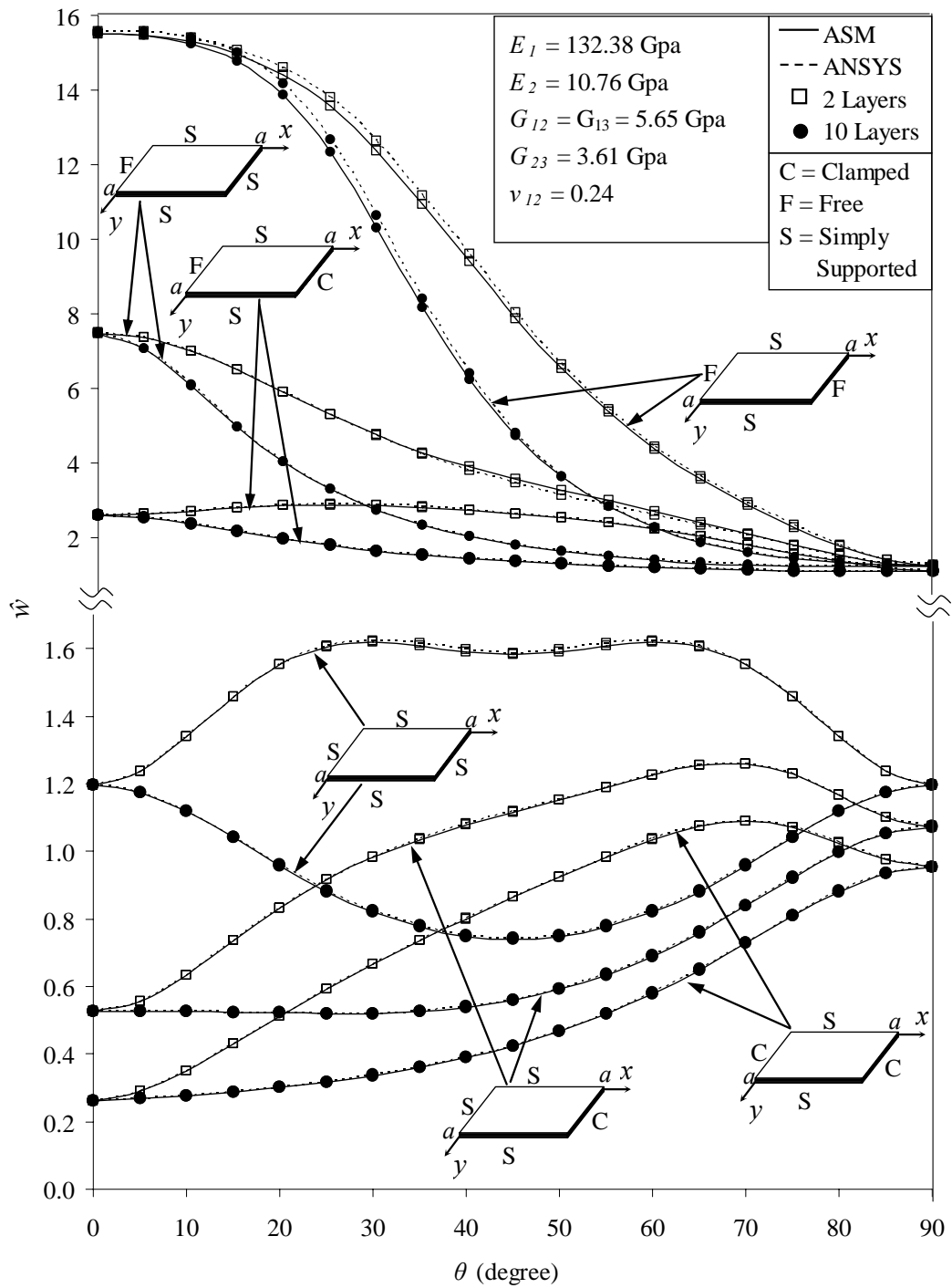


Figure 3.1. Deflection at the center of a uniformly loaded antisymmetric angle-ply square plate, $\hat{w}\left(\frac{a}{2}, \frac{a}{2}\right) = \left(\frac{100E_2h^3}{a^4q}\right)w$, versus ply orientation angle, θ , for different boundary conditions

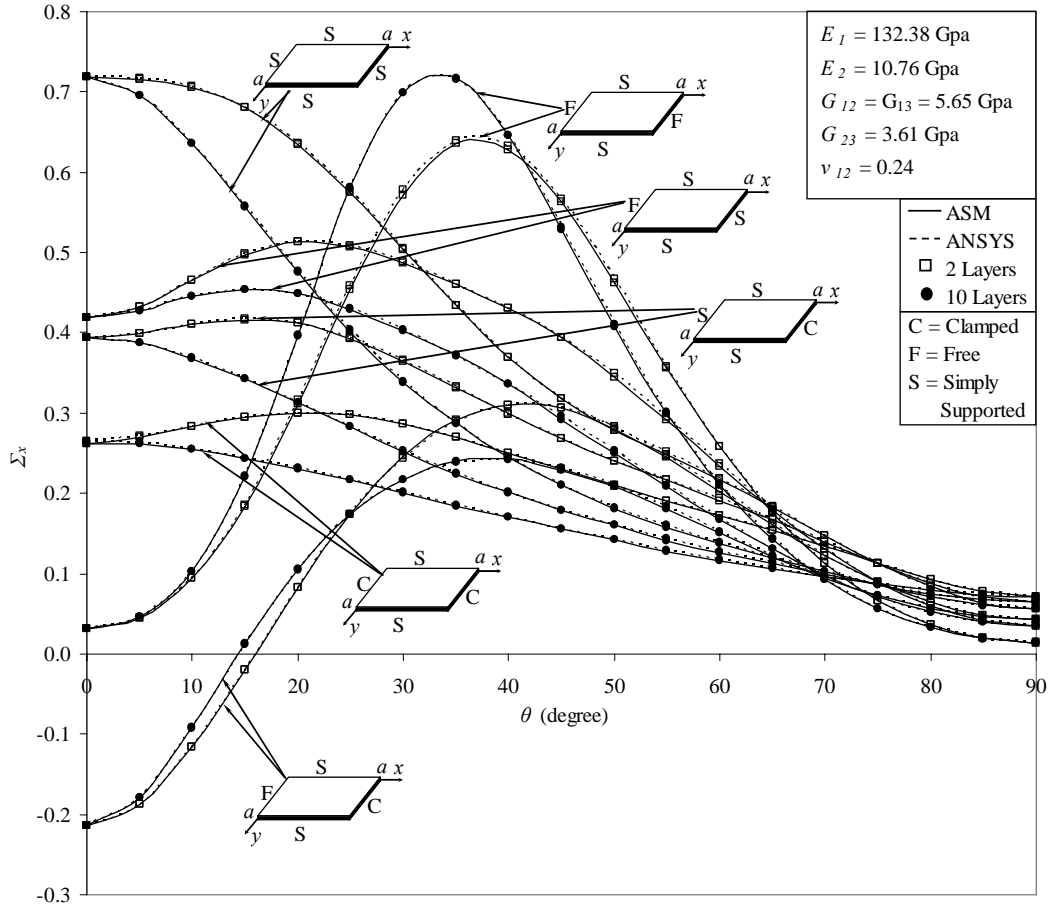


Figure 3.2a. Stress in the x -direction at the center of bottom surface on a uniformly loaded antisymmetric angle-ply square plate,

$$\Sigma_x \left(\frac{a}{2}, \frac{a}{2} \right) = \left(\frac{h^2}{a^2 q} \right) \sigma_x \text{ versus ply orientation angle, } \theta$$

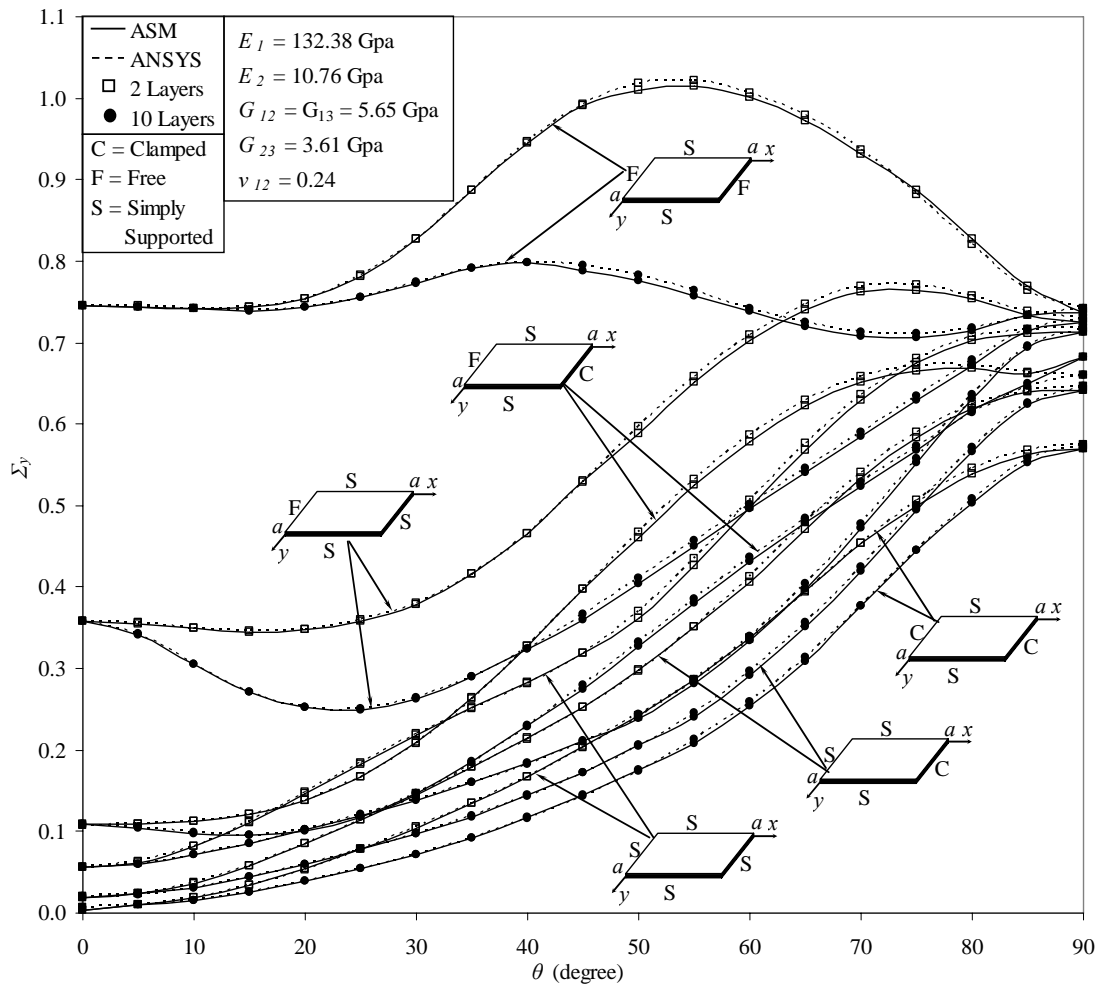


Figure 3.2b. Stress in the y-direction at the center of bottom surface on a uniformly loaded antisymmetric angle-ply square plate, $\Sigma_y\left(\frac{a}{2}, \frac{a}{2}\right) = \left(\frac{h^2}{a^2 q}\right)\sigma_y$ versus ply orientation angle, θ

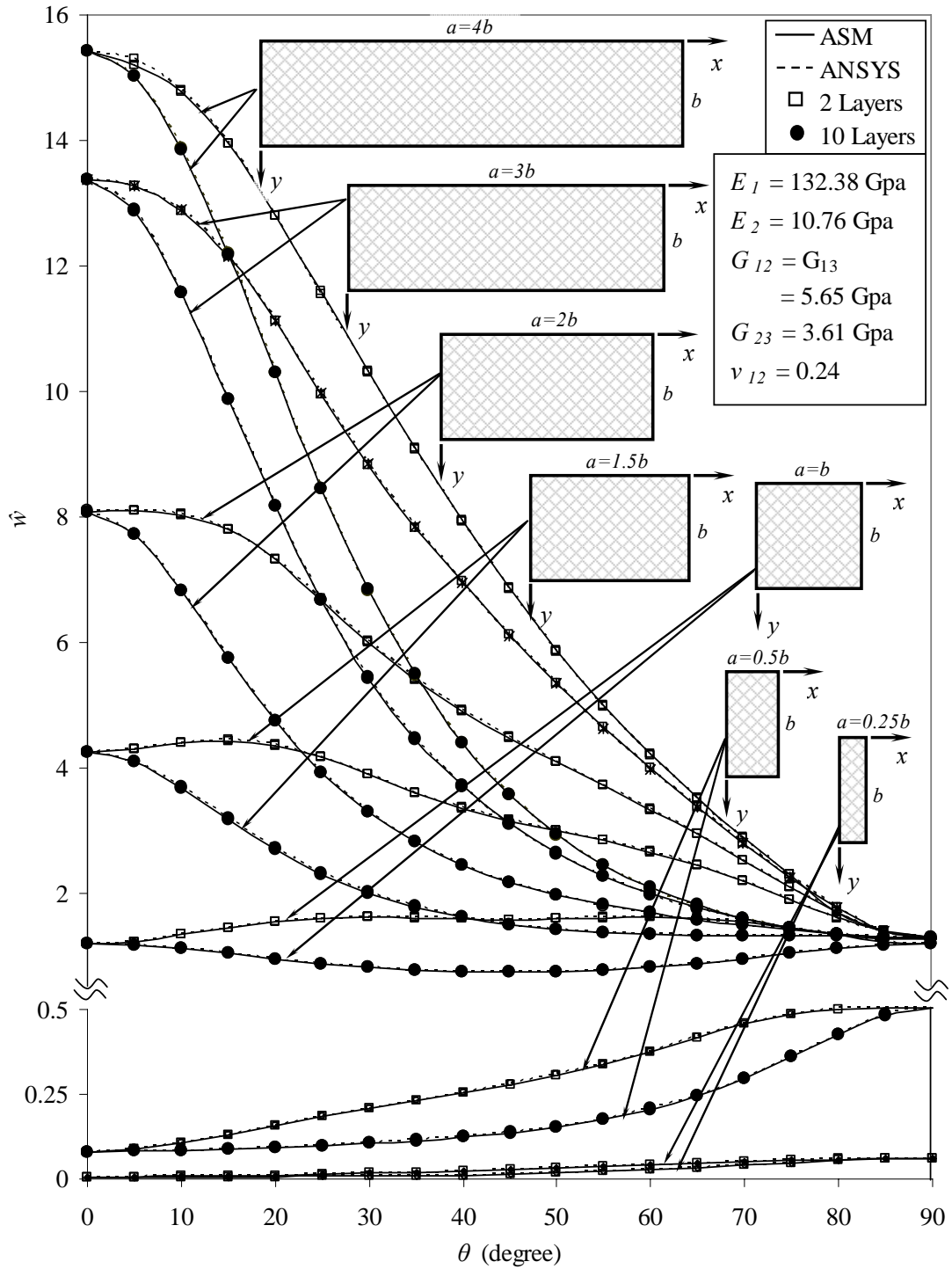


Figure 3.3. Deflection at the center of a uniformly loaded antisymmetric angle-ply rectangular plate with all sides simply supported, $\hat{w}\left(\frac{a}{2}, \frac{b}{2}\right) = \left(\frac{100E_2h^3}{b^4q}\right)w$ versus ply orientation angle, θ

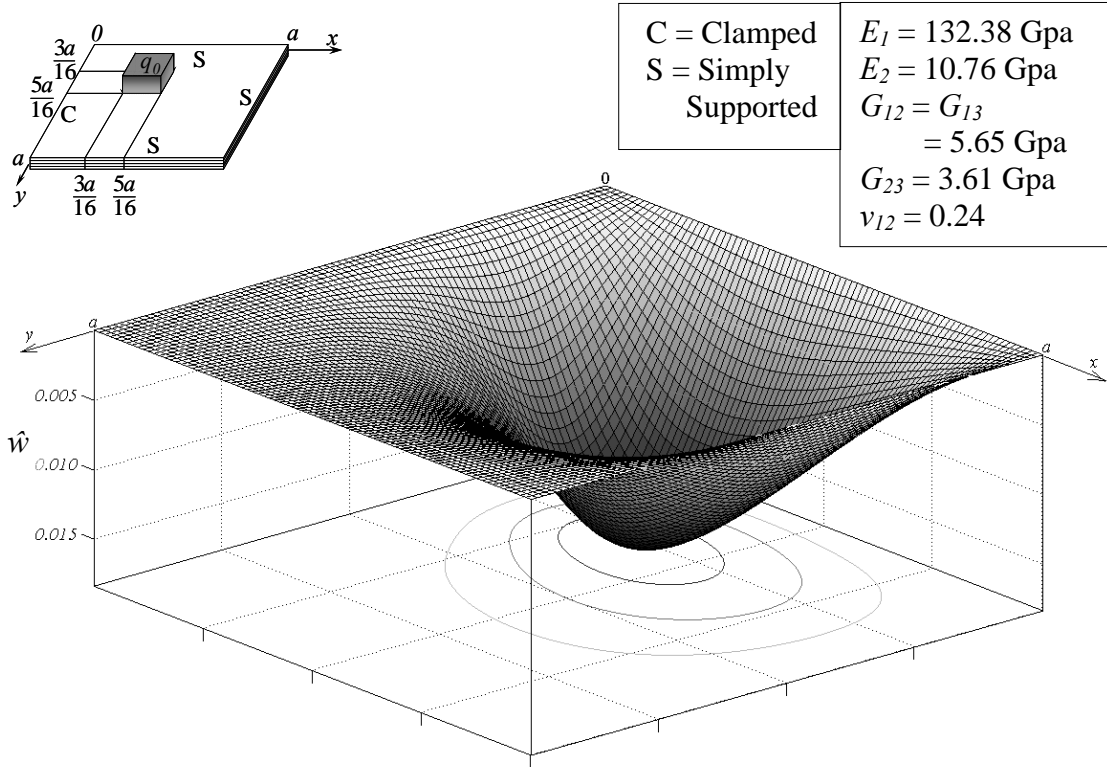


Fig. 3.4. Contour of the dimensionless deflection, $\hat{w} = \left(\frac{100E_2h^3}{a^4q} \right) w$ for an antisymmetric angle-ply 6-layer ($-15^\circ/-45^\circ/-75^\circ/75^\circ/45^\circ/15^\circ$) square laminated plate subjected to a patch load

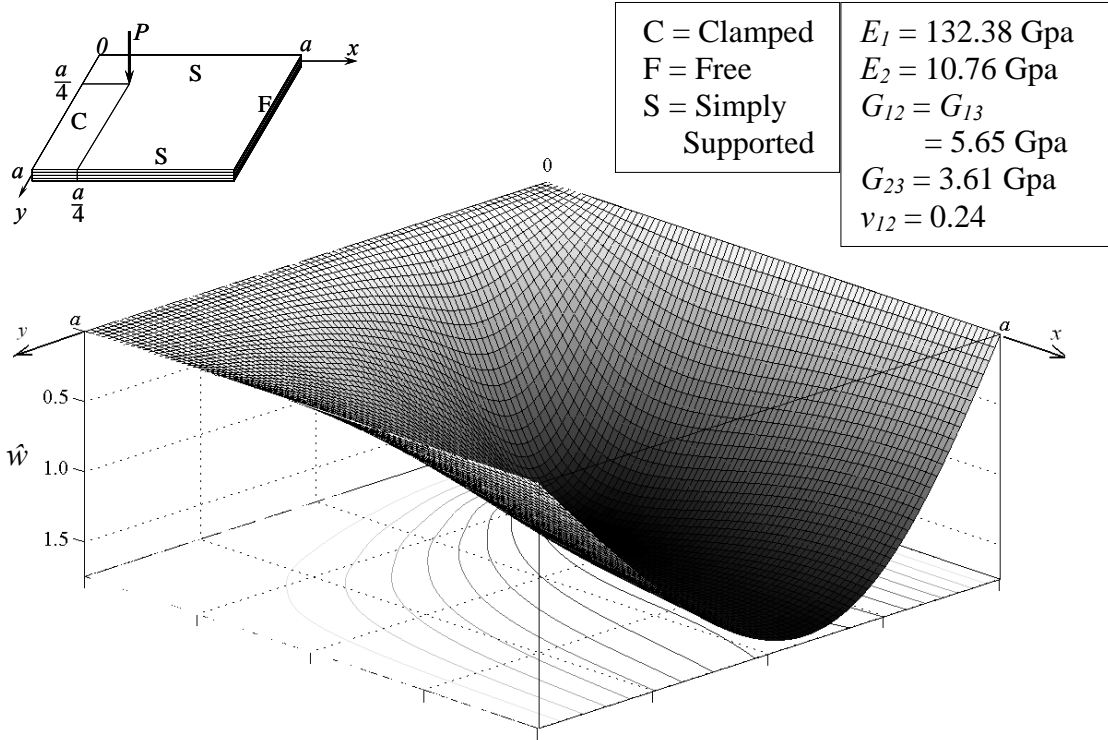


Fig. 3.5. Contour of the dimensionless deflection, $\hat{w} = \left(\frac{100E_2h^3}{a^2P} \right) w$ for an antisymmetric angle-ply 8-layer (-30°/-40°/-50°/-60°/60°/50°/40°/30°) square laminated plate subjected to a concentrated load, P

CHAPTER 4

BENDING-EXTENSION COUPLING OF STIFFENED AND CONTINUOUS ANTISYMMETRIC LAMINATED PLATES

4.1 Introduction

Stiffened plates are widely used in all kinds of circumstances, such as bridges, ship hulls or decks, and aircraft structures. An economical design is achieved through a proper selection of the plate and the stiffener sizes. Numerous studies have analyzed stiffened plates, and earlier researchers simulated stiffened plates with grillage models (Yettram and Hussain, 1965) or orthotropic models (Schade, 1940). A more accurate model is achieved by representing the plate and stiffeners separately, and maintaining compatibility between them. Different analytical methods and numerical techniques, such as the Rayleigh-Ritz method (Liew, Lam, and Chow, 1990; Liew, Xiang, Kitipornchai, and Meek, 1995; Xiang, Liew, and Kitipornchai, 1996; Liew and Lam, 1990), the finite element method (Deb and Booton, 1988; Biswal and Ghosh, 1994; Sadek and Tawfik, 2000), and the constraint method based on finite elements (Rossow and Ibrahimkhail, 1978) have been used to solve the problem. In this chapter, analytical solutions for bending-extension coupling of stiffened and continuous antisymmetric laminated plates (Figure 4.1) are obtained by using ASM.

4.2 Governing Differential Equation

For a stiffened and continuous antisymmetric laminated plate, subjected to a transverse load $q(x, y)$, the governing differential equation is the same as one shown in Equation 2.13:

$$A_1 \frac{\partial^8 \Phi}{\partial x^8} + A_3 \frac{\partial^8 \Phi}{\partial x^6 \partial y^2} + A_5 \frac{\partial^8 \Phi}{\partial x^4 \partial y^4} + A_7 \frac{\partial^8 \Phi}{\partial x^2 \partial y^6} + A_9 \frac{\partial^8 \Phi}{\partial y^8} = q(x, y) \quad (2.13)$$

The major difference between this kind of plate and a simple plate discussed in previous chapter is that beam elements are involved in stiffened and continuous plate. Solving a plate problem, with beams supported on edges or interior plate, is a very challenging topic for analytical methods. An endeavor will be made to solve this problem by the

analytical strip method, in this chapter in conjunction with beam elements as boundary and continuity conditions.

4.3 Beam Elements

For the J^{th} beam ($J = 1, 2, \dots, S$), located along the line $x = x_J$ ($J = 1, 2, \dots, S$) (Figure 4.1), the axial rotation is assumed to be fully restrained at the supports ($y = 0$ and $y = b$). Considering the bending, torsional and warping stresses, the following pair of differential equations can be derived from the equilibrium of the beam element (Salamoun and Harik, 1985; Harik and Salamoun, 1988):

$$Q_{bJ} = D_E \left(bK1_J \frac{d^4 W_{bJ}}{dy^4} \right) \quad (4.1)$$

$$T_{bJ} = D_E \left(-bK2_J \frac{d^2 \phi_{bJ}}{dy^2} + b^3 K3_J \frac{d^4 \phi_{bJ}}{dy^4} \right) \quad (4.2)$$

in which,

$$K1_J = \frac{E_{bJ} I_{bJ}}{D_E b}, \quad K2_J = \frac{G_{bJ} J_{bJ}}{D_E b}, \quad K3_J = \frac{E_{bJ} C_{wJ}}{D_E b^3} \quad (4.3)$$

$$D_E = \frac{E_x h^3}{12(1 - \nu_{12}\nu_{21})} \quad (4.4)$$

Q_{bJ} and T_{bJ} are lateral load and twisting moment per unit length, applied to the beam element at the line $x = x_J$ ($J = 1, 2, \dots, S$); D_E is equivalent flexural rigidity of orthotropic plate; W_{bJ} and ϕ_{bJ} are deflection and angle of twist of the beam; $K1$, $K2$, and $K3$ are dimensionless constants chosen for convenience; $E_b I_b$ = flexural rigidity of the beam; $G_b J_b$ = torsional rigidity of the beam; and, $E_b C_w$ = warping rigidity of the beam.

Because of this beam element, beam support conditions are added to boundary and continuity conditions in Equations (3.39) through (3.43). The boundary conditions at beam support location are:

$$w = W_b, \quad -\frac{\partial w}{\partial x} = \phi_b, \quad R_x = Q_b, \quad M_x = T_b \quad (4.5)$$

The continuity conditions at beam support location along the common edge, $x = x_i$ between strips I and $I+1$, are:

$$u_I = u_{(I+1)}, \quad v_I = v_{(I+1)}, \quad w_I = w_{(I+1)} = w_b, \quad \frac{\partial w_I}{\partial x} = \frac{\partial w_{(I+1)}}{\partial x} = -\phi_b, \quad (4.6)$$

$$T_b = M_{x(I+1)} - M_{xb}, \quad N_{xI} = N_{x(I+1)}, \quad Q_b = V_{x(I+1)} - V_{xI}, \quad N_{xyI} = N_{xy(I+1)} \quad (4.7)$$

4.4 Application

For illustrative purposes, the numerical applications address verifications of different loading and boundary conditions. All the layers are assumed to be of the same thickness and density, and they are made of the same orthotropic material. The following material parameters are used:

$$\begin{aligned} E_1 &= 132.38 \text{ GPa} (19.2 \times 10^6 \text{ psi}), & E_2 &= 10.76 \text{ GPa} (1.56 \times 10^6 \text{ psi}), \\ G_{12} &= G_{13} = 5.65 \text{ GPa} (0.82 \times 10^6 \text{ psi}), & G_{23} &= 3.61 \text{ GPa} (0.523 \times 10^6 \text{ psi}) \\ \nu_{12} &= 0.24 \end{aligned}$$

In the following plate bending analysis, uniformly distributed load, concentrated load, and patch load are considered. The edges $y = 0$ and $y = b$ are invariably assumed to be simply supported. Similarly to Chapter 3, the eight-node, Shell99 (ANSYS, Inc., 2007), and quadrilateral linear layered structural shell element of ANSYS, is used for the comparison.

4.4.1 Example 1: Edge beam effect for a square antisymmetric angle-ply plate

Uniformly-loaded antisymmetric angle-ply square plates, having a width in the x -direction to plate thickness ratio $a/h = 1000$, are studied in this section. The plates are simply supported along the edges at $y = 0$, $y = b$, and $x = 0$, with varied stiffness beam supported at $x = x_n = a$. The ply orientation angle is varied from $\theta = 0^\circ$ to $\theta = 90^\circ$. Plates with 2 layers and 10 layers are analyzed.

This study shows edge beam effect by changing beam stiffness, KI , which takes values 0.6221, 1.5, 10, and 30. For comparison, results using simply supported and clamped edges at $x = x_n = a$ are presented.

Figure 4.2 shows the dimensionless deflections $\left[\hat{w} = \left(\frac{100E_2h^3}{b^4q} \right) w \right]$ at the center of plate, obtained from ANSYS and ASM. The variation between ASM and ANSYS

results is negligible. When $KI= 0.6221$, which is the weakest beam stiffness in this investigation, the center deflection is greatest and tends to be like free edge. When $KI= 30$, which is the strongest beam stiffness in this investigation, the center deflection is least and approaches the result under the clamped edge. Under same loading and boundary conditions, the deflections with 2 layers plate are always larger than ones with 10 layers plate. It shows stronger bending-extension coupling effect in 2-layer antisymmetric angle-ply plate than in 10-layer antisymmetric angle-ply plate.

Table 4.1 shows the convergence study on the dimensionless center deflection of 2-layer and 10-layer uniformly loaded square laminated plates ($45^\circ/-45^\circ/\dots$), with four different boundary beams at $x = a$. It is clear that for any beam stiffness, sufficiently converged deflection results can be obtained as series item m up to 5.

Figure 4.3 shows the dimensionless stress $\left[\Sigma_x = \left(\frac{h^2}{qb^2} \right) \sigma_x \right]$ at the point with $x/a = 0.975$ and close to the beam support edge obtained from ANSYS and ASM. The maximum difference between ANSYS and ASM is 1.75%, which occurs when KI is 30 and ply orientation angle is 15 degree. The stress increases when KI (beam stiffness) increases. When $KI = 30$, the stress Σ_x closes to one under clamped edge condition. Under the same loading and boundary conditions, the stresses on the 2-layer plate are always larger than those on the 10-layer plate. It also shows a stronger bending-extension coupling effect in 2-layer antisymmetric angle-ply plate than in 10-layer antisymmetric angle-ply plate. Due to the moment capacity of the beam, the stresses on the observed point are always negative for all the beams with different stiffnesses.

Tables 4.2 shows the convergence study on the dimensionless center stresses of 2-layer and 10-layer uniformly loaded square angle-ply laminated plates ($45^\circ/-45^\circ/\dots$), with four different boundary beams at $x = a$. It indicates that sufficiently converged stress results can also be obtained when $m = 5$.

4.4.2 Example 2: Two interior beams for rectangular antisymmetric angle-ply plate

A uniformly-loaded antisymmetric angle-ply rectangular plates, having a width in

the y -direction to plate thickness ratio $b/h = 1000$ and $a/b = 2$ ($a - x$ direction length of plate, $b - y$ direction length of plate), is studied in this example. The plate is simply supported on $y = 0$ and $y = b$, free edges on $x = 0$ and $x = a = 2b$; two beams which are parallel to y -axis support the inside plate. One beam is located at $x/a = 0.25$, and another beam is placed at $x/a = 0.925$. Beam stiffness, $KI = 1.5$ for both beams is used.

This investigation shows the effect of the ply-orientation angle on deflections and stresses at center, edges, and beam positions of plate with two inside beam supports.

Figure 4.4 shows loading and support conditions for this example and displays the contour of dimensionless deflection $\left[\hat{w} = \left(\frac{100E_2h^3}{b^4q} \right) w \right]$ with 10-layer $(-45/45)_5$

rectangular laminated plate, obtained using ASM. Table 4.3 displays the effects of ply angle and number of layers on dimensionless deflections at left middle edge ($x = 0, y = b/2$), middle point of the beam 1 ($x = a/4, y = b/2$), center of the plate ($x = a/2, y = b/2$), middle point of the beam 2 ($x = 0.925a, y = b/2$), and the middle of right edge ($x = a, y = b/2$). The maximum difference in deflection between ANSYS and ASM is 1.664%, and that occurs at the middle of right edge of a 2-layer plate, when ply orientation-angle $\theta = 30^\circ$. Most of the deflection differences between ANSYS and ASM are smaller than 1.0% (Table 4.3).

The deflection of 2-layer plate is larger than the deflection of 10-layer plate, due to the effect of bending-extension coupling stiffness coefficients. All the minimum deflections for the five points observed on both 2-layer and 10-layer plate occur when $\theta = 90^\circ$, because ply is at the shortest distance at this orientation. The maximum deflections at the center of the two beam positions on both 2-layer and 10-layer plate occur when $\theta = 0^\circ$, because they take over maximum loads from adjacent areas. The deflections for the left edge and center of the plate follow similar trends, when ply orientation angle varies from 0° to 90° . Due to the bending-extension coupling effect, they start at same deflection for 2-layer and 10-layer plates as ply orientation angle is 0° ; increased deflection difference between 2-layer and 10-layer plates when ply orientation angle increases; and end at same deflection for 2-layer and 10-layer plates, when ply orientation angle reaches 90° . Whereas the deflections on other three points are not

pronouncedly affected by bending-extension coupling effect because of the beam effect (see Table 4.3).

Table 4.4 displays the effect of ply angle and number of layers on dimensionless stresses $\left[\Sigma_x = \left(\frac{h^2}{b^2 q} \right) \sigma_x, \Sigma_y = \left(\frac{h^2}{b^2 q} \right) \sigma_y, \text{ and } \Sigma_{xy} = \left(\frac{h^2}{b^2 q} \right) \sigma_{xy} \right]$, at the middle point of beam 1 ($x = a/4, y = b/2$), center of the plate ($x = a/2, y = b/2$), and the middle point of beam 2 ($x = 0.925a, y = b/2$). The maximum stress difference between ANSYS and ASM is 4.88% and that occurs at the center of 2-layer plate, when ply angle $\theta = 60^\circ$ for Σ_{xy} . Differences of Σ_x and Σ_y , between ANSYS and ASM, are smaller than the difference of Σ_{xy} between ANSYS and ASM. Most of the stress differences between ANSYS and ASM are smaller than 3.0% (Table 4.4). At the center of the plate, Σ_x decreases from maximum value at $\theta = 0^\circ$ to minimum value at $\theta = 90^\circ$, for both 2-layer and 10-layer plates; whereas Σ_y increases from minimum value at $\theta = 0^\circ$ to maximum value at $\theta = 90^\circ$, for both 2-layer and 10-layer plates. Shear stresses Σ_{xy} have similar values for 2-layer and 10-layer plates, are close to zero at points $\theta = 0^\circ$ and $\theta = 90^\circ$, and reach maximum values when $\theta = 60^\circ$. The stresses on two beam positions have similar trends.

4.4.3 Example 3: Two points supported rectangular antisymmetric angle-ply plate

The ASM can be applied to a laminated plate over point supports. A uniformly-loaded antisymmetric angle-ply rectangular plate, having a width in the y -direction to plate thickness ratio $b/h = 1000$ and $a/b = 2$ ($a - x$ direction length of plate, $b - y$ direction length of plate), is studied in this example. The plate is simply supported on $y = 0$ and $y = b$, and free edges on $x = 0$ and $x = a = 2b$. Two points support inside at $x = 0.4b, y = b/2$ and $x = 1.7b, y = b/2$, respectively.

The plate is divided into strips in such a way that the point supports are located along the edges of the strips. The solution to this problem is achieved by releasing the deflection at both point supports, and then by building the flexibility matrix to determine the supports' reactions, which are required to cancel these deflections. Figure 4.5 shows loading and support conditions for this example, and displays the contour of

dimensionless deflection $\left[\hat{w} = \left(\frac{100E_2h^3}{b^4q} \right) w \right]$ with 2-layer (-45/45) rectangular laminated plate obtained by using ASM.

Figure 4.6 shows the dimensionless deflections at middle edges of left and right plate, and the center of the plate. The maximum difference between ASM and ANSYS results is 3.22%, which occurs at middle right edge of 10-layer plate, when ply orientation angle $\theta = 90^\circ$. Most of the differences between the results from these two methods are less than 2%. Under a prescribed loading and boundary condition, the deflection at the center of the plate with 2 layers is always larger than one with 10 layers.

However, due to the effect from inside point support positions, deflections at both middle edges follow a different trend to the one in the middle of plate. At the middle point of left edge, the deflections of the 2-layer plate are smaller than those of the 10-layer plate, when the ply-orientation angle is less than 19° . At the middle point of right edge, the deflections of the 2-layer are smaller than those of the 10-layer, when the ply-orientation angle is less than 38° . They vary, by relative amounts, after these two points.

Figure 4.7 shows the dimensionless stresses $\left[\Sigma_x = \left(\frac{h^2}{b^2q} \right) \sigma_x, \Sigma_y = \left(\frac{h^2}{b^2q} \right) \sigma_y, \right.$ and $\left. \Sigma_{xy} = \left(\frac{h^2}{b^2q} \right) \sigma_{xy} \right]$ at the center of the plate by using ASM and ANSYS. The

maximum difference between ASM and ANSYS results is 1.578%, which happens at Σ_y on the 10-layer plate, when ply-orientation angle $\theta = 0^\circ$. Because of ply effect, the stress Σ_x decreases when the ply-orientation angle increases. On the other hand, the stress Σ_y increases when the ply-orientation angle increases. Under prescribed loading and boundary conditions, both stresses Σ_x and Σ_y on 2-layer plate are always larger than those of 10-layer plate. Unlike Σ_x and Σ_y , stress Σ_{xy} of 2-layer plate is greater than those of 10-layers plate, only between ply orientation angles ranging from 15 to 75 degrees (see Figure 4.7).

4.4.4 Example 4: Two beam supported antisymmetric angle-ply 6-layer square laminated plate, subjected to a patch load and a concentrated load P

This example presents a more complicated case for an antisymmetric angle-ply 6-layer square laminated plate with varied ply orientation angles (-15/-45/-75/75/45/15), subjected to a patch load and a concentrated load combination. This plate has simply supported on $y = 0$ and $y = b$, one beam ($KI = 1.5$) supported on the left edge, $x = 0$, and another beam ($KI = 10$) supported inside the plate at $x = 7a/8$. The patch load covers x from $a/10$ to $a/2$ and y from $a/10$ to $a/2$. The concentrated load is located at point $x = 37a/40$ and $y = 3a/4$.

Figure 4.8 shows loading and support conditions for this example, and displays the contour of dimensionless deflection $\left[\hat{w} = \left(\frac{100E_2h^3}{b^4q} \right) w \text{ for patch load and } \hat{w} = \left(\frac{100E_2h^3}{b^2P} \right) w \text{ for concentrated load} \right]$ for a square laminated plate, generated using ASM. This case is also analyzed using ANSYS. The differences of dimensionless deflections $\left(100 \frac{\hat{w}_{ANSYS} - \hat{w}_{ASM}}{\hat{w}_{ASM}} \right)$ on special points, such as middle point on left edge (0.214%), center of patch load (0.985%), middle point of inside beam (0.518%), the point concentrated load exerted on (4.065%), and the point of right edge, $x = a$ and $y = 3a/4$ (1.241%), are identified. The maximum difference is 4.065%, which happens at the concentrated load point. Others are less than 1.25%. The differences of dimensionless stresses $\left(100 \frac{\Sigma_{ANSYS} - \Sigma_{ASM}}{\Sigma_{ASM}} \right)$ at the center of the patch load are 1.158%, 2.28%, and 1.886% for Σ_x , Σ_y , and Σ_{xy} respectively. All of these results indicate that ASM can be used in more complicated loading and boundary conditions.

4.5 Summary and Conclusions

ASM is extended to the analysis of stiffened continuous antisymmetric laminated composite plates in this chapter. This method can be used to analyze stiffened continuous laminated composite plates, subjected to any combination of patch, uniform,

line, and concentrated loads. The sufficiently converged deflection and stress results are observed for antisymmetric laminated plates with beam supports. The results generated, using ASM, are compared with ones obtained using ANSYS. All the differences between ASM and ANSYS results of dimensionless deflections and stresses listed in this chapter, from four different examples from basic to more complicated combination of loading and boundary conditions, are matched very well. The proposed methodology enables researchers to analyze stiffened continuous antisymmetric composite laminated plates, with beam or point supports, subjected to any combination of patch, uniform, line, and concentrated loads, without resorting to approximate methods.

Table 4.1. Convergence study for ASM on the center deflection, $\hat{w}(a/2, a/2)^1$ of an antisymmetric angle-ply square plate (30°/-30°/30°/-30°/...) having three edges simply supported and the fourth edge ($x = a$) with varied beam supported, $a/h = 1000$, $E_1 = 132.38$ GPa, $E_2 = 10.76$ GPa, $G_{12} = G_{13} = 5.65$ GPa, $G_{23} = 3.61$ GPa, $\nu_{12} = 0.24$

θ°	n^2	m^2	KI^4			
			0.622	1.5	10	30
30°	2	1	1.71286	1.38606	1.12445	1.08903
		3	-0.03510	-0.03486	-0.03472	-0.03469
		5	0.00351	0.00350	0.00350	0.00350
		7	-0.00069	-0.00069	-0.00068	-0.00069
		9	0.00020	0.00020	0.00020	0.00020
		Sum ⁵	1.68078	1.35421	1.09275	1.05735
	10	1	1.07414	0.82507	0.59161	0.55645
		3	-0.02152	-0.02115	-0.02091	-0.02089
		5	0.00241	0.00240	0.00240	0.00241
		7	-0.00050	-0.00049	-0.00049	-0.00050
9		0.00015	0.00014	0.00014	0.00015	
	Sum	1.05468	0.80597	0.57275	0.53762	

$$^1 \hat{w} \left(\frac{a}{2}, \frac{a}{2} \right) = \left(\frac{100 E_2 h^3}{a^4 q} \right) w$$

² n = number of layers

³ m = mode of deflection

⁴ KI = dimensionless flexural rigidity of the beam

$$^5 \text{Sum} = \sum_{m=1,3}^{11}$$

Table 4.2. Convergence study for ASM on the center stresses $\Sigma(a/2, a/2) = (\sigma h^2/qa^2)$ of an antisymmetric angleply square plate (30°/-30°/30°/-30°/...) having three edges simply supported and the fourth edge ($x = a$) with varied beam supported, $a/h = 1000$, $E_1 = 132.38$ GPa, $E_2 = 10.76$ GPa, $G_{12} = G_{13} = 5.65$ GPa, $G_{23} = 3.61$ GPa, $\nu_{12} = 0.24$

θ°	n^1	m^2	KI^3											
			0.622			1.5			10			30		
			Σ_x	Σ_y	Σ_{xy}	Σ_x	Σ_y	Σ_{xy}	Σ_x	Σ_y	Σ_{xy}	Σ_x	Σ_y	Σ_{xy}
30°	2	1	0.4528	0.2207	0.1863	0.4254	0.1951	0.1743	0.4007	0.1739	0.1635	0.3972	0.1710	0.1619
		3	-0.0262	-0.0246	-0.0116	-0.0262	-0.0245	-0.0116	-0.0262	-0.0244	-0.0115	-0.0262	-0.0244	-0.0115
		5	0.0059	0.0065	0.0028	0.0059	0.0065	0.0028	0.0059	0.0065	0.0028	0.0059	0.0065	0.0028
		7	-0.0023	-0.0025	-0.0011	-0.0023	-0.0025	-0.0011	-0.0023	-0.0025	-0.0011	-0.0023	-0.0025	-0.0011
		9	0.0011	0.0012	0.0005	0.0011	0.0012	0.0005	0.0011	0.0012	0.0005	0.0011	0.0012	0.0005
	Sum ⁴	0.4313	0.2012	0.1769	0.4040	0.1758	0.1649	0.3793	0.1546	0.1541	0.3758	0.1517	0.1526	
	10	1	0.3456	0.1633	0.1720	0.3154	0.1403	0.1556	0.2816	0.1172	0.1377	0.2762	0.1136	0.1348
		3	-0.0256	-0.0185	-0.0137	-0.0254	-0.0182	-0.0136	-0.0252	-0.0181	-0.0135	-0.0252	-0.0181	-0.0135
		5	0.0066	0.0053	0.0036	0.0066	0.0053	0.0036	0.0066	0.0053	0.0036	0.0066	0.0053	0.0036
		7	-0.0025	-0.0021	-0.0014	-0.0025	-0.0021	-0.0014	-0.0025	-0.0021	-0.0014	-0.0025	-0.0021	-0.0014
9		0.0012	0.0010	0.0007	0.0012	0.0010	0.0007	0.0012	0.0010	0.0007	0.0012	0.0010	0.0007	
Sum	0.3253	0.1490	0.1612	0.2953	0.1263	0.1449	0.2616	0.1033	0.1271	0.2562	0.0998	0.1242		

¹ n = number of layers

² m = mode of deflection

³ KI = dimensionless flexural rigidity of the beam

⁴ Sum = $\sum_{m=1,3}^{11}$

Table 4.3. Effect of ply angle (θ°) and number of layers (n) on deflection \hat{w}^1 of a uniformly loaded rectangular antisymmetric angle-ply plate ($a/b = 2$, θ° - $\theta^\circ/\theta^\circ$.../ $-\theta^\circ$) with two beams supported inside, $b/h = 1000$, $E_1 = 132.38$ GPa, $E_2 = 10.76$ GPa, $G_{12} = G_{13} = 5.65$ GPa, $G_{23} = 3.61$ GPa, $\nu_{12} = 0.24$

θ°	n	Method	\hat{w}_{Left}^5	\hat{w}_{Beam1}^6	\hat{w}_{Center}^7	\hat{w}_{Beam2}^8	\hat{w}_{Right}^9
0	2	ASM ²	1.5526	0.9280	1.7092	0.6648	0.4768
		ANSYS ³	1.5475	0.9288	1.7160	0.6647	0.4711
		Diff. (%) ⁴	0.327	-0.085	-0.395	0.008	1.206
	10	ASM	1.5526	0.9280	1.7092	0.6648	0.4768
		ANSYS	1.5475	0.9288	1.7160	0.6647	0.4711
		Diff. (%)	0.327	-0.085	-0.395	0.008	1.206
30	2	ASM	2.1361	0.8821	2.2322	0.6423	0.5459
		ANSYS	2.1380	0.8827	2.2360	0.6430	0.5370
		Diff. (%)	-0.089	-0.062	-0.169	-0.107	1.664
	10	ASM	1.6263	0.8743	1.5267	0.6380	0.5656
		ANSYS	1.6220	0.8748	1.5290	0.6377	0.5573
		Diff. (%)	0.266	-0.057	-0.148	0.054	1.493
45	2	ASM	2.2034	0.8107	2.2366	0.5945	0.5641
		ANSYS	2.2070	0.8111	2.2420	0.5947	0.5576
		Diff. (%)	-0.163	-0.045	-0.241	-0.041	1.170
	10	ASM	1.5177	0.7518	1.3600	0.5624	0.5569
		ANSYS	1.5220	0.7524	1.3630	0.5623	0.5518
		Diff. (%)	-0.285	-0.073	-0.220	0.017	0.926
60	2	ASM	2.1750	0.6818	2.1453	0.5110	0.5244
		ANSYS	2.1650	0.6801	2.1320	0.5094	0.5181
		Diff. (%)	0.460	0.243	0.621	0.310	1.224
	10	ASM	1.3698	0.5815	1.2269	0.4489	0.4824
		ANSYS	1.3680	0.5802	1.2210	0.4476	0.4784
		Diff. (%)	0.134	0.223	0.483	0.283	0.839
90	2	ASM	1.2648	0.3514	1.1640	0.2941	0.3289
		ANSYS	1.2630	0.3512	1.1610	0.2939	0.3244
		Diff. (%)	0.139	0.044	0.258	0.065	1.402
	10	ASM	1.2648	0.3514	1.1640	0.2941	0.3289
		ANSYS	1.2630	0.3512	1.1610	0.2939	0.3244
		Diff. (%)	0.139	0.044	0.258	0.065	1.402

$$^1 \hat{w} = \left(\frac{100 E_2 h^3}{a^4 q} \right) w$$

² ASM - Analytical Strip Method

³ ANSYS - Finite Element Analysis program (ANSYS Inc., 2007)

$$^4 \text{Diff. (\%)} = \left(100 \frac{\hat{w}_{ANSYS} - \hat{w}_{ASM}}{\hat{w}_{ASM}} \right)$$

⁵ \hat{w}_{Left} - \hat{w} at $x=0$ and $y=b/2$

⁶ \hat{w}_{Beam1} - \hat{w} at $x=a/4$ (beam 1 position) and $y=b/2$

⁷ \hat{w}_{Center} - \hat{w} at $x=a/2$ and $y=b/2$

⁸ \hat{w}_{Beam2} - \hat{w} at $x=0.925a$ (beam 2 position) and $y=b/2$

⁹ \hat{w}_{Right} - \hat{w} at $x=a$ and $y=b/2$

Table 4.4. Effect of ply angle (θ°) and number of layers (n) on stress Σ^I at center plate and middle beams of a uniformly loaded rectangular antisymmetric angle-ply plate ($a/b = 2$, $\theta^\circ/-\theta^\circ/\theta^\circ/\dots/-\theta^\circ$) with two beams supported inside plate, $b/h = 1000$, $E_1 = 132.38$ GPa, $E_2 = 10.76$ GPa, $G_{12} = G_{13} = 5.65$ GPa, $G_{23} = 3.61$ GPa, $\nu_{12} = 0.24$

θ°	n	Method	Middle Beam 1			Center			Middle Beam 2		
			Σ_x	Σ_y	Σ_{xy}	Σ_x	Σ_y	Σ_{xy}	Σ_x	Σ_y	Σ_{xy}
0	2	ASM ²	-0.7757	0.0297	0.0000	0.4122	0.0758	0.0000	-0.6537	0.0193	0.0000
		ANSYS ³	-0.7775	0.0296	0.0000	0.4140	0.0769	0.0000	-0.6524	0.0191	0.0000
		Diff. (%) ⁴	-0.226	0.543	0.009	-0.446	-1.465	0.063	0.199	0.908	0.001
	10	ASM	-0.7757	0.0297	0.0000	0.4122	0.0758	0.0000	-0.6537	0.0193	0.0000
		ANSYS	-0.7775	0.0296	0.0000	0.4140	0.0769	0.0000	-0.6524	0.0191	0.0000
		Diff. (%)	-0.226	0.543	0.009	-0.446	-1.465	0.063	0.199	0.908	0.001
30	2	ASM	-0.6517	-0.1326	-0.2438	0.4110	0.2209	0.1733	-0.6230	-0.1362	-0.2279
		ANSYS	-0.6552	-0.1334	-0.2452	0.4166	0.2263	0.1762	-0.6265	-0.1373	-0.2307
		Diff. (%)	-0.531	-0.590	-0.573	-1.371	-2.423	-1.679	-0.559	-0.841	-1.218
	10	ASM	-0.3855	-0.0668	-0.1728	0.3325	0.1769	0.1690	-0.3754	-0.0767	-0.1697
		ANSYS	-0.3849	-0.0667	-0.1725	0.3315	0.1757	0.1684	-0.3731	-0.0762	-0.1687
		Diff. (%)	0.146	0.148	0.172	0.298	0.667	0.336	0.623	0.672	0.610
45	2	ASM	-0.3979	-0.1797	-0.1866	0.3174	0.3660	0.2207	-0.4112	-0.2055	-0.1989
		ANSYS	-0.3995	-0.1805	-0.1874	0.3216	0.3724	0.2240	-0.4109	-0.2049	-0.1981
		Diff. (%)	-0.404	-0.452	-0.451	-1.317	-1.751	-1.487	0.062	0.310	0.381
	10	ASM	-0.1861	-0.0683	-0.1013	0.2534	0.2934	0.2176	-0.2114	-0.1031	-0.1251
		ANSYS	-0.1872	-0.0689	-0.1019	0.2570	0.2982	0.2209	-0.2115	-0.1030	-0.1251
		Diff. (%)	-0.576	-0.757	-0.605	-1.405	-1.620	-1.504	-0.054	0.080	0.038
60	2	ASM	-0.2473	-0.0969	-0.0665	0.2234	0.5907	0.2326	-0.2637	-0.1439	-0.0852
		ANSYS	-0.2396	-0.0940	-0.0636	0.2150	0.5702	0.2213	-0.2544	-0.1412	-0.0825
		Diff. (%)	3.119	2.962	4.415	3.749	3.469	4.877	3.528	1.906	3.212
	10	ASM	-0.1120	-0.0029	-0.0200	0.1649	0.4696	0.2238	-0.1315	-0.0558	-0.0455
		ANSYS	-0.1082	-0.0028	-0.0195	0.1586	0.4482	0.2139	-0.1270	-0.0546	-0.0443
		Diff. (%)	3.377	1.433	2.607	3.841	4.551	4.438	3.420	2.101	2.506
90	2	ASM	-0.1216	0.1841	0.0000	0.0396	0.7162	0.0000	-0.1244	0.1487	0.0000
		ANSYS	-0.1187	0.1795	0.0000	0.0395	0.6926	0.0000	-0.1213	0.1442	0.0000
		Diff. (%)	2.357	2.521	0.002	0.501	3.296	0.001	2.467	3.028	0.003
	10	ASM	-0.1216	0.1841	0.0000	0.0396	0.7162	0.0000	-0.1244	0.1487	0.0000
		ANSYS	-0.1187	0.1795	0.0000	0.0395	0.6926	0.0000	-0.1213	0.1442	0.0000
		Diff. (%)	2.357	2.521	0.002	0.501	3.296	0.001	2.467	3.028	0.003

$$^1 \Sigma = \left(\frac{h^2}{a^2 q} \right) \sigma$$

² ASM - Analytical Strip Method

³ ANSYS - Finite Element Analysis program (ANSYS Inc., 2007)

$$^4 \text{Diff. (\%)} = \left(100 \frac{\Sigma_{ANSYS} - \Sigma_{ASM}}{\Sigma_{ASM}} \right)$$

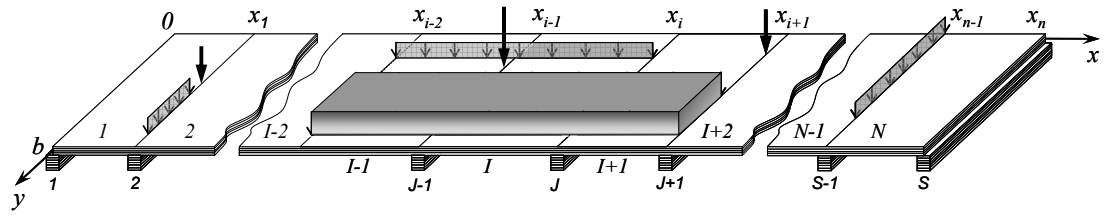


Figure 4.1. Stiffened plate with strip and edge loadings (beams are concentric and only half beams on bottom are shown for clarity)

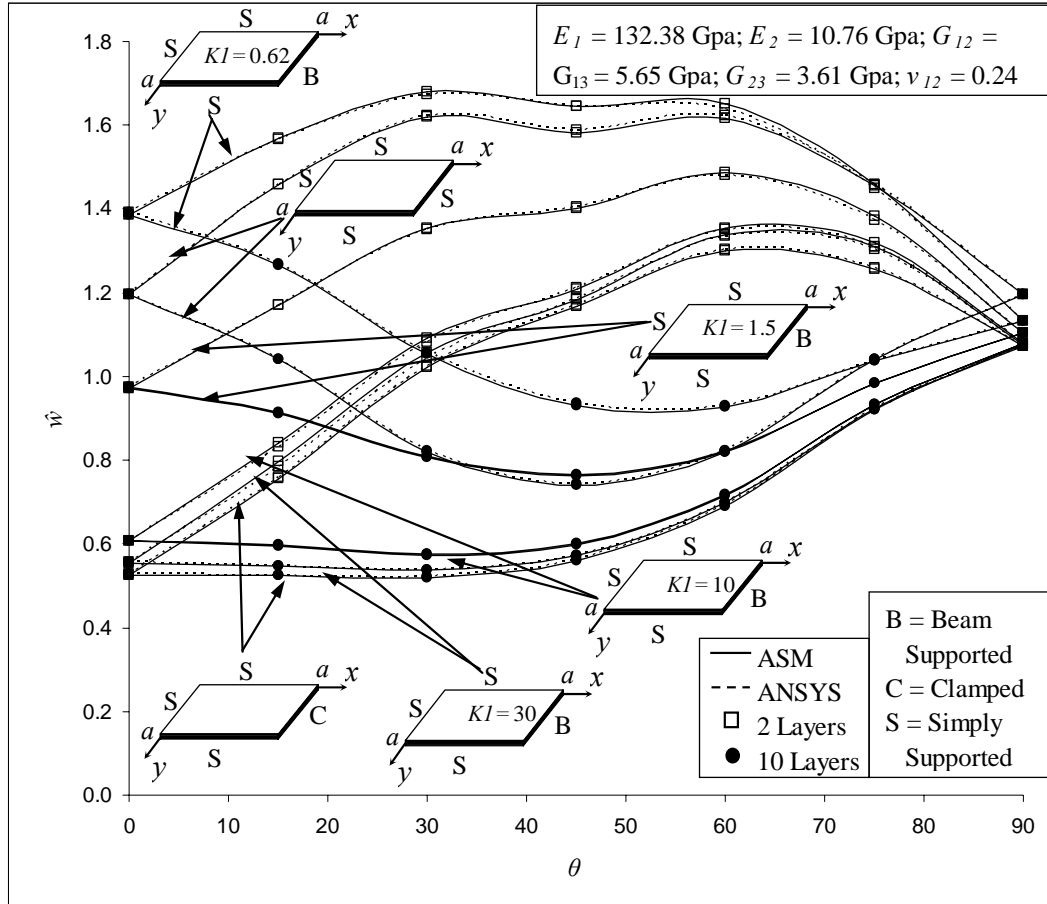


Figure 4.2. Deflection $\hat{w}\left(\frac{a}{2}, \frac{a}{2}\right) = \left(\frac{100E_2h^3}{a^4q}\right)w$ at the center of a uniformly loaded antisymmetric angle-ply square plate having three edges simply supported and the fourth edge ($x = a$) with varied beam supported, versus fiber orientation angle, θ

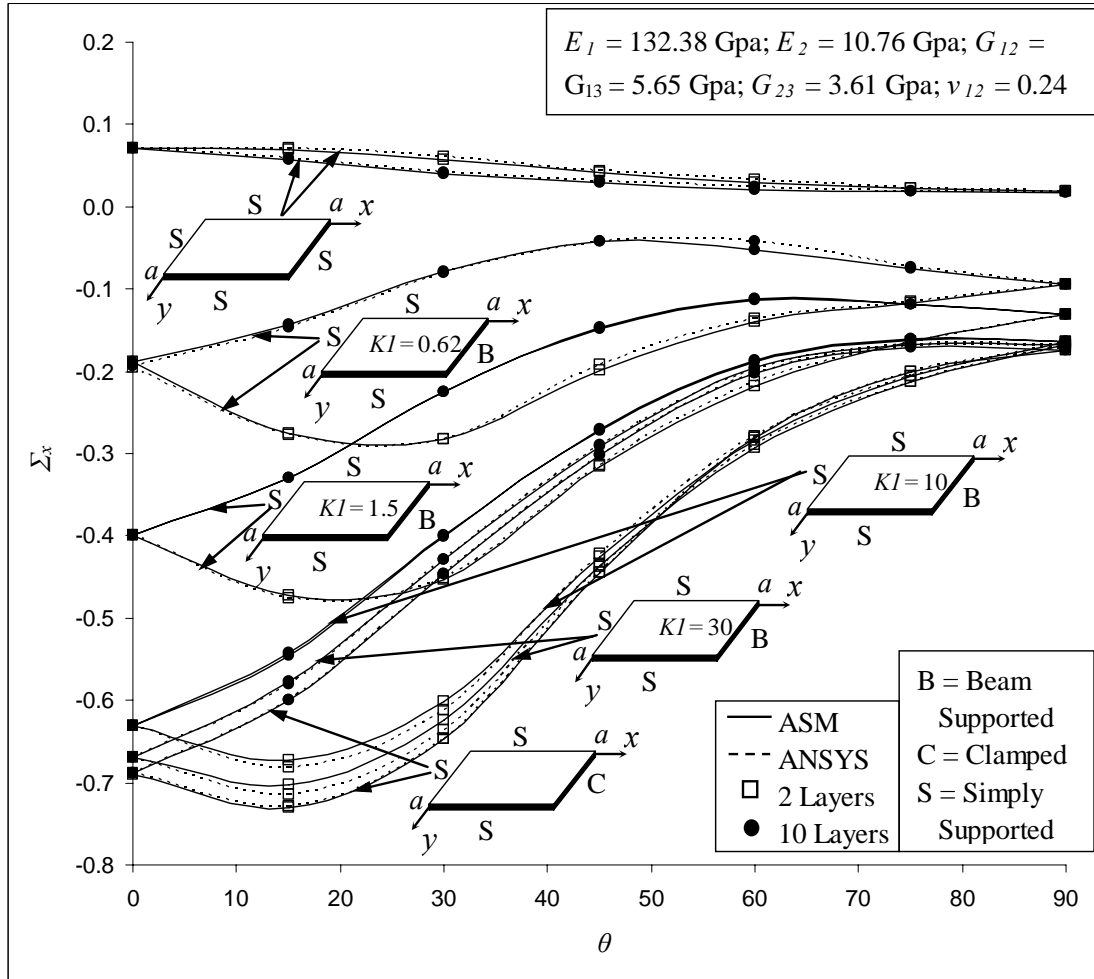
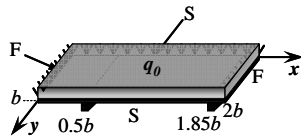
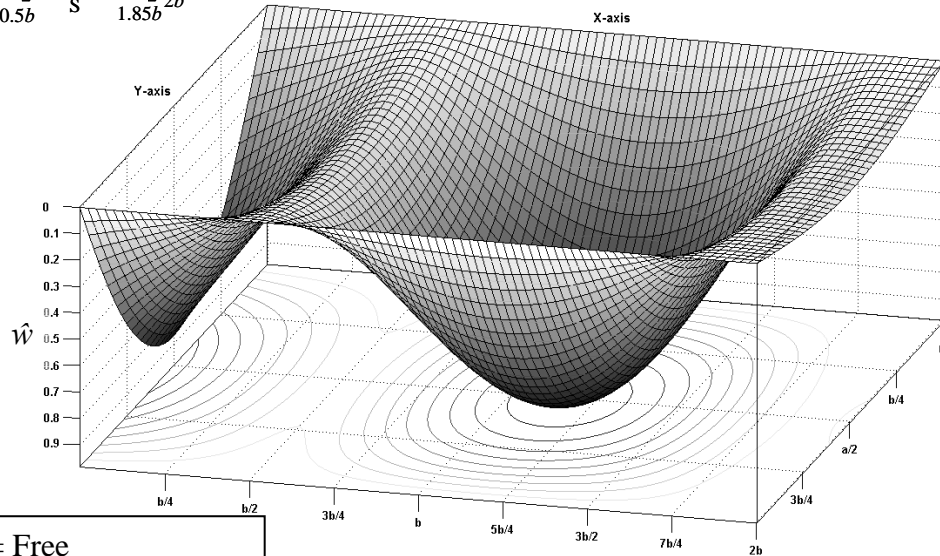


Figure 4.3. Stress $\Sigma_x \left(0.975a, \frac{a}{2} \right) = \left(\frac{h^2}{qa^2} \right) \sigma_x$ close to beam edge of a uniformly loaded antisymmetric angle-ply square plate having three edges simply supported and fourth edge ($x = a$) with varied beam supported, versus fiber orientation angle, θ



$$E_1 = 132.38 \text{ Gpa}; E_2 = 10.76 \text{ Gpa}; G_{12} = G_{13} = 5.65 \text{ Gpa}; G_{23} = 3.61 \text{ Gpa}; \nu_{12} = 0.24$$



F = Free
S = Simply Supported

Figure 4.4. Contour of dimensionless deflection, $\hat{w} = \left(\frac{100E_2h^3}{b^4q} \right) w$ for a uniformly

loaded antisymmetric angle-ply 10-layer $(-45/45)_5$ rectangular laminated plate having $a/b = 2$, simply supported at $y = 0$ and $y = b$, beams supported at $x = 0.5b$ and $x = 1.85b$, free at $x = 0$ and $x = 2b$

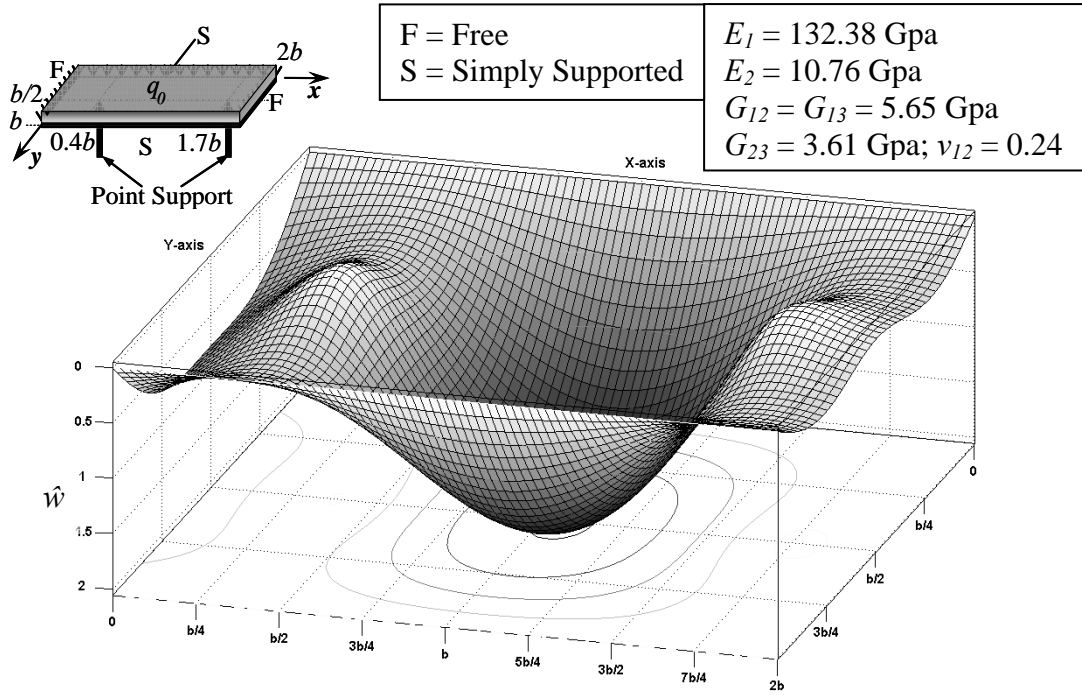


Figure 4.5. Contour of dimensionless deflection, $\hat{w} = \left(\frac{100E_2h^3}{b^4q} \right) w$ for a uniformly loaded antisymmetric angle-ply 2-layer (-45/45) rectangular laminated plate ($a/b = 2$) having simply supported on $y = 0$ and $y = b$, two point supports at $x = 0.4b, y = b/2$ and $x = 1.7b, y = b/2$, free at $x = 0$ and $x = 2b$

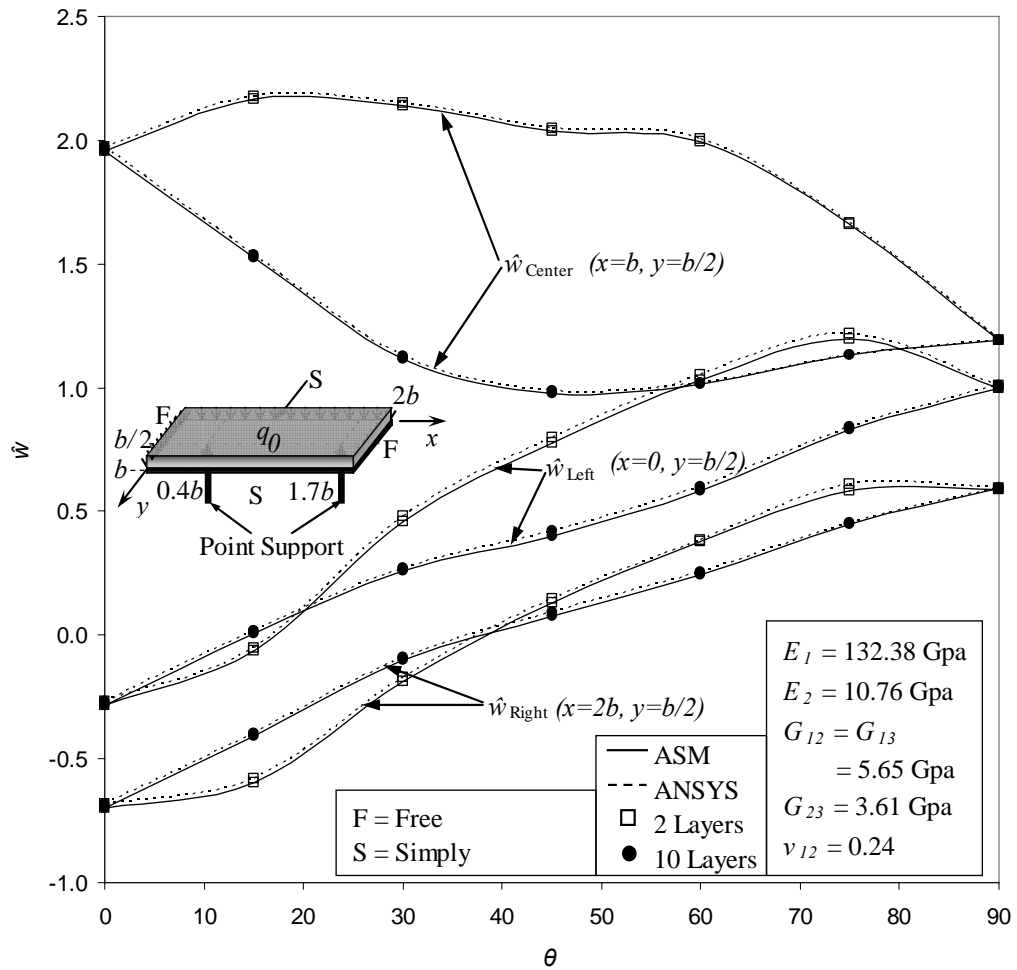


Figure 4.6. Dimensionless deflections at middle edges of left and right plate, and the center of plate of a uniformly loaded antisymmetric angle-ply rectangular laminated plate, having $a/b = 2$, simply supported at $y = 0$ and $y = a$, two points supported at $x = 0.4b, y = b/2$ and $x = 1.7b, y = b/2$, free at $x = 0$ and $x = 2b$,

$$\hat{w} = \left(\frac{100E_2h^3}{b^4q} \right) w \text{ versus ply orientation angle, } \theta$$

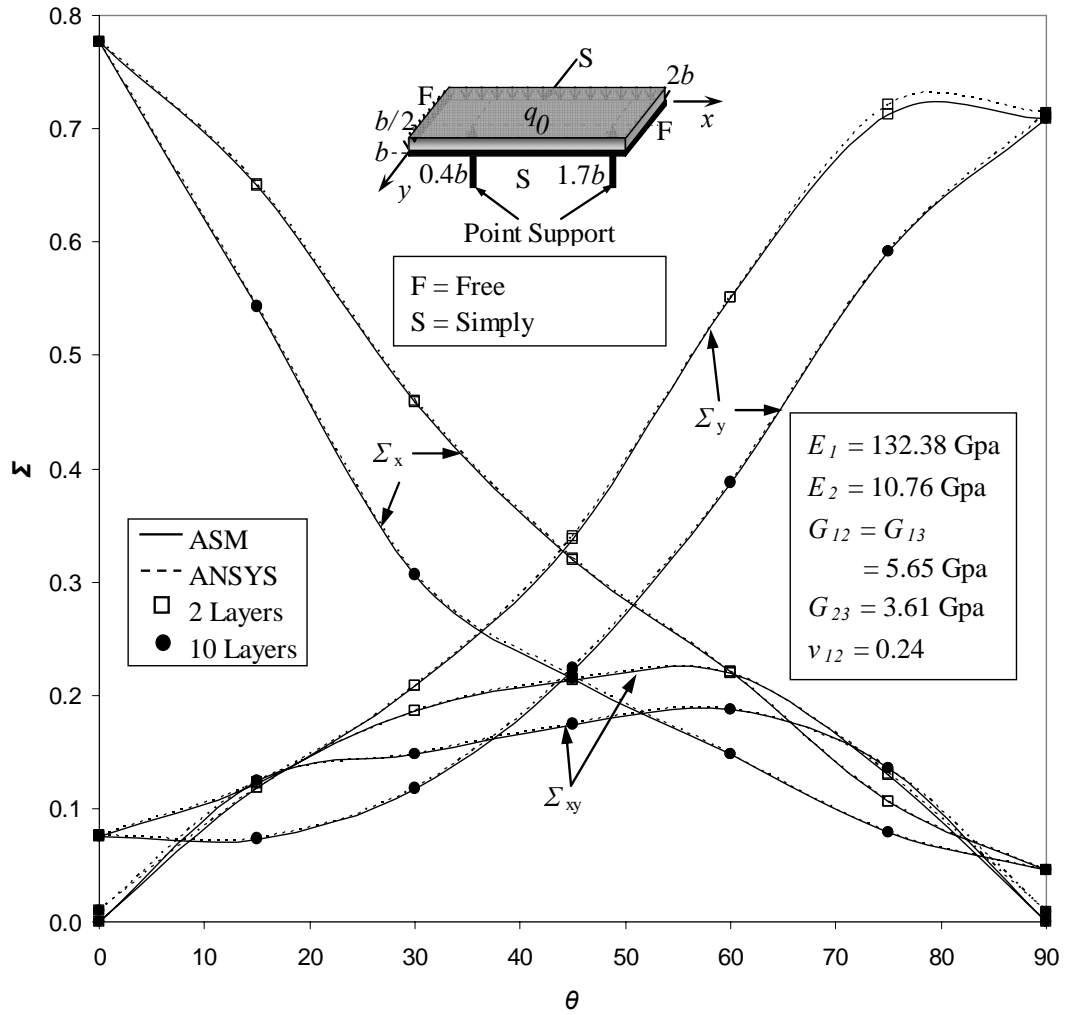


Figure 4.7. Dimensionless stresses at the center of plates of a uniformly loaded antisymmetric angle-ply rectangular laminated plate, having $a/b = 2$, simply supported at $y = 0$ and $y = a$, two points supported at $x = 0.4b, y = b/2$ and $x = 1.7b, y = b/2$, free at $x = 0$ and $x = 2b$, $\Sigma\left(\frac{a}{2}, \frac{b}{2}\right) = \left(\frac{h^2}{b^2 q}\right)\sigma$ versus ply orientation angle, θ

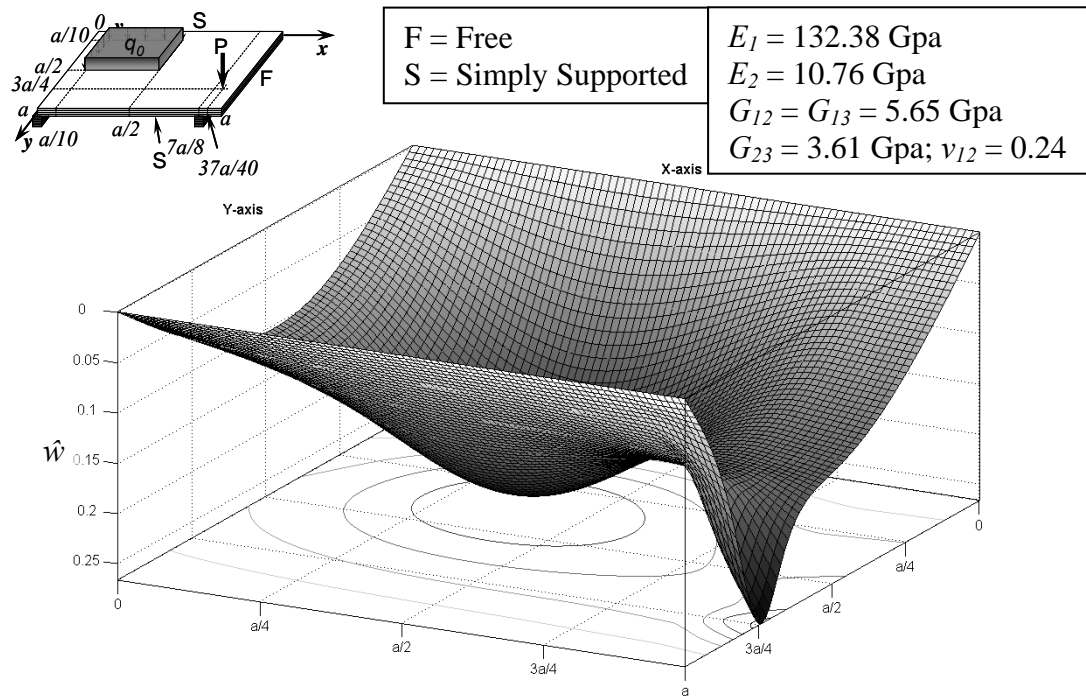


Figure 4.8. Contour of dimensionless deflection for an antisymmetric angle-ply 6-layer (-15/-45/-75/75/45/15) square laminated plate with simply supported on $y = 0$ and $y = a$, one beam at $x = 0$, and another beam at $x = 7a/8$ having a patch load and concentrated load

CHAPTER 5
FREE VIBRATION OF STIFFENED
ANTISYMMETRIC LAMINATED PLATES

5.1 Introduction

Stiffened laminated composite plates are being increasingly used in the aeronautical and aerospace industry, as well as in other fields of modern technology. They are structural components, consisting of plates reinforced by a system of ribs or beams to enhance their load-carrying capacity, and they are preferred in situations where the structures are subject to severe dynamic loads. The stiffened laminated plates are taking the place of many metallic components in aircrafts, such as in wings, fuselages, and floors.

A number of papers, pertaining to the free vibration of stiffened laminated plate, have been published. Mukherjee and Mukhopadhyay (1986) and Mukhopadhyay and Mukherjee (1989) have surveyed different approaches to vibration analysis of conventional stiffened plate problems. Many of these approaches can be utilized with the finite element method (FEM). Zhao *et al.* (2002), using an energy approach, investigated the free vibration of the stiffened simply supported rotating cross-ply laminated cylindrical shells. Sadek and Tawfik (2000) presented a higher-order finite element model, and studied the behavior of concentrically and eccentrically stiffened laminated plates. Rikards *et al.* (2001) developed a triangular finite element model, and studied the free vibrations of stiffened laminated composite shells. Guo *et al.* (2002) developed a layerwise finite element formulation, and made a free vibration analysis of stiffened laminated plates. Qing *et al.* (2006) analyzed a novel mathematical model, based on the state-vector equation theory, for the free vibration analysis of stiffened laminated plates.

In this chapter, ASM is developed for the free vibration analysis of antisymmetric cross-ply and angle-ply stiffened laminated composite plate (Figure 5.1) with bending-extension coupling.

5.2 Free Vibration Analysis

For an antisymmetric cross-ply or angle-ply plate in harmonic vibration, the

governing differential Equation 2.13 can be written as (Reddy, 2004):

$$\left(A_1 \frac{\partial^8 \Phi}{\partial x^8} + A_3 \frac{\partial^8 \Phi}{\partial x^6 \partial y^2} + A_5 \frac{\partial^8 \Phi}{\partial x^4 \partial y^4} + A_7 \frac{\partial^8 \Phi}{\partial x^2 \partial y^6} + A_9 \frac{\partial^8 \Phi}{\partial y^8} \right) \sin(\omega t) + I_0 \frac{\partial^2 W}{\partial t^2} - I_2 \left(\frac{\partial^4 W}{\partial x^2 \partial t^2} + \frac{\partial^4 W}{\partial y^2 \partial t^2} \right) = 0 \quad (5.1)$$

where,

$$I_0 = \sum_{k=1}^L \rho^k (z_{k+1} - z_k) \quad (5.2)$$

$$I_2 = \frac{1}{3} \sum_{k=1}^L \rho^k (z_{k+1}^3 - z_k^3) \quad (5.3)$$

$$W = w \sin(\omega t) \quad (5.4)$$

L is total layers of laminated plate; ρ^k is material density of the k^{th} layer. For an antisymmetric cross-ply plate, w can be written as:

$$w = a_7 \frac{\partial^4 \Phi}{\partial x^4} + a_8 \frac{\partial^4 \Phi}{\partial x^2 \partial y^2} + a_9 \frac{\partial^4 \Phi}{\partial y^4} \quad (2.16)$$

Equation 5.1 can be written as:

$$\left\{ A_1 \frac{\partial^8 \Phi}{\partial x^8} + A_3 \frac{\partial^8 \Phi}{\partial x^6 \partial y^2} + A_5 \frac{\partial^8 \Phi}{\partial x^4 \partial y^4} + A_7 \frac{\partial^8 \Phi}{\partial x^2 \partial y^6} + A_9 \frac{\partial^8 \Phi}{\partial y^8} - I_0 \omega^2 \left(a_7 \frac{\partial^4 \Phi}{\partial x^4} + a_8 \frac{\partial^4 \Phi}{\partial x^2 \partial y^2} + a_9 \frac{\partial^4 \Phi}{\partial y^4} \right) + I_2 \omega^2 \left[a_7 \frac{\partial^6 \Phi}{\partial x^6} + (a_7 + a_8) \frac{\partial^6 \Phi}{\partial x^4 \partial y^2} + (a_8 + a_9) \frac{\partial^6 \Phi}{\partial x^2 \partial y^4} + a_9 \frac{\partial^6 \Phi}{\partial y^6} \right] \right\} \sin(\omega t) = 0 \quad (5.5)$$

If Equation 5.5 keeps always true, the following must be valid:

$$A_1 \frac{\partial^8 \Phi}{\partial x^8} + A_3 \frac{\partial^8 \Phi}{\partial x^6 \partial y^2} + A_5 \frac{\partial^8 \Phi}{\partial x^4 \partial y^4} + A_7 \frac{\partial^8 \Phi}{\partial x^2 \partial y^6} + A_9 \frac{\partial^8 \Phi}{\partial y^8} - I_0 \omega^2 \left(a_7 \frac{\partial^4 \Phi}{\partial x^4} + a_8 \frac{\partial^4 \Phi}{\partial x^2 \partial y^2} + a_9 \frac{\partial^4 \Phi}{\partial y^4} \right) + I_2 \omega^2 \left[a_7 \frac{\partial^6 \Phi}{\partial x^6} + (a_7 + a_8) \frac{\partial^6 \Phi}{\partial x^4 \partial y^2} + (a_8 + a_9) \frac{\partial^6 \Phi}{\partial x^2 \partial y^4} + a_9 \frac{\partial^6 \Phi}{\partial y^6} \right] = 0 \quad (5.6)$$

5.3 Method of Solution

Using a procedure similar to that used in 3.3 for strip I , the characteristic equation of Equation 5.6 is:

$$\begin{aligned} & (A_1\gamma_m^8 - A_3\gamma_m^6 + A_5\gamma_m^4 - A_7\gamma_m^2 + A_9)\beta_m^8 - I_0\omega^2(a_7\gamma_m^4 - a_8\gamma_m^2 + a_9)\beta_m^4 \\ & + I_2\omega^2[a_7\gamma_m^6 - (a_7 + a_8)\gamma_m^4 + (a_8 + a_9)\gamma_m^2 - a_9] \beta_m^6 = 0 \end{aligned} \quad (5.7)$$

Since $\beta_m = \frac{m\pi}{b} \neq 0$, for $m = 1, 2, \dots, \infty$, Equation 5.7 leads to:

$$A_1^*\gamma_m^8 - A_3^*\gamma_m^6 + A_5^*\gamma_m^4 - A_7^*\gamma_m^2 + A_9^* = 0 \quad (5.8)$$

in which,

$$A_1^* = A_1 \quad (5.9a)$$

$$A_3^* = A_3 - I_2\omega^2 \frac{a_7}{\beta_m^2} \quad (5.9b)$$

$$A_5^* = A_5 - I_0\omega^2 \frac{a_7}{\beta_m^4} - I_2\omega^2 \frac{a_7 + a_8}{\beta_m^2} \quad (5.9c)$$

$$A_7^* = A_7 - I_0\omega^2 \frac{a_8}{\beta_m^4} - I_2\omega^2 \frac{a_8 + a_9}{\beta_m^2} \quad (5.9d)$$

$$A_9^* = A_9 - I_0\omega^2 \frac{a_9}{\beta_m^4} - I_2\omega^2 \frac{a_9}{\beta_m^2} \quad (5.9e)$$

The corresponding coefficients A_1^* , A_3^* , A_5^* , A_7^* , and A_9^* , for an antisymmetric angle-ply plate, are obtained by replacing a_7 , a_8 , and a_9 by b_7 , b_8 , and b_9 , respectively (Equation 2.30).

Similar to 3.3.1, Equation 5.8 can be reduced to a quartic equation, leading to the following general expression for I^{th} strip solution, $\phi_{ml}(x)$:

$$\begin{aligned} \phi_{ml}(x) = & [C_{1ml} \cosh(\gamma_{1ml}\beta_{ml}x) + C_{2ml} \sinh(\gamma_{1ml}\beta_{ml}x)] \cos(\gamma_{2ml}\beta_{ml}x) \\ & + [C_{3ml} \cosh(\gamma_{1ml}\beta_{ml}x) + C_{4ml} \sinh(\gamma_{1ml}\beta_{ml}x)] \sin(\gamma_{2ml}\beta_{ml}x) \\ & + [C_{5ml} \cosh(\gamma_{3ml}\beta_{ml}x) + C_{6ml} \sinh(\gamma_{3ml}\beta_{ml}x)] \cos(\gamma_{4ml}\beta_{ml}x) \\ & + [C_{7ml} \cosh(\gamma_{3ml}\beta_{ml}x) + C_{8ml} \sinh(\gamma_{3ml}\beta_{ml}x)] \sin(\gamma_{4ml}\beta_{ml}x) \end{aligned} \quad (5.10)$$

For a rectangular plate with N -plate strips (Figure 5.1), which depends on the number of beams and material/geometric discontinuities, all the boundary and continuity conditions

in (3.39) through (3.43) and (4.5) through (4.7) can be expressed in terms of constants C_{dml} ($d = 1, 2, \dots, 8; I = 1, 2, \dots, N$), and the roots of Equation 5.8. The constants C_{dml} ($d = 1, 2, \dots, 8; I = 1, 2, \dots, N$) are determined for each mode of plate m ($m = 1, 2, \dots, \infty$).

The coefficients of Equation 5.8 contain two unknowns, ω and m . m is fixed *a priori*, and it can be identified with the number of half-waves along y -direction deformation; it takes integer values, depending on the mode of deformation. Substitution of the solution $\phi_m(x)$, given by Equation 5.10 in a set of eight boundary, and continuity conditions, leads to a set of $8N$ algebraic equations. The determinant of the coefficients C_{dml} ($d = 1, 2, \dots, 8; I = 1, 2, \dots, N$), set to zero, leads to a transcendental equation for ω and m . For a given integer value of m , the value of ω , which makes the determinant zero, obtained by a method of hit and trial involving a bisection search strategy. The minimum value of ω , which satisfies this condition, is the lowest natural frequency (fundamental frequency). The MATLAB programs are then written to obtain fundamental frequencies ω for antisymmetric angle-ply and cross-ply plates with various aspect ratios, ply orientation angle and different number of layers.

5.4 Application

For illustrative purpose, the numerical applications address verifications of beam/stiffener boundary condition and supports inside the plate. All the layers are assumed to be of the same thickness and density, and made of the same orthotropic material. The plates with 2 layers and 10 layers are analyzed in all examples.

When comparing the results of the ASM solution with ones obtained from the finite element program ANSYS (ANSYS, Inc., 2007), an eight-node quadrilateral linear-layered structural shell element (Shell99) is used to model the laminated plates.

5.4.1 Example 1: Effects of aspect ratio (a/b), beam rigidity (KI) and number of layers

(n) on the dimensionless fundamental frequency
$$\left[\bar{\omega} = \left(\frac{b^2}{h} \sqrt{\frac{\rho}{E_2}} \right) \omega \right]$$

Antisymmetric cross-ply rectangular laminated plates ($0^\circ/90^\circ/0^\circ/90^\circ/\dots$, $a/b = 0.5$, 1, 2, 3, 5), having a width in the y -direction to plate thickness ratio $b/h = 1000$, simply

supported on $y = 0$ and $y = b$, beam supported at $x = 0$ and $x = a$, are used in this example. The material properties are: $\frac{E_1}{E_2} = 20$, $\frac{G_{12}}{E_2} = \frac{G_{13}}{E_2} = 0.6$, $\frac{G_{23}}{E_2} = 0.5$, $\nu_{12} = 0.25$.

Table 5.1 illustrates effects of aspect ratio (a/b), beam rigidity (KI), and number of layers (n) on fundamental frequency, $\bar{\omega}$, of a rectangular cross-ply plate ($0^\circ/90^\circ/0^\circ/90^\circ/...$). For given beam rigidity (KI) and plate layer (n), $\bar{\omega}$ decreases as aspect ratio (a/b) increases. This is true when a/b increases, and when plate stiffness decreases so does the $\bar{\omega}$. For given aspect ratio (a/b) and plate layer (n), $\bar{\omega}$ increases as beam rigidity (KI) increases. The stronger beam rigidity (KI) reinforces plate stiffness. As a result, $\bar{\omega}$ increases as well. For given beam rigidity (KI) and aspect ratio (a/b), $\bar{\omega}$ with 10 layers is always greater than $\bar{\omega}$ with 2 layers.

The bending-extension coupling effect from 2-layer laminated plate is greater than the bending-extension coupling effect of 10-layer laminated plate. The stronger bending-extension coupling effect lowers $\bar{\omega}$. The beam rigidity (KI) shows a greater effect when a/b is smaller. We can see greater differences from $\bar{\omega}$ among different beam rigidities when a/b equals 0.5. On the other hand, at the greatest value of a/b , $a/b = 5$, for example, $\bar{\omega}$ is approximately same when beam rigidity (KI) changes from 0.6 to 80. This means when a/b gets equal to or greater than a certain value, the effect of the boundary beams vanishes.

The difference between results obtained by ASM and by ANSYS decreases as a/b increases. When a/b equals 1, these differences are less than 1.41%, and when a/b equals 5, they are less than 0.14%. The results obtained by ASM and by ANSYS are identical when $a/b = 5$, $n = 10$, and $KI \geq 10$. However, when $a/b = 0.5$ and $KI \leq 10$, the results obtained by ASM and by ANSYS are not very well matched. The maximum difference between them $\left(100 \frac{\bar{\omega}_{ANSYS} - \bar{\omega}_{ASM}}{\bar{\omega}_{ASM}}\right)$ reaches -3.61%, which happens at $a/b = 0.5$, $KI = 0.6$, and $n = 2$, because boundary restriction on beam rotary and warping becomes a strong side effect on laminated plate in the ANSYS model. As the beam stiffness increases or a/b ratio increases, this side effect of boundary restriction is

dominated by the beam or is ignored by bigger plate size a . That is why the differences are diminished to smaller than 0.80% when $a/b = 0.5$ and $KI \geq 40$, or to smaller than 0.12% when $a/b = 5$.

5.4.2 Example 2: Effects of orthotropicity ratio (E_1/E_2), beam rigidity (KI) and number of layers (n) on the dimensionless fundamental frequency $\left[\bar{\omega} = \left(\frac{a^2}{h} \sqrt{\frac{\rho}{E_2}} \right) \omega \right]$

An antisymmetric angle-ply square plate ($45^\circ/-45^\circ/45^\circ/-45^\circ\dots$, $a/b = 1$), having a width in the x -direction to plate thickness ratio $a/h = 1000$, simply supported on $y = 0$ and $y = b$, beam supported at $x = 0$ and $x = a$ is used in this example. The material properties are: $\frac{E_1}{E_2} = 3, 10, 20, 30, \text{ and } 40$, $\frac{G_{12}}{E_2} = \frac{G_{13}}{E_2} = 0.6$, $\frac{G_{23}}{E_2} = 0.5$, $\nu_{12} = 0.25$.

Table 5.2 illustrates the effects of orthotropicity ratio (E_1/E_2), beam rigidity (KI), and number of layers (n) on fundamental frequency, $\bar{\omega}$, of a square angle-ply plate ($45^\circ/-45^\circ/45^\circ/-45^\circ\dots$). For given beam rigidity (KI) and plate layer (n), $\bar{\omega}$ increases as orthotropicity ratio (E_1/E_2) increases. This is true when E_1/E_2 increases, and when plate stiffness increases, so does the $\bar{\omega}$. For given orthotropicity ratio (E_1/E_2) and plate layer (n), $\bar{\omega}$ increases as beam rigidity (KI) increases. The stronger beam rigidity (KI) reinforces plate stiffness. As a result, $\bar{\omega}$ increases as well. For given beam rigidity (KI) and orthotropicity ratio (E_1/E_2), $\bar{\omega}$ with 10 layers is always greater than $\bar{\omega}$ with 2 layers.

The bending-extension coupling effect, of 2-layer laminated plate is greater than the bending-extension coupling effect of 10-layer laminated plate. The stronger bending-extension coupling effect lowers $\bar{\omega}$. This effect becomes more evident when the orthotropicity ratio (E_1/E_2) increases. When E_1/E_2 equals 3, there are only small differences, *i.e.* from 2.96% to 8.73% when KI varies from 1 to 80, between $\bar{\omega}$ with 10-layer and with 2-layer plates. On the other hand, when E_1/E_2 equals 40, there are larger differences, *i.e.* from 37.58% to 69.97% when KI varies from 1 to 80, between $\bar{\omega}$ with 10-layers and with 2-layer plates. It shows stronger bending-extension coupling effect when orthotropicity ratio (E_1/E_2) increases.

The difference $\left(100 \frac{\bar{\omega}_{ANSYS} - \bar{\omega}_{ASM}}{\bar{\omega}_{ASM}}\right)$ between results obtained by ASM and by

ANSYS decreases as E_1/E_2 or KI increases. The greatest difference, *i.e.* 4.78% occurs at $E_1/E_2 = 3$, $KI = 1$, and $n = 2$. This is due to a situation similar to that in 5.4.1, in which boundary restriction on beam rotary and warping is a strong side effect on laminated plate in ANSYS model, when E_1/E_2 decreases. As E_1/E_2 increases, this boundary restriction side effect is dominated by plies in the plate. That is why the differences are reduced to less than 1.63%, when $E_1/E_2 = 40$.

5.4.3 Example 3: Effects of ply angle (θ) and number of layers (n) on the dimensionless

$$\text{fundamental frequency } \left[\bar{\omega} = \left(\frac{b^2}{h} \sqrt{\frac{\rho}{E_2}} \right) \omega \right]$$

An antisymmetric angle-ply rectangular plate ($\theta/-\theta/\theta/-\theta/...$, $a/b = 2$), having a width in the y -direction to plate thickness ratio $b/h = 1000$, simply supported on $y = 0$ and $y = b$, three beams with $KI = 1$ supported at $x = 0$, $x = a/2$ and $x = a$, is used in this example. The material properties are: $\frac{E_1}{E_2} = 20$, $\frac{G_{12}}{E_2} = \frac{G_{13}}{E_2} = 0.6$, $\frac{G_{23}}{E_2} = 0.5$, $\nu_{12} = 0.25$.

Table 5.3 illustrates effects of ply angle (θ) and number of layers (n) on $\bar{\omega}$ of a rectangular angle-ply plate ($\theta/-\theta/\theta/-\theta/...$). $\bar{\omega}$ varies as ply angle changes. For 2-layer laminated plate, the minimum value of $\bar{\omega}$ occurs at ply-orientation angle $\theta = 50^\circ$; whereas for 10-layer laminated plate, the maximum value of $\bar{\omega}$ happens at ply-orientation angle $\theta = 65^\circ$. For given ply angle, $\bar{\omega}$ in 10-layer plate is greater than that in 2-layer plate. Most of the differences $\left(100 \frac{\bar{\omega}_{ANSYS} - \bar{\omega}_{ASM}}{\bar{\omega}_{ASM}}\right)$ between results obtained by ASM and by ANSYS are less than 1%. Only at one point is the difference greater than 3%, which reaches -3.21%, and this occurs when $\theta = 75^\circ$ and $n = 2$.

5.4.4 Example 4: Maximizing fundamental frequency $\left[\bar{\omega} = \left(\frac{b^2}{h} \sqrt{\frac{\rho}{E_2}} \right) \omega \right]$ by varying

inside beam position for cross-ply (0/90/0/90/...) and angle-ply (θ /- θ /0/- θ /...) laminated plates, with varied boundary conditions

Antisymmetric cross-ply ($a/b = 1$ and $a/b = 2.5$) and antisymmetric angle-ply ($a/b = 2.5$) laminated plates having a width in the y -direction to plate thickness ratio $b/h = 1000$, simply supported at $y = 0$ and $y = b$, and varied boundary conditions at $x = 0$ and $x = a$ are used in this example. The material properties are: $\frac{E_1}{E_2} = 40$ (for cross-ply)

and $\frac{E_1}{E_2} = 20$ (for angle-ply), $\frac{G_{12}}{E_2} = \frac{G_{13}}{E_2} = 0.6$, $\frac{G_{23}}{E_2} = 0.5$, $\nu_{12} = 0.25$.

Figure 5.2 shows boundary condition and beam layout, and displays searching results by varying inside beam position for a cross-ply square plate in maximizing procedure. Inside beam position has an effect on $\bar{\omega}$ of a plate. Opposite to what was expected, these positions are different for laminated plates that have different layers. $\bar{\omega}_{\max}$ for 2-layer plate is 22.909, and occurs at $x_b/b = 0.55$; whereas $\bar{\omega}_{\max}$ for 10-layer plate is 26.470 and occurs at $x_b/b = 0.58$. It is reasonable that the position of the inside beam is not at $a/2$, because the beam on the left boundary is much stronger, $KI = 2.0$, than the beam on the right boundary, $KI = 0.6$.

Further maximizing results for $\bar{\omega}$ for a cross-ply rectangular plate ($a/b = 2.5$), with different boundary conditions at $x = 0$ and $x = a$, are shown in Table 5.4. For a same layer plate, with the weakest boundary condition, *i.e.* free boundary condition, the maximized $\bar{\omega}$ has the least values, 10.096 and 15.277, for 2-layer and 10-layer plates respectively. The positions of the inside beams are closest to boundaries, $x_b/b = 0.57$ and $x_b/b = 0.55$ for 2-layer and 10-layer plates respectively.

When boundary conditions at both sides $x = 0$ and $x = a$ get stronger, from $KI = 0.6$ to clamped condition, the maximized $\bar{\omega}$ increases. Under clamped condition, the maximized $\bar{\omega}$ are 16.787 and 21.557 for 2-layer and 10-layer plates respectively. At this time, the positions of the inside beams are the farthest away from plate boundaries. They are $x_b/b = 0.90$ and $x_b/b = 0.97$, for 2-layer and 10-layer plates respectively.

Similar to the results in Figure 5.2, the inside beam positions, where \bar{w} are maximized, are different for 2-layer and 10-layer plates under the same boundary condition.

More interesting results are illustrated in Table 5.5, for angle-ply rectangular plate ($a/b = 2.5$), with beam supported boundary conditions at $x = 0$ and $x = a$. For any given layer, \bar{w}_{\max} is not only inside-beam position dependent, but it is also ply-angle dependent. The larger the ply angle, the smaller x_b/b . \bar{w}_{\max} are, 15.263, which happens at $\theta = 90$ and when $x_b/b = 0.85$ in a 2-layer plate, and 15.337, which happens at $\theta = 80$ and $x_b/b = 0.85$ in a 10-layer plate. These maximized values have only a 0.48% difference.

For the same ply-angles, the biggest difference between \bar{w} for 2-layer and 10-layer plates is 24.09%. At this point, \bar{w} is 12.030 under $x_b/b = 0.87$, for 2-layer plate, and 14.928 under $x_b/b = 0.88$, for 10-layer plate; this happens at $\theta = 65$. At two end points, where $\theta = 0^\circ$ or $\theta = 90^\circ$, there are not differences between \bar{w} in 2- and 10-layer laminated plates, since the bending-extension coupling effect is 0.

5.5 Summary and Conclusions

ASM is extended to the analysis of free vibration for antisymmetric laminated composite plates in this chapter. The results obtained using ASM are compared with ones obtained by using ANSYS (ANSYS, Inc., 2007). Most of the results are match well, with less than 1% difference (5.4.1 through 5.4.3). Because boundary restriction on beam rotary and warping has a strong side effect on laminated plate in the ANSYS model, when beam rigidity is small (e.g. $KI = 0.6$ or 1), plate-dimension ratio is small (e.g. $a/b = 0.5$), or orthotropicity ratio is small (e.g. $E_1/E_2 = 3$), the results obtained by these two approaches are not well matched. The difference between them reaches -3.61%, which occurs at $a/b = 0.5$, $KI = 0.6$, and $n = 2$; and 4.78%, which occurs at $E_1/E_2 = 3$, $KI = 1$, and $n = 2$.

As the beam rigidity increases, or as the orthotropicity ratio increases, \bar{w} also increases. On the other hand, as aspect ratio increases, \bar{w} declines. It is shown that the effect of coupling between bending and extension upon \bar{w} is noticeable. For given beam rigidity, aspect ratio of the plate, orthotropicity ratio of the plate, and ply angle (for

angle-ply plate), $\bar{\omega}$ of 10-layer plate is always greater than $\bar{\omega}$ of 2-layer plate, except at the points $\theta = 0^\circ$ or $\theta = 90^\circ$ where there is no bending-extension coupling effect at all ($B_{ij} = 0$ at $\theta = 0^\circ$ and 90°).

The proposed method, ASM, can be easily used to maximize $\bar{\omega}$ for antisymmetric stiffened laminated composite plates. For given laminated plate and stiffener, $\bar{\omega}_{\max}$, depends on the stiffener's position and ply angle (for angle-ply plate). The inside stiffener positions, where $\bar{\omega}$ is maximized, are different for 2-layer and 10-layer laminated plates under the same boundary conditions. For a designer, this may indicate that it is necessary to analyze every laminated plate, when $\bar{\omega}_{\max}$ is pursued for different layer plate.

Table 5.1. Effects of aspect ratio (a/b), beam rigidity (Kl) and number of layers (n) on the dimensionless fundamental frequency (ϖ^1) of a rectangular cross-ply laminated plate ($0^\circ/90^\circ/0^\circ/90^\circ/\dots$, $b/h = 1000$, $E_1/E_2=20$, $G_{12} = G_{13} = 0.6E_2$, $G_{23} = 0.5E_2$, $\nu_{12} = 0.25$)

Kl	Method	a/b									
		0.5		1		2		3		5	
		$n = 2$	$n = 10$	$n = 2$	$n = 10$	$n = 2$	$n = 10$	$n = 2$	$n = 10$	$n = 2$	$n = 10$
0.6	ASM ²	19.411	20.821	11.134	14.041	6.801	10.142	6.107	9.461	5.847	9.216
	ANSYS ³	18.710	20.330	11.140	14.110	6.871	10.200	6.138	9.476	5.853	9.218
	Diff. (%) ⁴	-3.61	-2.36	0.06	0.49	1.02	0.58	0.50	0.16	0.11	0.02
1	ASM	23.597	25.369	12.139	15.612	6.887	10.319	6.124	9.497	5.849	9.221
	ANSYS	22.880	24.700	12.260	15.750	6.967	10.380	6.157	9.510	5.856	9.222
	Diff. (%)	-3.04	-2.64	0.99	0.88	1.17	0.59	0.53	0.14	0.12	0.01
2	ASM	30.344	33.484	13.294	17.893	6.969	10.520	6.140	9.534	5.851	9.226
	ANSYS	29.630	32.460	13.480	18.110	7.054	10.570	6.174	9.544	5.858	9.226
	Diff. (%)	-2.35	-3.06	1.40	1.21	1.22	0.47	0.56	0.10	0.12	0.01
10	ASM	45.276	58.884	14.678	21.697	7.052	10.760	6.155	9.574	5.853	9.230
	ANSYS	45.050	57.220	14.860	21.830	7.134	10.780	6.189	9.577	5.860	9.230
	Diff. (%)	-0.50	-2.83	1.24	0.61	1.16	0.18	0.56	0.03	0.12	0.00
40	ASM	51.084	75.507	15.007	22.837	7.070	10.817	6.158	9.583	5.854	9.231
	ANSYS	51.170	74.910	15.170	22.880	7.151	10.820	6.192	9.584	5.860	9.231
	Diff. (%)	0.17	-0.79	1.09	0.19	1.15	0.03	0.56	0.01	0.11	0.00
80	ASM	52.215	79.531	15.064	23.047	7.073	10.827	6.158	9.585	5.854	9.231
	ANSYS	52.330	79.300	15.220	23.070	7.154	10.830	6.192	9.585	5.861	9.231
	Diff. (%)	0.22	-0.29	1.04	0.10	1.15	0.03	0.55	0.00	0.13	0.00

$$^1 \varpi = \frac{\omega b^2}{h} \sqrt{\frac{\rho}{E_2}}$$

² ASM - Analytical Strip Method (present method)

³ ANSYS - Finite Element Analysis program (ANSYS Inc., 2007)

$$^4 \text{Diff. (\%)} = \left(100 \frac{\varpi_{ANSYS} - \varpi_{ASM}}{\varpi_{ASM}} \right)$$

Table 5.2. Effects of in-plane orthotropy ratio (E_1/E_2), beam rigidity (KI) and number of layers (n) on the dimensionless fundamental frequency (ϖ^1) of a square angle-ply laminated plate ($45^\circ/-45^\circ/45^\circ/-45^\circ\dots$, $b/h = 1000$, $G_{12} = G_{13} = 0.6E_2$, $G_{23} = 0.5E_2$, $\nu_{12} = 0.25$)

KI	Method	E_1/E_2									
		3		10		20		30		40	
		$n = 2$	$n = 10$	$n = 2$	$n = 10$	$n = 2$	$n = 10$	$n = 2$	$n = 10$	$n = 2$	$n = 10$
1	ASM	6.883	7.087	9.994	11.635	12.473	15.882	14.337	19.143	15.908	21.885
	ANSYS	6.554	6.829	9.721	11.410	12.380	15.760	14.420	19.140	16.160	22.000
	Diff. (%)	-4.78	-3.64	-2.73	-1.93	-0.75	-0.77	0.58	-0.01	1.58	0.52
5	ASM	9.335	9.932	12.208	15.766	14.714	21.306	16.731	25.552	18.487	29.098
	ANSYS	9.057	9.633	12.110	15.600	14.720	21.310	16.820	25.780	18.650	29.570
	Diff. (%)	-2.98	-3.01	-0.80	-1.05	0.04	0.02	0.53	0.89	0.88	1.62
10	ASM	9.912	10.659	12.615	16.718	15.111	22.589	17.159	27.134	18.957	30.953
	ANSYS	9.734	10.459	12.560	16.610	15.110	22.600	17.200	27.290	19.040	31.270
	Diff. (%)	-1.80	-1.88	-0.44	-0.65	-0.01	0.05	0.24	0.57	0.44	1.02
20	ASM	10.236	11.075	12.833	17.254	15.323	23.323	17.388	28.058	19.210	32.061
	ANSYS	10.133	10.960	12.800	17.190	15.320	23.320	17.400	28.130	19.240	32.220
	Diff. (%)	-1.01	-1.04	-0.26	-0.37	-0.02	-0.01	0.07	0.26	0.16	0.50
30	ASM	10.350	11.222	12.908	17.442	15.396	23.583	17.466	28.389	19.297	32.462
	ANSYS	10.275	11.141	12.880	17.390	15.390	23.570	17.470	28.420	19.310	32.550
	Diff. (%)	-0.72	-0.72	-0.22	-0.30	-0.04	-0.05	0.02	0.11	0.07	0.27
40	ASM	10.407	11.297	12.946	17.537	15.432	23.715	17.506	28.559	19.341	32.669
	ANSYS	10.348	11.234	12.920	17.500	15.420	23.700	17.500	28.570	19.350	32.720
	Diff. (%)	-0.57	-0.56	-0.20	-0.21	-0.08	-0.06	-0.04	0.04	0.05	0.16
80	ASM	10.495	11.411	13.003	17.683	15.488	23.918	17.566	28.819	19.408	32.988
	ANSYS	10.459	11.376	12.980	17.650	15.470	23.890	17.560	28.800	19.400	32.980
	Diff. (%)	-0.34	-0.31	-0.18	-0.19	-0.12	-0.12	-0.04	-0.07	-0.04	-0.02

$$^1 \varpi = \frac{\omega b^2}{h} \sqrt{\frac{\rho}{E_2}}$$

² ASM - Analytical Strip Method (present method)

³ ANSYS - Finite Element Analysis program (ANSYS Inc., 2007)

$$^4 \text{Diff. (\%)} = \left(100 \frac{\varpi_{ANSYS} - \varpi_{ASM}}{\varpi_{ASM}} \right)$$

Table 5.3. Effects of ply angle (θ) and number of layers (n) on the dimensionless fundamental frequency (ϖ^1) of a rectangular angle-ply laminated plate ($a/b = 2$, $b/h = 1000$, $E_1/E_2=20$, $G_{12} = G_{13} = 0.6E_2$, $G_{23} = 0.5E_2$, $\nu_{12} = 0.25$) with beams at $x = 0$, $x = a/2$ and $x = a$ respectively, $KI = 1$ for all 3 beams

Angle (θ)	2 Layers			10 Layers		
	ASM ²	ANSYS ³	Diff.(%) ⁴	ASM	ANSYS	Diff.(%)
0	12.908	12.897	-0.08	12.908	12.903	-0.04
5	12.811	12.790	-0.16	12.927	12.918	-0.07
10	12.581	12.541	-0.32	12.990	12.969	-0.16
15	12.324	12.280	-0.36	13.096	13.060	-0.28
20	12.108	12.067	-0.34	13.243	13.188	-0.41
25	11.946	11.910	-0.30	13.427	13.353	-0.55
30	11.834	11.799	-0.29	13.647	13.554	-0.68
35	11.758	11.722	-0.31	13.901	13.791	-0.79
40	11.709	11.666	-0.37	14.181	14.060	-0.85
45	11.679	11.623	-0.48	14.477	14.348	-0.89
50	11.667	11.585	-0.71	14.768	14.638	-0.88
55	11.674	11.547	-1.09	15.030	14.904	-0.84
60	11.705	11.521	-1.58	15.229	15.115	-0.75
65	11.795	11.542	-2.15	15.335	15.238	-0.64
70	12.018	11.686	-2.76	15.328	15.251	-0.50
75	12.480	12.080	-3.21	15.206	15.150	-0.37
80	13.267	12.875	-2.96	15.012	14.975	-0.25
85	14.249	14.047	-1.42	14.835	14.816	-0.13
90	14.765	14.723	-0.29	14.765	14.760	-0.04

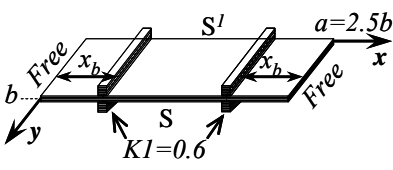
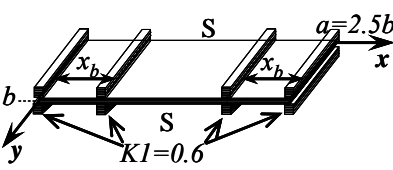
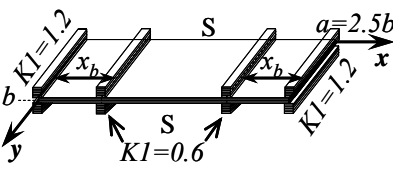
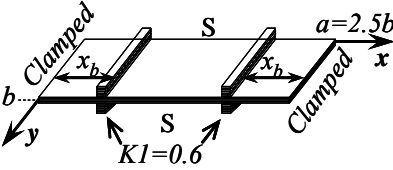
$$^1 \varpi = \frac{\omega b^2}{h} \sqrt{\frac{\rho}{E_2}}$$

² ASM - Analytical Strip Method (present method)

³ ANSYS - Finite Element Analysis program (ANSYS Inc., 2007)

$$^4 \text{Diff. (\%)} = \left(100 \frac{\varpi_{ANSYS} - \varpi_{ASM}}{\varpi_{ASM}} \right)$$

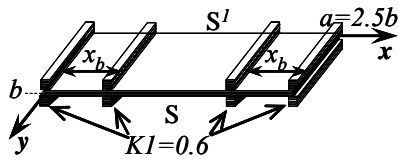
Table 5.4. Effect of boundary condition and positions of two inside beams on maximized dimensionless fundamental frequency for a rectangular cross-ply laminated plate ($0^\circ/90^\circ/0^\circ/90^\circ/\dots$, $b/h = 1000$, $E_1/E_2=40$, $G_{12} = G_{13} = 0.6E_2$, $G_{23} = 0.5E_2$, $\nu_{12} = 0.25$)

Boundary Condition	2 Layers		10 Layers	
	ϖ_{\max}^2	x_b/b	ϖ_{\max}	x_b/b
	10.096	0.57	15.277	0.55
	15.607	0.85	19.704	0.87
	16.082	0.87	20.288	0.90
	16.787	0.90	21.557	0.97

¹ S – Simply Supported

$$^2 \varpi = \frac{\omega b^2}{h} \sqrt{\frac{\rho}{E_2}}$$

Table 5.5. Effect of ply angle and positions of two inside beams on maximized dimensionless fundamental frequency for a rectangular angle-ply laminated plate ($\theta/\theta/\theta/\dots$, $b/h = 1000$, $E_1/E_2=20$, $G_{12} = G_{13} = 0.6E_2$, $G_{23} = 0.5E_2$, $\nu_{12} = 0.25$) with two boundary beams at $x = 0$ and $x = a$



Angle (θ)	2 Layers		10 Layers	
	ϖ_{max}	x_b/b	ϖ_{max}	x_b/b
0	11.536	0.90	11.536	0.90
5	11.502	0.90	11.552	0.90
10	11.425	0.89	11.604	0.90
15	11.345	0.89	11.694	0.90
20	11.288	0.88	11.826	0.90
25	11.260	0.88	12.006	0.90
30	11.261	0.88	12.242	0.90
35	11.290	0.87	12.538	0.90
40	11.346	0.87	12.892	0.90
45	11.425	0.87	13.296	0.90
50	11.527	0.87	13.731	0.89
55	11.656	0.87	14.171	0.89
60	11.817	0.87	14.581	0.89
65	12.030	0.87	14.928	0.88
70	12.345	0.87	15.179	0.87
75	12.861	0.87	15.312	0.86
80	13.682	0.87	15.337	0.85
85	14.721	0.85	15.309	0.85
90	15.289	0.85	15.289	0.85

¹ S – Simply Supported

$$^2 \varpi = \frac{\omega b^2}{h} \sqrt{\frac{\rho}{E_2}}$$

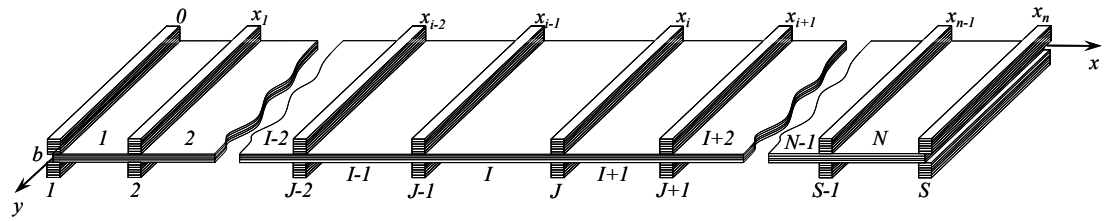


Figure 5.1. Stiffened plate with stiffeners parallel to y -axis

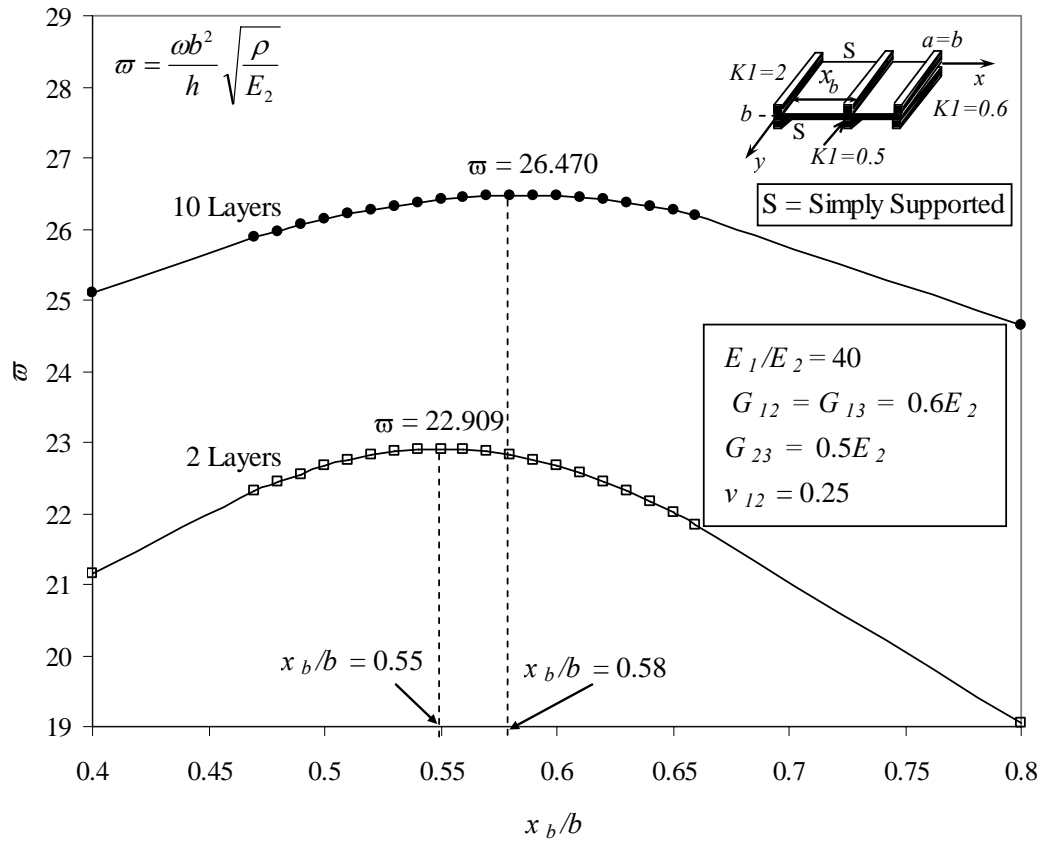


Figure 5.2. Maximizing dimensionless fundamental frequency by varying inside beam position for a square cross-ply laminated plate ($0^\circ/90^\circ/0^\circ/90^\circ/\dots$, $b/h = 1000$) with two boundary beams at $x = 0$ and $x = a$

CHAPTER 6
BUCKLING OF STIFFENED
ANTISYMMETRIC LAMINATED PLATES

6.1 Introduction

The study of buckling of stiffened laminated plates has a long history. In the early stages, a stiffened plate was idealized as an orthotropic plate. In fact, the study of orthotropic plates was stimulated by the need to establish a simplified model for the analysis of stiffened isotropic plates a half century ago (Troitsky, 1976). The earliest published work found was presented by Bryan in 1891.

Based on the classical plate theory, Timoshenko and Gere (1961) presented numerical tables for buckling coefficients of rectangular plates, stiffened by longitudinal and lateral stiffeners. Experimental investigations have been carried out on graphite/epoxy laminated stiffened plates (Williams and Stein, 1976; Starnes *et al.*, 1985.

Habib and Nahas (1997) have investigated, experimentally and analytically, the buckling of glass/polyster composite stiffened panels, with Z-shape/Angle stiffeners, under uniaxial compression. The finite strip method has been applied for the stability analysis of composite blade stiffened panels under in-plane loads (Cheung, 1976; Loughland and Delaunoy, 1993). Guo *et al.* (2002) developed a layerwise finite element formulation, and made a buckling analysis of stiffened laminated plates.

In this chapter, ASM is applied to the buckling analysis of antisymmetric cross-ply and angle-ply stiffened laminated composite plate (Figure 6.1), with bending-extension coupling.

6.2 Buckling Analysis

For an antisymmetric cross-ply or angle-ply plate subjected to in-plane loads N_x and/or N_y (Figure 6.1) per unit width, the governing Equation 2.13 can be written as (Reddy, 2004):

$$A_1 \frac{\partial^8 \Phi}{\partial x^8} + A_3 \frac{\partial^8 \Phi}{\partial x^6 \partial y^2} + A_5 \frac{\partial^8 \Phi}{\partial x^4 \partial y^4} + A_7 \frac{\partial^8 \Phi}{\partial x^2 \partial y^6} + A_9 \frac{\partial^8 \Phi}{\partial y^8} = -N_x \frac{\partial^2 w}{\partial x^2} - N_y \frac{\partial^2 w}{\partial y^2} \quad (6.1)$$

For an antisymmetric cross-ply plate, w can be written as:

$$w = a_7 \frac{\partial^4 \Phi}{\partial x^4} + a_8 \frac{\partial^4 \Phi}{\partial x^2 \partial y^2} + a_9 \frac{\partial^4 \Phi}{\partial y^4} \quad (2.16)$$

Equation 6.1 can be written as:

$$\begin{aligned} & A_1 \frac{\partial^8 \Phi}{\partial x^8} + A_3 \frac{\partial^8 \Phi}{\partial x^6 \partial y^2} + A_5 \frac{\partial^8 \Phi}{\partial x^4 \partial y^4} + A_7 \frac{\partial^8 \Phi}{\partial x^2 \partial y^6} + A_9 \frac{\partial^8 \Phi}{\partial y^8} \\ & + N_x \left(a_7 \frac{\partial^6 \Phi}{\partial x^6} + a_8 \frac{\partial^6 \Phi}{\partial x^4 \partial y^2} + a_9 \frac{\partial^6 \Phi}{\partial x^2 \partial y^4} \right) \\ & + N_y \left(a_7 \frac{\partial^6 \Phi}{\partial x^4 \partial y^2} + a_8 \frac{\partial^6 \Phi}{\partial x^2 \partial y^4} + a_9 \frac{\partial^6 \Phi}{\partial y^6} \right) = 0 \end{aligned} \quad (6.2)$$

6.3 Method of Solution

Using a similar procedure as used in 5.3, for strip I , the characteristic equation of Equation 6.2 is:

$$\begin{aligned} & (A_1 \gamma_m^8 - A_3 \gamma_m^6 + A_5 \gamma_m^4 - A_7 \gamma_m^2 + A_9) \beta_m^8 \\ & - \left[N_x (-a_7 \gamma_m^6 + a_8 \gamma_m^4 - a_9 \gamma_m^2) + N_y (a_7 \gamma_m^4 - a_8 \gamma_m^2 + a_9) \right] \beta_m^6 = 0 \end{aligned} \quad (6.3)$$

Since $\beta_m = \frac{m\pi}{b} \neq 0$, $m = 1, 2, \dots, \infty$, Equation 6.3 leads to:

$$A_1^* \gamma_n^8 - A_3^* \gamma_n^6 + A_5^* \gamma_n^4 - A_7^* \gamma_n^2 + A_9^* = 0 \quad (6.4)$$

in which,

$$A_1^* = A_1 \quad (6.5a)$$

$$A_3^* = A_3 - \frac{1}{\beta_m^2} a_7 N_x \quad (6.5b)$$

$$A_5^* = A_5 - \frac{1}{\beta_m^2} (a_8 N_x + a_7 N_y) \quad (6.5c)$$

$$A_7^* = A_7 - \frac{1}{\beta_m^2} (a_9 N_x + a_8 N_y) \quad (6.5d)$$

$$A_9^* = A_9 - \frac{1}{\beta_m^2} a_9 N_y \quad (6.5e)$$

The corresponding coefficients A_1^* , A_3^* , A_5^* , A_7^* , and A_9^* , for an antisymmetric

angle-ply plate, are obtained by replacing a_7 , a_8 , and a_9 with b_7 , b_8 , and b_9 respectively (Equation 2.30).

Similarly to 5.3, Equation 6.4 can be reduced to a quartic equation and leads to the following general expression for strip I solution, $\phi_{ml}(x)$

$$\begin{aligned} \phi_{ml}(x) = & [C_{1ml} \cosh(\gamma_{1ml} \beta_{ml} x) + C_{2ml} \sinh(\gamma_{1ml} \beta_{ml} x)] \cos(\gamma_{2ml} \beta_{ml} x) \\ & + [C_{3ml} \cosh(\gamma_{1ml} \beta_{ml} x) + C_{4ml} \sinh(\gamma_{1ml} \beta_{ml} x)] \sin(\gamma_{2ml} \beta_{ml} x) \\ & + [C_{5ml} \cosh(\gamma_{3ml} \beta_{ml} x) + C_{6ml} \sinh(\gamma_{3ml} \beta_{ml} x)] \cos(\gamma_{4ml} \beta_{ml} x) \\ & + [C_{7ml} \cosh(\gamma_{3ml} \beta_{ml} x) + C_{8ml} \sinh(\gamma_{3ml} \beta_{ml} x)] \sin(\gamma_{4ml} \beta_{ml} x) \end{aligned} \quad (6.6)$$

For a rectangular plate, with N -plate strips (Figure 6.1), which depends on the number of beams and material/geometric discontinuities, all the boundary and continuity conditions in (3.39) through (3.43) and (4.5) through (4.7) can be expressed in terms of constants C_{dml} ($d = 1, 2, \dots, 8; I = 1, 2, \dots, N$) and the roots of Equation 6.4. The constants C_{dml} ($d = 1, 2, \dots, 8; I = 1, 2, \dots, N$) are determined for each mode of plate m ($m = 1, 2, \dots, \infty$).

The coefficients of Equation 6.4 contain three unknowns, N_x , N_y , and m . m is fixed *a priori* and it is identified with the number of half-waves along y -direction deformation; it takes integer value, depending on the mode of deformation. If $N_x = 0$, it is uniaxial compression by N_y . If $N_y = 0$, it is uniaxial compression by N_x . For a biaxial compression, assume $N_y = k_N N_x$, k_N is fixed *a priori* and can be any number. Substitution of solution $\phi_m(x)$, given by Equation 6.6 in a set of eight boundary, and continuity conditions, leads to a set of $8N$ algebraic equations.

The determinant of the coefficients C_{dml} ($d = 1, 2, \dots, 8; I = 1, 2, \dots, N$), set to zero, leads to a transcendental equation in N_x/N_y and m . The elements of this equation contain N_x/N_y and m as unknowns. For a given integer value of m , the value of N_x/N_y which makes this determinant zero, is obtained by a method of hit and trial that involves a bisection search strategy. The minimum value of N_x/N_y which satisfies this condition is the critical buckling load, $N_{x_{cr}} / N_{y_{cr}}$. A MATLAB program is then written to obtain the critical value of N_x/N_y , for antisymmetric angle-ply and cross-ply plates, with various aspect ratios, ply-orientation angles and any number of layers.

6.4 Application

For illustrative purpose the numerical applications address verifications of the beam/stiffener boundary condition and supports inside the plate. All the layers are assumed to be of the same thickness and density, and they are made of the same orthotropic material. The plates with 2 layers and 10 layers are analyzed for all examples.

When comparing the results of the ASM solution, with those obtained from the finite element program ANSYS (ANSYS, Inc., 2007), an 8-node quadrilateral linear-layered structural shell element (Shell99) is used to model the laminated plates.

6.4.1 Example 1: Effects of aspect ratio (a/b), beam rigidity (KI) and number of layers

(n) on the dimensionless uniaxial buckling load $\left[\bar{N}_y = \left(\frac{b^2}{E_2 h^3} \right) N_y \right]$ and bi-axial

buckling loads $\left[\bar{N}_y = \bar{N}_x = \left(\frac{b^2}{E_2 h^3} \right) N_x \right]$

An antisymmetric cross-ply rectangular plate ($0^\circ/90^\circ/0^\circ/90^\circ\dots$, $a/b = 0.5, 1, 2, 3, 5$), having a width in the y -direction to plate thickness ratio $b/h = 1000$, simply supported on $y = 0$ and $y = b$, beam supported at $x = 0$ and $x = a$, is used for this study. The material properties are: $\frac{E_1}{E_2} = 20$, $\frac{G_{12}}{E_2} = \frac{G_{13}}{E_2} = 0.6$, $\frac{G_{23}}{E_2} = 0.5$, $\nu_{12} = 0.25$.

Table 6.1 illustrates effects of aspect ratio (a/b), beam rigidity (KI), and number of layers (n) on dimensionless of a uniaxial buckling load (\bar{N}_y) of a rectangular cross-ply plate ($0/90/0/90/\dots$). For given beam rigidity (KI) and plate layer (n), \bar{N}_y decreases as aspect ratio (a/b) increases. So, when a/b increases, plate stiffness decreases; \bar{N}_y decreases as well. For given aspect ratio (a/b) and plate layer (n), \bar{N}_y increases as beam rigidity, KI , increases. The stronger KI gets, the stiffer the plate becomes. As a result, \bar{N}_y increases as well. For given KI and aspect ratio (a/b), \bar{N}_y in 10-layer plate is always greater than \bar{N}_y in 2-layer plate.

The bending-extension coupling effect for 2-layer laminated plate is greater than

the bending-extension coupling effect for 10-layer laminated plate. A stronger bending-extension coupling effect lowers \bar{N}_y . KI demonstrates greater effect when a/b is smaller. We can see greater differences from \bar{N}_y among different beam rigidities, when a/b equals 0.5. On the other hand, at the greatest value of a/b , $a/b = 5$, for example, \bar{N}_y maintains approximately the same value, when KI changes from 0.6 to 80. That means when a/b is equal to or greater than a certain value, the effect of boundary beams vanishes.

The difference $\left(100 \frac{\bar{N}_{y,ANSYS} - \bar{N}_{y,ASM}}{\bar{N}_{y,ASM}} \right)$ between results obtained by ASM and by

ANSYS decreases as a/b increases. When a/b is equal to 0.5, this difference reaches 5.11%; when a/b is equal to 5, they are smaller than or equal to 0.60%. When $a/b \leq 1$, the results obtained by ASM and by ANSYS are not very well matched. The maximum difference between them reaches 5.11%, which happens when $a/b = 0.5$, $KI = 0.6$, and $n = 2$, because boundary restriction on beam rotary and warping increases the side effect on laminated plate in the ANSYS model. As the beam stiffness increases or a/b ratio increases, the side effect from boundary restriction is dominated by the beam, or it is ignored by the larger plate size a . That is why the differences are reduced to less than 3.0% when $a/b = 0.5$ and $KI \geq 40$, and to less than 0.61% when $a/b = 5$.

A similar situation exists for bi-axial buckling loads. Table 6.2 lists bi-axial buckling loads when \bar{N}_x is equal to \bar{N}_y . Comparing Table 6.2 with Table 6.1, the loads under the bi-axial condition are always lesser than ones under a uniaxial condition.

From Tables 6.1 and 6.2, we can see marked differences between the uniaxial buckling load and bi-axial buckling load, when a/b is small, say $a/b = 0.5$ or 1.0. On the other hand, difference is getting smaller when a/b increases (see Tables 6.1 and 6.2). This means that short direction, y -axial for this case, controls bi-axial load when a/b gets bigger.

6.4.2 Example 2: Effects of orthotropy ratio (E_1/E_2), beam rigidity (KI) and number of layers (n) on the dimensionless uniaxial buckling load $\left[\bar{N}_y = \left(\frac{b^2}{E_2 h^3} \right) N_y \right]$

An antisymmetric angle-ply square plate ($45^\circ/-45^\circ/45^\circ/-45^\circ\dots$, $a/b = 1$), having a width in the x -direction to plate thickness ratio $a/h = 1000$, simply supported on $y = 0$ and $y = b$, beam supported at $x = 0$ and $x = a$, is used for this study. The material properties are: $\frac{E_1}{E_2} = 3, 10, 20, 30, \text{ and } 40$, $\frac{G_{12}}{E_2} = \frac{G_{13}}{E_2} = 0.6$, $\frac{G_{23}}{E_2} = 0.5$, $\nu_{12} = 0.25$.

Table 6.3 illustrates effects of orthotropy ratio (E_1/E_2), beam rigidity, KI , and number of layers, n , on \bar{N}_y of a square angle-ply plate ($45^\circ/-45^\circ/45^\circ/-45^\circ\dots$). For given KI and n , \bar{N}_y increases as orthotropy ratio (E_1/E_2) increases. This is true when E_1/E_2 increases, and when plate stiffness increases, so does the \bar{N}_y . For given orthotropy ratio, E_1/E_2 , and plate layer (n), \bar{N}_y increases as KI increases. The stronger KI reinforces the plate and makes it stiffer. As a result, \bar{N}_y increases as well. For given KI and E_1/E_2 , \bar{N}_y of 10-layer plate is always greater than \bar{N}_y of 2-layer plate.

The bending-extension coupling effect for a 2-layer laminated plate is greater than the bending-extension coupling effect for 10-layer laminated plate. The stronger bending-extension coupling effect lowers \bar{N}_y . This effect becomes more evident when E_1/E_2 increases. When E_1/E_2 equals 3, there are only small differences, *i.e.* from 6.00% to 18.89%, when KI varies from 1 to 80, between dimensionless uniaxial buckling loads for plates with 10 layers and those with 2 layers. On the other hand, when E_1/E_2 equals 40, there are larger differences, *i.e.* from 89.27% to 193.08%, when KI varies from 1 to 80, between dimensionless buckling loads with 10 layers and with 2 layers. This shows a stronger bending-extension coupling effect, when orthotropy ratio (E_1/E_2) increases.

6.4.3 Example 3: Effects of ply angle (θ) and number of layers (n) on the dimensionless

uniaxial buckling load $\left[\bar{N}_y = \left(\frac{b^2}{E_2 h^3} \right) N_y \right]$

An antisymmetric angle-ply rectangular plate ($\theta/-\theta/\theta/-\theta/...$, $a/b = 2$), having a width in the y -direction to plate thickness ratio $b/h = 1000$, simply supported on $y = 0$ and $y = b$, three beams with $KI = 1$ supported at $x = 0$, $x = a/2$ and $x = a$, is used in this example. The material properties are: $\frac{E_1}{E_2} = 20$, $\frac{G_{12}}{E_2} = \frac{G_{13}}{E_2} = 0.6$, $\frac{G_{23}}{E_2} = 0.5$, $\nu_{12} = 0.25$.

Table 6.4 illustrates the effects of ply angle, θ , and number of layers, n , on \bar{N}_y of a rectangular angle-ply plate ($\theta/-\theta/\theta/-\theta/...$). \bar{N}_y varies as the ply angle changes. For 2-layer laminated plate, the minimum value of \bar{N}_y occurs at ply-orientation angle $\theta = 50^\circ$; whereas for 10-layer laminated plate, the maximum value of \bar{N}_y occurs at ply-orientation angle $\theta = 65^\circ$. For a given ply angle, \bar{N}_y for a 10-layer plate is greater than one for 2-layer plate, except at points where $\theta = 0^\circ$ or $\theta = 90^\circ$ when they are the same values.

Because boundary restriction on beam rotary and warping has a strong side effect when the ply-orientation angle decreases in the ANSYS model, the maximum difference between results obtained by ASM and by ANSYS reaches 6.97%; this occurs at the ply-orientation angle $\theta = 0^\circ$ for the 10-layer plate. Conversely, the minimum difference between results obtained by ASM and by ANSYS reaches 0.01% when the ply-orientation angle $\theta = 75^\circ$, for a 10-layer plate.

6.4.4 Maximizing dimensionless uniaxial buckling load $\left[\bar{N}_y = \left(\frac{b^2}{E_2 h^3} \right) N_y \right]$ by

varying inside beam position for cross-ply ($0/90/0/90/...$) and angle-ply ($\theta/-\theta/\theta/-\theta/...$) laminated plates with varied boundary conditions

Antisymmetric cross-ply ($a/b = 1$ and $a/b = 2.5$) and antisymmetric angle-ply ($a/b = 2.5$) laminated plates, having a width in the y -direction to plate thickness ratio b/h

= 1000, simply supported on $y = 0$ and $y = b$, with varied boundary conditions at $x = 0$ and $x = a$, are used in this example. The material properties are: $\frac{E_1}{E_2} = 20$, $\frac{G_{12}}{E_2} = \frac{G_{13}}{E_2} = 0.6$, $\frac{G_{23}}{E_2} = 0.5$, $\nu_{12} = 0.25$.

Figure 6.2 shows the boundary condition and beam layout, and it displays searching results by varying inside beam position for a cross-ply square plate in a maximizing procedure. Inside beam position has an effect on \bar{N}_y of a plate. These positions are different when laminated plates have different layers. The maximum dimensionless uniaxial buckling load, $\bar{N}_{y,\max}$ for 2-layer plate is 29.382, and this occurs at $x_b/b = 0.56$; whereas $\bar{N}_{y,\max}$ for 10-layer plate is 37.806, and it occurs at $x_b/b = 0.60$. It is reasonable that the position for the inside beam is not at $a/2$, since the beam on the left boundary is much stronger, $KI = 2.0$, than beam on the right boundary, $KI = 0.6$.

Further maximizing results for \bar{N}_y for a cross-ply rectangular plate ($a/b = 2.5$), with different boundary conditions at $x = 0$ and $x = a$, are shown in Table 6.5. For the same layer plate, with the weakest boundary condition, *i.e.* free boundary condition the maximized \bar{N}_y is the smallest, 7.270 and 13.848, for 2-layer and 10-layer plates respectively. The positions of inside beams are closest to boundaries, $x_b/b = 0.58$ and $x_b/b = 0.56$, for 2-layer and 10-layer plates respectively.

When boundary conditions at both sides $x = 0$ and $x = a$ increase, from $KI = 0.6$ to the clamped condition, the maximized \bar{N}_y increases. Under the clamped condition, the maximized dimensionless uniaxial buckling loads are 15.951 and 24.120, for 2-layer and 10-layer plates respectively. At this time, the positions of the inside beams are the farthest away from boundaries. They are $x_b/b = 0.91$ and $x_b/b = 0.97$, for 2-layer and 10-layer plates respectively. Similar to the results in Figure 6.2, the inside-beam positions, where \bar{N}_y is maximized, are different for 2-layer and 10-layer plates under the same boundary condition.

More interesting results are illustrated in Table 6.6 for angle-ply rectangular plate ($a/b = 2.5$) with a beam supported boundary condition at $x = 0$ and $x = a$. For any given

layer, $\bar{N}_{y,\max}$ is not only inside beam position dependent, but also ply-angle dependent. The larger the ply angle, the smaller x_b/b . For the same ply angle, the biggest difference of dimensionless uniaxial buckling loads between 2-layer and 10-layer plates is 53.99% $\left(100 \frac{\bar{N}_{y,10} - \bar{N}_{y,2}}{\bar{N}_{y,2}}\right)$. At this point, the dimensionless uniaxial buckling loads are 14.663 under $x_b/b = 0.87$ for 2-layer plate, and 22.580 under $x_b/b = 0.88$ for 10-layer plate; this occurs at $\theta = 65^\circ$. At two end points, where $\theta = 0^\circ$ or $\theta = 90^\circ$, there are no differences between dimensionless uniaxial buckling loads with 10- and 2-layer laminated plates, since the bending-extension coupling effect is 0.

6.5 Summary and Conclusions

An analytical method, ASM, is extended to the buckling analysis for antisymmetric laminated composite plates in this chapter. The results obtained using ASM are compared with ones obtained by using ANSYS (ANSYS, Inc., 2007). The examples show that there is big difference between uniaxial and bi-axial ($\bar{N}_x = \bar{N}_y$) buckling loads, when the aspect ratio (a/b) is small, *i.e.* $a/b = 0.5$. However, they are close to each other when the aspect ratio (a/b) is greater, *i.e.* $a/b = 5$. This indicates that short direction, y -axial for this case, controls bi-axial load when a/b increases.

As the beam rigidity increases, or as the orthotropy ratio increases, \bar{N}_y also rises. On the other hand, as aspect ratio increases, \bar{N}_y declines. Due to bending-extension coupling effect, for a given beam rigidity, aspect ratio of the plate, orthotropy ratio of the plate and ply angle (for angle-ply plate), \bar{N}_y with 10 layers is always greater than one with 2 layers except at the points $\theta = 0^\circ$ or $\theta = 90^\circ$ where there are not bending-extension coupling effect.

The proposed method, ASM, can be easily used to maximize \bar{N}_y for antisymmetric stiffened laminated composite plates. For given laminated plate and stiffener, the maximum \bar{N}_y depends on the stiffener's position and ply-orientation angle (for angle-ply plate). The inside stiffener positions, where buckling load is maximized, are different for 2-layer and 10-layer laminated plates under prescribed conditions. As

expected, and similar to situations of free vibration, the clamped boundary condition provides the strongest stiffening effect, and the free boundary condition has the weakest stiffening effect. It is evident that the various solutions trend to be independent of the number of layers at extreme values of ply-orientation angles owing to the absence of coupling stiffness ($B_{ij} = 0$ at $\theta = 0^\circ$ and $\theta = 90^\circ$ for antisymmetric laminated angle-ply plate).

Table 6.1. Effects of aspect ratio (a/b), beam rigidity (KI) and number of layers (n) on the dimensionless uniaxial buckling load (\bar{N}_y^1) of a rectangular cross-ply laminated plate ($0^\circ/90^\circ/0^\circ/90^\circ/\dots$, $b/h = 1000$, $E_1/E_2=20$, $G_{12} = G_{13} = 0.6E_2$, $G_{23} = 0.5E_2$, $\nu_{12} = 0.25$)

KI	Method	a/b									
		0.5		1		2		3		5	
		$n = 2$	$n = 10$	$n = 2$	$n = 10$	$n = 2$	$n = 10$	$n = 2$	$n = 10$	$n = 2$	$n = 10$
0.6	ASM ²	38.133	41.937	13.090	19.628	4.722	9.556	3.278	7.097	2.578	5.693
	ANSYS ³	40.080	43.840	13.680	20.570	4.767	9.508	3.283	7.070	2.593	5.708
	Diff. (%) ⁴	5.11	4.54	4.50	4.80	0.94	-0.51	0.16	-0.38	0.60	0.27
1	ASM	55.493	63.441	15.763	25.558	4.983	10.552	3.346	7.412	2.591	5.764
	ANSYS	57.730	65.580	16.410	26.570	5.060	10.480	3.357	7.377	2.606	5.778
	Diff. (%)	4.03	3.37	4.10	3.96	1.54	-0.68	0.34	-0.47	0.58	0.24
2	ASM	80.568	110.11	19.030	34.824	5.233	11.669	3.407	7.728	2.603	5.830
	ANSYS	82.900	112.50	19.800	36.160	5.332	11.520	3.421	7.677	2.617	5.842
	Diff. (%)	2.89	2.17	4.04	3.84	1.89	-1.28	0.40	-0.66	0.55	0.21
10	ASM	82.497	199.40	22.100	51.702	5.482	12.999	3.466	8.066	2.614	5.895
	ANSYS	85.070	200.40	22.790	53.290	5.593	12.680	3.479	7.980	2.627	5.903
	Diff. (%)	3.12	0.50	3.12	3.07	2.03	-2.45	0.38	-1.07	0.52	0.13
40	ASM	82.870	201.77	22.182	53.532	5.534	13.316	3.478	8.142	2.616	5.910
	ANSYS	85.060	201.40	22.930	54.870	5.646	12.930	3.490	8.042	2.629	5.916
	Diff. (%)	2.64	-0.18	3.37	2.50	2.02	-2.90	0.34	-1.23	0.51	0.11
80	ASM	82.932	202.17	22.196	53.622	5.543	13.372	3.480	8.155	2.616	5.912
	ANSYS	85.150	201.70	22.940	54.760	5.656	12.970	3.492	8.052	2.630	5.918
	Diff. (%)	2.67	-0.23	3.35	2.12	2.03	-3.00	0.34	-1.26	0.53	0.10

$$^1 \bar{N}_y = \frac{N_y b^2}{E_2 h^3}$$

² ASM - Analytical Strip Method (present method)

³ ANSYS - Finite Element Analysis program (ANSYS Inc., 2007)

$$^4 \text{Diff. (\%)} = \left(100 \frac{\bar{N}_{ANSYS} - \bar{N}_{ASM}}{\bar{N}_{ASM}} \right)$$

Table 6.2. Effects of aspect ratio (a/b), beam rigidity (KI) and number of layers (n) on the dimensionless bi-axial buckling loads ($\bar{N}_x = \bar{N}_y$ ¹) of a rectangular cross-ply laminated plate ($0^\circ/90^\circ/0^\circ/90^\circ/\dots$, $b/h = 1000$, $E_1/E_2=20$, $G_{12} = G_{13} = 0.6E_2$, $G_{23} = 0.5E_2$, $\nu_{12} = 0.25$)

KI	Method	a/b									
		0.5		1		2		3		5	
		$n = 2$	$n = 10$	$n = 2$	$n = 10$	$n = 2$	$n = 10$	$n = 2$	$n = 10$	$n = 2$	$n = 10$
0.6	ASM ²	23.901	33.741	8.667	15.853	3.948	8.500	2.989	6.631	2.485	5.524
	ANSYS ³	24.800	35.310	8.957	16.600	4.084	8.668	3.022	6.687	2.507	5.573
	Diff. (%) ⁴	3.76	4.65	3.35	4.71	3.43	1.98	1.10	0.84	0.87	0.89
1	ASM	28.173	44.028	9.465	18.733	4.073	9.085	3.028	6.836	2.494	5.574
	ANSYS	28.970	46.030	9.649	19.340	4.228	9.213	3.062	6.874	2.515	5.616
	Diff. (%)	2.83	4.55	1.94	3.24	3.80	1.41	1.13	0.56	0.85	0.76
2	ASM	32.587	60.078	10.186	22.107	4.184	9.677	3.062	7.031	2.501	5.619
	ANSYS	32.790	59.150	10.260	21.860	4.355	9.739	3.097	7.046	2.522	5.655
	Diff. (%)	0.62	-1.54	0.72	-1.12	4.09	0.64	1.16	0.21	0.83	0.64
10	ASM	36.566	80.870	10.826	25.639	4.284	10.280	3.092	7.226	2.508	5.662
	ANSYS	35.530	78.250	10.870	24.950	4.477	10.260	3.129	7.212	2.528	5.691
	Diff. (%)	-2.83	-3.24	0.40	-2.69	4.50	-0.19	1.19	-0.19	0.81	0.51
40	ASM	37.302	84.714	10.951	26.339	4.304	10.407	3.098	7.267	2.509	5.671
	ANSYS	36.030	81.660	11.040	25.390	4.506	10.370	3.136	7.247	2.530	5.698
	Diff. (%)	-3.41	-3.60	0.82	-3.60	4.68	-0.36	1.21	-0.27	0.84	0.48
80	ASM	37.423	85.325	10.971	26.455	4.308	10.429	3.099	7.274	2.509	5.672
	ANSYS	36.080	81.970	11.080	25.480	4.512	10.390	3.137	7.253	2.530	5.699
	Diff. (%)	-3.59	-3.93	0.99	-3.69	4.74	-0.37	1.21	-0.28	0.83	0.47

$$^1 \bar{N}_x = \frac{N_y b^2}{E_2 h^3} \quad \bar{N}_y = \frac{N_x b^2}{E_2 h^3}$$

² ASM - Analytical Strip Method (present method)

³ ANSYS - Finite Element Analysis program (ANSYS Inc., 2007)

$$^4 \text{Diff. (\%)} = \left(100 \frac{\bar{N}_{ANSYS} - \bar{N}_{ASM}}{\bar{N}_{ASM}} \right)$$

Table 6.3. Effects of in-plane orthotropy ratio (E_1/E_2), beam rigidity (KI) and number of layers (n) on the dimensionless uniaxial buckling load (\bar{N}_y^1) of a square angle-ply laminated plate ($45^\circ/-45^\circ/45^\circ/-45^\circ\dots$, $b/h = 1000$, $G_{12} = G_{13} = 0.6E_2$, $G_{23} = 0.5E_2$, $\nu_{12} = 0.25$)

KI	Method	E_1/E_2									
		3		10		20		30		40	
		n = 2	n = 10	n = 2	n = 10	n = 2	n = 10	n = 2	n = 10	n = 2	n = 10
1	ASM ²	4.801	5.089	10.120	13.716	15.763	25.558	20.827	37.128	25.640	48.529
	ANSYS ³	4.667	5.062	10.560	14.040	16.410	26.570	21.470	38.720	26.570	50.670
	Diff. (%) ⁴	-2.78	-0.52	4.34	2.36	4.10	3.96	3.09	4.29	3.63	4.41
5	ASM	8.829	9.996	15.099	25.185	21.937	45.993	28.346	66.155	34.629	85.787
	ANSYS	9.165	10.470	15.670	26.110	22.650	47.480	29.420	68.800	35.300	89.300
	Diff. (%)	3.80	4.74	3.78	3.67	3.25	3.23	3.79	4.00	1.94	4.09
10	ASM	9.956	11.512	15.536	28.320	22.100	51.702	29.832	74.601	34.802	97.076
	ANSYS	10.410	12.050	16.100	29.290	22.790	53.290	29.470	78.920	35.290	101.60
	Diff. (%)	4.56	4.68	3.63	3.43	3.12	3.07	-1.21	5.79	1.40	4.66
20	ASM	10.132	12.033	15.581	29.070	22.155	53.353	28.544	77.614	34.882	101.86
	ANSYS	10.600	12.510	16.130	29.950	22.860	54.720	29.360	79.210	35.170	102.00
	Diff. (%)	4.62	3.97	3.52	3.03	3.18	2.56	2.86	2.06	0.82	0.14
30	ASM	10.148	12.058	15.597	29.132	22.173	53.472	28.566	77.793	34.909	102.10
	ANSYS	10.650	12.520	16.140	30.100	22.910	54.820	29.300	79.220	35.080	101.90
	Diff. (%)	4.95	3.83	3.48	3.32	3.32	2.52	2.57	1.83	0.49	-0.20
40	ASM	10.156	12.070	15.604	29.163	22.182	53.532	28.578	77.884	34.923	102.23
	ANSYS	10.680	12.530	16.150	30.140	22.930	54.870	29.260	79.190	35.030	101.80
	Diff. (%)	5.16	3.81	3.50	3.35	3.37	2.50	2.39	1.68	0.31	-0.42
80	ASM	10.168	12.089	15.616	29.210	22.196	53.622	28.594	78.019	34.943	102.41
	ANSYS	10.710	12.540	16.160	30.180	22.940	54.760	29.170	79.050	34.910	101.60
	Diff. (%)	5.33	3.73	3.48	3.32	3.35	2.12	2.01	1.32	-0.09	-0.79

$$^1 \bar{N}_y = \frac{N_y b^2}{E_2 h^3}$$

² ASM - Analytical Strip Method (present method)

³ ANSYS - Finite Element Analysis program (ANSYS Inc., 2007)

$$^4 \text{Diff. (\%)} = \left(100 \frac{\bar{N}_{ANSYS} - \bar{N}_{ASM}}{\bar{N}_{ASM}} \right)$$

Tab 6.4. Effects of ply angle (θ) and number of layers (n) on the dimensionless uniaxial buckling load (\bar{N}_y ¹) of a rectangular angle-ply laminated plate ($a/b = 2$, $b/h = 1000$, $E_1/E_2=20$, $G_{12} = G_{13} = 0.6E_2$, $G_{23} = 0.5E_2$, $\nu_{12} = 0.25$) with beams at $x = 0$, $x = a/2$ and $x = a$ respectively, $KI = 1$ for all 3 beams

Angle (θ)	2 Layers			10 Layers		
	ASM ²	ANSYS ³	Diff.(%) ⁴	ASM	ANSYS	Diff.(%)
0	16.881	18.040	6.87	16.881	18.060	6.99
5	16.629	17.660	6.20	16.933	17.980	6.19
10	16.037	16.980	5.88	17.097	18.010	5.34
15	15.390	16.290	5.85	17.378	18.380	5.77
20	14.853	15.590	4.96	17.769	18.570	4.51
25	14.460	15.130	4.63	18.268	19.060	4.34
30	14.189	14.790	4.24	18.871	19.660	4.18
35	14.008	14.490	3.44	19.578	20.190	3.12
40	13.891	14.340	3.23	20.376	21.010	3.11
45	13.821	14.170	2.52	21.235	21.760	2.47
50	13.793	14.040	1.79	22.099	22.400	1.36
55	13.807	14.050	1.76	22.887	23.150	1.15
60	13.883	14.030	1.06	23.498	23.710	0.90
65	14.096	13.950	-1.04	23.828	24.010	0.76
70	14.634	14.280	-2.42	23.804	23.990	0.78
75	15.782	15.310	-2.99	23.428	23.430	0.01
80	17.834	17.270	-3.16	22.835	22.730	-0.46
85	20.571	19.870	-3.41	22.299	22.150	-0.67
90	22.090	21.830	-1.18	22.090	21.940	-0.68

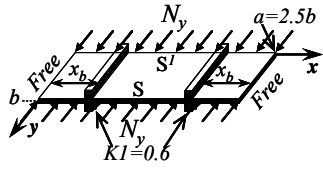
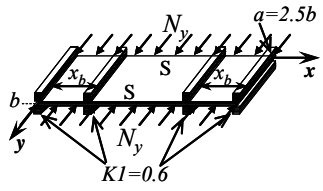
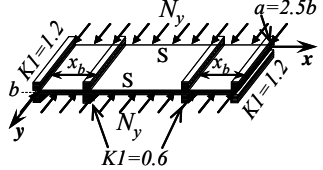
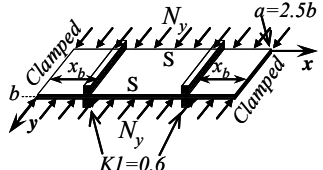
$$^1 \bar{N}_y = \frac{N_y b^2}{E_2 h^3}$$

² ASM - Analytical Strip Method (present method)

³ ANSYS - Finite Element Analysis program (ANSYS Inc., 2007)

$$^4 \text{Diff. (\%)} = \left(100 \frac{\bar{N}_{ANSYS} - \bar{N}_{ASM}}{\bar{N}_{ASM}} \right)$$

Table 6.5. Effect of boundary condition and positions of two inside beams on maximized dimensionless uniaxial buckling load for a rectangular cross-ply laminated plate ($0^\circ/90^\circ/0^\circ/90^\circ/\dots$, $b/h = 1000$, $E_1/E_2=20$, $G_{12} = G_{13} = 0.6E_2$, $G_{23} = 0.5E_2$, $\nu_{12} = 0.25$)

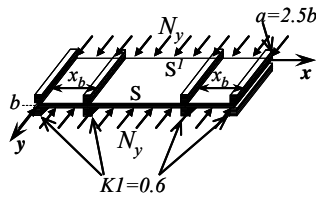
Boundary Condition	2 Layers		10 Layers	
	$\bar{N}_{y,\max}^2$	x_b/b	$\bar{N}_{y,\max}$	x_b/b
	7.270	0.58	13.848	0.56
	13.949	0.86	20.439	0.88
	14.813	0.88	21.813	0.92
	15.951	0.91	24.120	0.97

¹ S – Simply Supported

$$^2 \bar{N}_y = \frac{N_y b^2}{E_2 h^3}$$

Table 6.6. Effect of ply angle and positions of two inside beams on maximized dimensionless uniaxial buckling load, \bar{N}_y for a rectangular angle-ply laminated plate ($\theta/-\theta/\theta/-\theta/\dots$, $b/h = 1000$, $E_1/E_2=20$, $G_{12} = G_{13} = 0.6E_2$, $G_{23} = 0.5E_2$, $\nu_{12} = 0.25$) with two boundary beams at $x = 0$ and $x = a$

Angle (θ)	2 Layers		10 Layers	
	$\bar{N}_{y,\max}^2$	x_b/b	$\bar{N}_{y,\max}$	x_b/b
0	13.483	0.90	13.483	0.90
5	13.405	0.90	13.522	0.90
10	13.227	0.89	13.643	0.90
15	13.041	0.89	13.855	0.90
20	12.909	0.88	14.169	0.90
25	12.845	0.88	14.605	0.90
30	12.848	0.88	15.185	0.90
35	12.915	0.87	15.927	0.90
40	13.043	0.87	16.841	0.90
45	13.219	0.88	17.913	0.90
50	13.464	0.87	19.104	0.89
55	13.766	0.87	20.347	0.89
60	14.150	0.87	21.542	0.89
65	14.663	0.87	22.580	0.88
70	15.441	0.87	23.344	0.87
75	16.760	0.87	23.757	0.86
80	18.967	0.87	23.834	0.85
85	21.958	0.85	23.745	0.85
90	23.685	0.85	23.685	0.85



¹ S – Simply Supported

$$^2 \bar{N}_y = \frac{N_y b^2}{E_2 h^3}$$

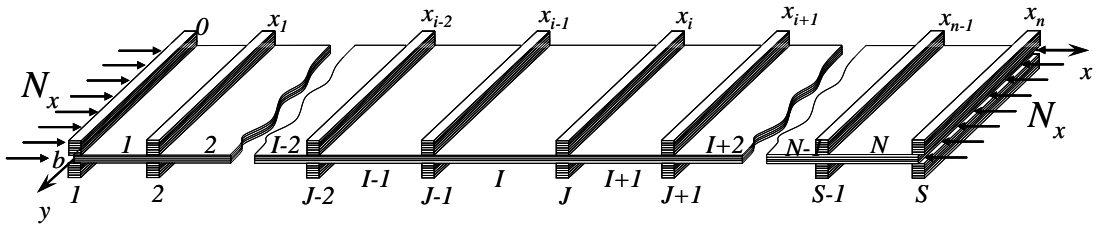


Figure 6.1a. Stiffened plate subject to in-plane loads N_x

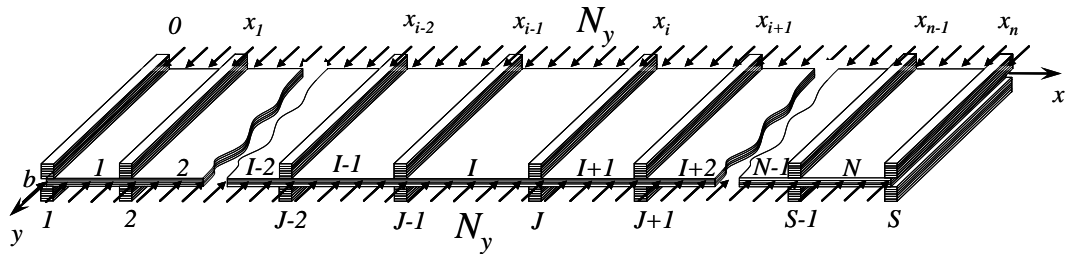


Figure 6.1b. Stiffened plate subject to in-plane loads N_y

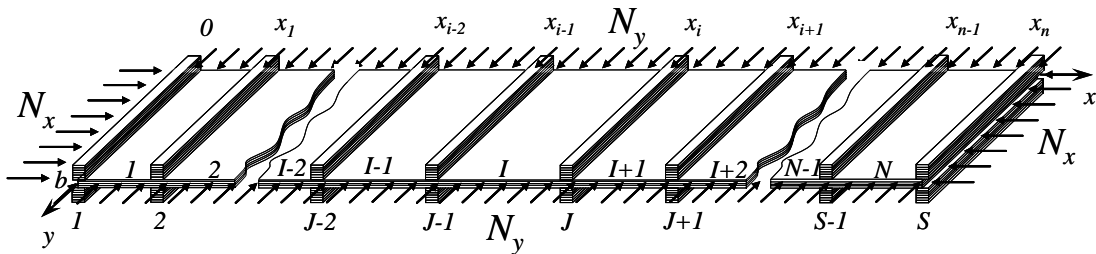


Figure 6.1c. Stiffened plate subject to in-plane loads N_x and N_y

Figure 6.1. Stiffened plate subject to in-plane loads

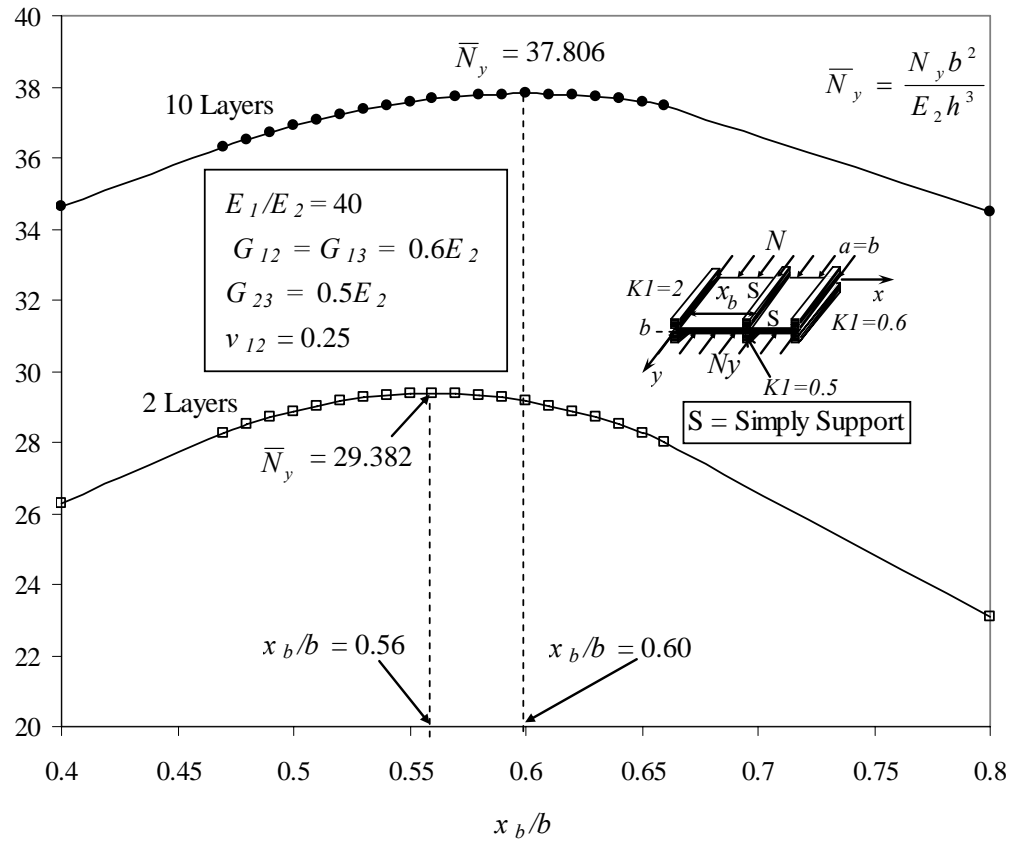


Figure 6.2. Maximizing dimensionless uniaxial buckling load (\bar{N}_y) by varying inside beam position for a square cross-ply laminated plate ($0^\circ/90^\circ/0^\circ/90^\circ/\dots$, $b/h = 1000$) with two boundary beams at $x = 0$ and $x = a$

CHAPTER 7

CONCLUSIONS AND FURTHER RESEARCH NEEDS

7.1 General Summary

An Analytical Strip Method (ASM) has been presented for the bending, free vibration and buckling of antisymmetric cross-ply and angle-ply laminated plates. Whenever possible, the results from the present study were compared with published ones, or compared with results by ANSYS. Most of the results among them are very well matched.

With the Analytical Strip Method, the analyst has the ability to analyze bending-extension coupling for antisymmetric cross-ply and angle-ply laminated plates, with various boundary and/or internal support and loading conditions. A system of three well-known equations of equilibrium is suitably combined into a single eighth-order partial differential equation, in terms of a displacement function. The series form solutions to the deflection, buckling, and natural frequency problems for antisymmetric cross-ply and angle-ply plates are also found.

7.2 Bending of Laminated Plate

The Analytical Strip Method (ASM) is applied to the bending-extension coupling of antisymmetric laminated composite plates and stiffened continuous antisymmetric laminated composite plates. Graphical and tabular results are presented for the deflections and stresses. A convergence study indicates that both deflection and stress results obtained by using ASM for antisymmetric laminated plates converge rapidly with deflections converging earlier compared to the stresses. This implies that the developed ASM can attain the desired accuracy, with reasonably fewer number of series. The results obtained using ASM are validated by comparing them with existing results, obtained using CLPT or ANSYS. All the results of deflections and stresses, listed for laminated plate obtained from ASM, CLPT, and ANSYS, are well matched. The proposed methodology enables researchers to analyze composite laminated plates and stiffened continuous antisymmetric composite laminated plates, with beam or point supports, subjected to any combination of patch, uniform, line, and concentrated loads

without resorting to approximating methods.

7.3 Free Vibration and Buckling of Laminated Plate

Based on ASM, the same method of hit and trial that involves a bisection search strategy is used to solve free vibration and buckling problems of antisymmetric laminated plate. The results obtained using ASM are compared with ones obtained by ANSYS. For free vibration, tables in Chapter 5 list the effects of in-plane orthotropy ratio of individual layers, ply-orientation angle (for angle-ply plate), number of layers, and aspect ratio on $\bar{\omega}$ of cross-ply and angle-ply plates. The agreement between results obtained by ASM and by ANSYS is excellent.

For buckling analysis, tables in Chapter 6 list effects of in-plane orthotropy ratio of individual layers, ply-orientation angle (for angle-ply plate), number of layers, and aspect ratio on \bar{N}_y of cross-ply and angle-ply plates. The agreement between buckling load results, obtained by ASM and by ANSYS, is not as good as one for free vibration. The maximum difference between buckling loads, obtained from ASM and ANSYS, reaches 6.97%, when ply orientation angle, $\theta = 0^\circ$ and plate layers $n = 10$.

ASM can be easily used to maximize fundamental frequency or buckling load capacity for antisymmetric angle-ply and cross-ply laminated plate. The maximized values can be reached by varying beam position and ply-orientation angle (for angle-ply plate).

7.4 Recommendation for Future Research

An Analytical Strip Method (ASM) has been developed for the bending, free vibration and buckling of antisymmetric cross-ply and angle-ply laminated plates, by solving a single eighth order partial differential equation, in terms of a displacement function. Based on the current work, recommendations for future research include:

- Plates with varied thicknesses and varied properties: All laminated plates considered in this study have been uniform thickness or equal property for the whole target plate. ASM can be extended to laminated plates with varied thicknesses and varied properties. Laminated plates can be divided to strips,

based on discontinuous lines at which thickness or property changes. More complicated mathematic derivation and matrix solving procedure should be used to pursue these solutions.

- Fundamental frequency under in-plane loads: In general engineering practice, it is normal to find fundamental frequency for laminated plates with in-plane loading. It is interesting and convenient to study fundamental frequency for laminated plate with in-plane loading, using ASM.
- The presented work could be a starting point for optimization of the antisymmetric cross-ply and angle-ply laminated plates. Obtaining an efficient antisymmetric structural design, which meets all requirements of a specific application, can be achieved by sizing cross-sectional areas and by tailoring material properties through selective choice of ply orientation, number of stiffeners, position of stiffeners and stacking sequence of laminae.
- The proposed methodology can be possibly extended to antisymmetric cross-ply and angle-ply laminated sector plates.

Appendix A
HOMOGENOUS SOLUTIONS, $\Phi_H(x, y)$, OF GDE FOR
ANTISYMMETRIC LAMINATED PLATES

For an antisymmetric laminated plate, subjected to a transverse load $q(x, y)$, the governing differential equation is shown in Equation 2.13:

$$A_1 \frac{\partial^8 \Phi}{\partial x^8} + A_3 \frac{\partial^8 \Phi}{\partial x^6 \partial y^2} + A_5 \frac{\partial^8 \Phi}{\partial x^4 \partial y^4} + A_7 \frac{\partial^8 \Phi}{\partial x^2 \partial y^6} + A_9 \frac{\partial^8 \Phi}{\partial y^8} = q(x, y) \quad (2.13)$$

For a rectangular plate, simply supported along two edges parallel to the x -axis, the solution to Equation 2.13 can be presented in a single series form:

$$\Phi(x, y) = \sum_n^{\infty} \phi_n(x) \cdot \sin(\beta_n y) \quad (3.1)$$

in which,

$$\beta_n = \frac{n\pi}{b} \quad (3.2)$$

and b is the length of the plate along the y -axis.

With solution in Equation 3.1, Equation 2.13 can be reduced to:

$$\begin{aligned} \sum_m^{\infty} \left[A_1 \frac{d^8 \phi_m(x)}{dx^8} - A_3 \beta_m^2 \frac{d^6 \phi_m(x)}{dx^6} + A_5 \beta_m^4 \frac{d^4 \phi_m(x)}{dx^4} - A_7 \beta_m^6 \frac{d^2 \phi_m(x)}{dx^2} + A_9 \beta_m^8 \phi_m(x) \right] \\ = \sum_m^{\infty} \left[\frac{2}{b} \int_0^b q(x, y) \sin(\beta_m y) dy \right] \end{aligned} \quad (3.5)$$

This is an infinite set of ordinary differential equations for $\phi_m(x)$ ($m = 1, 2, 3, \dots, \infty$). It is a unidirectional and linear 8^{th} order differential equation, which can be solved by the superposition of the homogeneous part, $\Phi_H(x, y)$, and the particular part of the equation, $\Phi_P(x, y)$.

$$\Phi(x, y) = \Phi_H(x, y) + \Phi_P(x, y) \quad (3.6a)$$

or

$$\sum_m^{\infty} \phi_m(x) \sin(\beta_m y) = \sum_m^{\infty} \phi_{Hm}(x) \sin(\beta_m y) + \sum_m^{\infty} \phi_{Pm}(x) \sin(\beta_m y) \quad (3.6b)$$

The characteristic equation of the homogeneous part of Equation 3.5 for mode m

is:

$$A_1\gamma_m^8\beta_m^8 - A_3\gamma_m^6\beta_m^8 + A_5\gamma_m^4\beta_m^8 - A_7\gamma_m^2\beta_m^8 + A_9\beta_m^8 = 0 \quad (3.8)$$

in which, $\gamma_m\beta_m$ are the characteristic roots for function $\phi_{Hm}(x)$. Since $\beta_m \neq 0$,

Equation 3.8 can be simplified as:

$$A_1\gamma_m^8 - A_3\gamma_m^6 + A_5\gamma_m^4 - A_7\gamma_m^2 + A_9 = 0 \quad (3.9)$$

There are 9 possible root combinations for solutions of Equation 3.9. Corresponding to each characteristic root combination, there are 9 homogenous solutions, $\Phi_H(x, y)$ as follows:

Case 1:

For roots, $\pm\gamma_{1m} \pm i\gamma_{2m}$ and $\pm\gamma_{3m} \pm i\gamma_{4m}$, the homogeneous solution, $\Phi_H(x, y)$:

$$\Phi_H(x, y) = \sum_m \left\{ \begin{array}{l} [C_{1m} \cosh(\gamma_{1m}\beta_m x) + C_{2m} \sinh(\gamma_{1m}\beta_m x)] \cos(\gamma_{2m}\beta_m x) \\ + [C_{3m} \cosh(\gamma_{1m}\beta_m x) + C_{4m} \sinh(\gamma_{1m}\beta_m x)] \sin(\gamma_{2m}\beta_m x) \\ + [C_{5m} \cosh(\gamma_{3m}\beta_m x) + C_{6m} \sinh(\gamma_{3m}\beta_m x)] \cos(\gamma_{4m}\beta_m x) \\ + [C_{7m} \cosh(\gamma_{3m}\beta_m x) + C_{8m} \sinh(\gamma_{3m}\beta_m x)] \sin(\gamma_{4m}\beta_m x) \end{array} \right\} \sin(\beta_m y) \quad (3.32)$$

Case 2:

For roots, $\pm\gamma_{1m} \pm i\gamma_{2m}$, $\pm\gamma_{3m}$ and $\pm i\gamma_{4m}$, the homogeneous solution, $\Phi_H(x, y)$:

$$\Phi_H(x, y) = \sum_m \left\{ \begin{array}{l} [C_{1m} \cosh(\gamma_{1m}\beta_m x) + C_{2m} \sinh(\gamma_{1m}\beta_m x)] \cos(\gamma_{2m}\beta_m x) \\ + [C_{3m} \cosh(\gamma_{1m}\beta_m x) + C_{4m} \sinh(\gamma_{1m}\beta_m x)] \sin(\gamma_{2m}\beta_m x) \\ + C_{5m} \cosh(\gamma_{3m}\beta_m x) + C_{6m} \sinh(\gamma_{3m}\beta_m x) \\ + C_{7m} \cos(\gamma_{4m}\beta_m x) + C_{8m} \sin(\gamma_{4m}\beta_m x) \end{array} \right\} \sin(\beta_m y) \quad (A.1)$$

Case 3:

For roots, $\pm i\gamma_{1m}$, $\pm i\gamma_{2m}$ and $\pm\gamma_{3m} \pm i\gamma_{4m}$, the homogeneous solution,

$\Phi_H(x, y)$:

$$\Phi_H(x, y) = \sum_m \left\{ \begin{array}{l} C_{1m} \cos(\gamma_{1m}\beta_m x) + C_{2m} \sin(\gamma_{1m}\beta_m x) \\ + C_{3m} \cos(\gamma_{2m}\beta_m x) + C_{4m} \sin(\gamma_{2m}\beta_m x) \\ + [C_{5m} \cosh(\gamma_{3m}\beta_m x) + C_{6m} \sinh(\gamma_{3m}\beta_m x)] \cos(\gamma_{4m}\beta_m x) \\ + [C_{7m} \cosh(\gamma_{3m}\beta_m x) + C_{8m} \sinh(\gamma_{3m}\beta_m x)] \sin(\gamma_{4m}\beta_m x) \end{array} \right\} \sin(\beta_m y) \quad (\text{A.2})$$

Case 4:

For roots, $\pm i\gamma_{1m}$, $\pm i\gamma_{2m}$, $\pm i\gamma_{3m}$ and $\pm i\gamma_{4m}$, the homogeneous solution,

$\Phi_H(x, y)$:

$$\Phi_H(x, y) = \sum_m \left\{ \begin{array}{l} C_{1m} \cos(\gamma_{1m}\beta_m x) + C_{2m} \sin(\gamma_{1m}\beta_m x) \\ + C_{3m} \cos(\gamma_{2m}\beta_m x) + C_{4m} \sin(\gamma_{2m}\beta_m x) \\ + C_{5m} \cos(\gamma_{3m}\beta_m x) + C_{6m} \sin(\gamma_{3m}\beta_m x) \\ + C_{7m} \cos(\gamma_{4m}\beta_m x) + C_{8m} \sin(\gamma_{4m}\beta_m x) \end{array} \right\} \sin(\beta_m y) \quad (\text{A.3})$$

Case 5:

For roots, $\pm i\gamma_{1m}$, $\pm i\gamma_{2m}$, $\pm\gamma_{3m}$ and $\pm i\gamma_{4m}$, the homogeneous solution,

$\Phi_H(x, y)$:

$$\Phi_H(x, y) = \sum_m \left\{ \begin{array}{l} C_{1m} \cos(\gamma_{1m}\beta_m x) + C_{2m} \sin(\gamma_{1m}\beta_m x) \\ + C_{3m} \cos(\gamma_{2m}\beta_m x) + C_{4m} \sin(\gamma_{2m}\beta_m x) \\ + C_{5m} \cosh(\gamma_{3m}\beta_m x) + C_{6m} \sinh(\gamma_{3m}\beta_m x) \\ + C_{7m} \cos(\gamma_{4m}\beta_m x) + C_{8m} \sin(\gamma_{4m}\beta_m x) \end{array} \right\} \sin(\beta_m y) \quad (\text{A.4})$$

Case 6:

For roots, $\pm i\gamma_{1m}$, $\pm i\gamma_{2m}$, $\pm \gamma_{3m}$ and $\pm \gamma_{4m}$, the homogeneous solution,

$\Phi_H(x, y)$:

$$\Phi_H(x, y) = \sum_m^{\infty} \left\{ \begin{array}{l} C_{1m} \cos(\gamma_{1m}\beta_m x) + C_{2m} \sin(\gamma_{1m}\beta_m x) \\ + C_{3m} \cos(\gamma_{2m}\beta_m x) + C_{4m} \sin(\gamma_{2m}\beta_m x) \\ + C_{5m} \cosh(\gamma_{3m}\beta_m x) + C_{6m} \sinh(\gamma_{3m}\beta_m x) \\ + C_{7m} \cosh(\gamma_{4m}\beta_m x) + C_{8m} \sinh(\gamma_{4m}\beta_m x) \end{array} \right\} \sin(\beta_m y) \quad (\text{A.5})$$

Case 7:

For roots, $\pm \gamma_{1m}$, $\pm \gamma_{2m}$ and $\pm \gamma_{3m} \pm i\gamma_{4m}$, the homogeneous solution, $\Phi_H(x, y)$:

$$\Phi_H(x, y) = \sum_m^{\infty} \left\{ \begin{array}{l} C_{1m} \cosh(\gamma_{1m}\beta_m x) + C_{2m} \sinh(\gamma_{1m}\beta_m x) \\ + C_{1m} \cosh(\gamma_{2m}\beta_m x) + C_{2m} \sinh(\gamma_{2m}\beta_m x) \\ + [C_{5m} \cosh(\gamma_{3m}\beta_m x) + C_{6m} \sinh(\gamma_{3m}\beta_m x)] \cos(\gamma_{4m}\beta_m x) \\ + [C_{7m} \cosh(\gamma_{3m}\beta_m x) + C_{8m} \sinh(\gamma_{3m}\beta_m x)] \sin(\gamma_{4m}\beta_m x) \end{array} \right\} \sin(\beta_m y) \quad (\text{A.6})$$

Case 8:

For roots, $\pm \gamma_{1m}$, $\pm \gamma_{2m}$, $\pm \gamma_{3m}$ and $\pm i\gamma_{4m}$, the homogeneous solution,

$\Phi_H(x, y)$:

$$\Phi_H(x, y) = \sum_m^{\infty} \left\{ \begin{array}{l} C_{1m} \cosh(\gamma_{1m}\beta_m x) + C_{2m} \sinh(\gamma_{1m}\beta_m x) \\ + C_{3m} \cosh(\gamma_{2m}\beta_m x) + C_{4m} \sinh(\gamma_{2m}\beta_m x) \\ + C_{5m} \cosh(\gamma_{3m}\beta_m x) + C_{6m} \sinh(\gamma_{3m}\beta_m x) \\ + C_{7m} \cos(\gamma_{4m}\beta_m x) + C_{8m} \sin(\gamma_{4m}\beta_m x) \end{array} \right\} \sin(\beta_m y) \quad (\text{A.7})$$

Case 9:

For roots, $\pm \gamma_{1m}$, $\pm \gamma_{2m}$, $\pm \gamma_{3m}$ and $\pm \gamma_{4m}$, the homogeneous solution,

$\Phi_H(x, y)$:

$$\Phi_H(x, y) = \sum_m^{\infty} \left\{ \begin{array}{l} C_{1m} \cosh(\gamma_{1m} \beta_m x) + C_{2m} \sinh(\gamma_{1m} \beta_m x) \\ + C_{3m} \cosh(\gamma_{2m} \beta_m x) + C_{4m} \sinh(\gamma_{2m} \beta_m x) \\ + C_{5m} \cosh(\gamma_{3m} \beta_m x) + C_{6m} \sinh(\gamma_{3m} \beta_m x) \\ + C_{7m} \cosh(\gamma_{4m} \beta_m x) + C_{8m} \sinh(\gamma_{4m} \beta_m x) \end{array} \right\} \sin(\beta_m y) \quad (\text{A.8})$$

BIBLIOGRAPHY

- ANSYS, Inc. (2007). *Documentation for ANSYS*, Revision 11.0. Canonsburg, PA, USA.
- Biswal, K.C. and Ghosh, A.K. (1994). "Finite element analysis for stiffened laminated plates using higher order shear deformation theory." *Computers & Structures*, 53(1), 161-171.
- Cheung, Y.K. (1976). *Finite Strip Method in Structural Analysis*. UK: Pergamon Press.
- Cheung, Y.K., Fan, S.C. and Wu, C.Q. (1982) "Spline finite strip in structure analysis." Proceedings of the International Conference on Finite Element Method, Shanghai, Science Press, Beijing, China, Gordon and Breach, Science Publishers, Inc., N.Y., 704-709.
- Deb, A. and Booton, M. (1988). "Finite element models for stiffened plates under transverse loading." *Computers & Structures*, 28(3), 361-372.
- Editing Group of the Manual of Mathematics (1979). "Roots for Quartic Equation." *Manual of Mathematics*, People's Education Press, Beijing, China, (Chinese), 87-90.
- Guo, M., Harik, I. E., and Ren, W. X. (2002). "Free vibration analysis of stiffened laminated plates using layered finite element method." *Structural Engineering and Mechanics*, 14(3), 245-262.
- Habib, S.S., Nahas, M.N. (1997). "Failure of composite stiffened plates loaded in compression." *Journal of Reinforced Plastics Composites*, 16(4), 332-340.
- Harik, I.E. and Salamoun, G.L. (1986). "Analytical Strip Solution to Rectangular Plates." *Journal of Engineering Mechanics*, 112(1), 105-118.
- Harik, I.E. and Salamoun, G.L. (1988). "The Analytical Strip Method of Solution for Stiffened Rectangular Plates." *Computers & Structures*, 29(2), 283-291.
- Jones, R.M. (1975). *Mechanics of Composite Materials*, Scripta, Washington, DC.
- Khdeir, A.A. (1989). "Comparison between Shear Deformable and Kirchhoff Theories for Bending, Buckling and Vibration of Antisymmetric Angle-ply Laminated Plates." *Composite Structures*, 13(3), 159-172.
- Khdeir, A.A. (1996). "Remark on the state-space concept applied to bending, buckling and free vibration of composite laminates." *Computers and Structures*, 59(5), 813-817.
- Khdeir, A.A. and Reddy, J.N. (1991). "Analytical Solutions of Refined Plate Theories of Cross-Ply Composite Laminates," *Journal of Pressure Vessel Technology*, 113(4), 570-578.
- Liew, K.M. and Lam, K.Y. (1990). "Application of two-dimensional orthogonal plate function to flexural vibration of skew plates." *Journal of Sound and Vibration*, 139(2), 241-252.
- Liew, K.M., Lam, K.Y., and Chow, S.T. (1990). "Free vibration analysis of rectangular plates using orthogonal plate function." *Computers and Structures*, 34(1), 79-85.
- Liew, K.M., Xiang, Y., Kitipornchai, S. and Meek, J.L. (1995). "Formulation of Mindlin-Engesser model for stiffened plate vibration." *Computer Methods in Applied Mechanics and Engineering*, 120(3-4), 339-353.
- Loughland J., Delaunoy J.M. (1993). "The buckling of composite stiffened plates with

- some emphasis on the effects of fiber orientation and on loading configuration.” *Composite Structures*, 25, 485-494.
- Mukherjee, A., Mukhopadhyay, M. (1986). “A review of dynamic behavior of stiffened plates.” *The Shock and Vibration Digest*, 18, 3-8.
- Mukhopadhyay, M., Mukherjee, A. (1989). “Recent advances on the dynamic behavior of stiffened plates.” *The Shock and Vibration Digest*, 21, 6-9.
- Qing, G., Qiu, J., and Liu, Y. (2006). “Free vibration analysis of stiffened laminated plates.” *International Journal of Solids and Structures*, 43, 1357–1371.
- Reddy, J.N. (1984). “A Simple Higher-Order Theory for Laminated Composite Plates.” *ASME Journal of Applied Mechanics*, 51(4), 745–752.
- Reddy, J.N. (2004). *Mechanics of Laminated Composite Plates and Shells, Theory and Analysis*, 2nd Ed., CRC Press LLC, New York.
- Rikards, R., Chate, A., Ozolinsh, O. (2001). “Analysis for buckling and vibrations of composite stiffened shells and plates.” *Composite Structures*, 51, 361–370.
- Rossow, M.P. and Ibrahimkhail, A.K. (1978). “Constraint method analysis of stiffened plates.” *Computers & Structures*, 8(1), 51-60.
- Sadek, E.A. and Tawfik, S.A. (2000). “Finite element model for the analysis of stiffened laminated plates.” *Computers & Structures*, 75(4), 369-383.
- Salamoun, G.L. and Harik, I.E. (1985). “Analytical Strip Solution for Stiffened and Continuous Orthotropic Rectangular Plates.” *Report No. UKCE8503*, Department of Civil Engineering, University of Kentucky, Lexington, KY.
- Schade, H.A. (1940). “The orthogonally stiffened plate under uniform lateral load.” *ASME Journal of the Applied Mechanics*, 7(4), 143-146.
- Sharma, S., Iyengar, N.G.R., and Murthy, P.N. (1980). “Buckling of Antisymmetric Cross- and Angle-ply Laminated Plates.” *International Journal of Mechanical Sciences*, 22(10), 607-620.
- Starnes Jr. J.H., Knight Jr N.F., Rouse M. (1985). “Post buckling behaviour of selected flat stiffened graphite epoxy panels loaded in compression.” *AIAA Journal*, 23 (8), 1236-1246.
- Szilar, R. (1974). *Theory and Analysis of Plate, Classical and Numerical Method*, Prentice-Hall, Englewood Cliffs, NJ.
- Timoshenko, S. and Gere, J.M. (1961). *Theory of Elastic Stability* (2nd Edition), McGraw-Hill, New York.
- Troitsky, M. S. (1976). “Stiffened Plates: Bending, Stability and Vibrations.” *Elsevier Scientific Publishing Company*, New York.
- Ugural, A. C. (1999). *Stresses in Plates and Shells* (2nd Edition), WCB/McGraw-Hill, Boston.
- Vel, S.S. and Batra, R.C. (1999). “Analytical Solution for Rectangular Thick Laminated Plates Subjected to Arbitrary Boundary Conditions.” *AIAA Journal*, 37(11), 1464-1473.
- Whitney, J.M. and Leissa, A.W. (1969). “Analysis of Heterogeneous Anisotropic Plates.” *ASME Journal of Applied Mechanics*, 36(2), 261–266.

- Williams J.G., Stein M. (1976). "Buckling behaviour and structural efficiency of open stiffened composite compressions panels." *AIAA Journal*. Vol. 14, No. 11, 1618-1826.
- Xiang, Y., Liew, K.M., and Kitipornchai, S. (1996). "Vibration of circular and annular plates with internal ring stiffeners." *Journal of the Acoustical Society of America*, 100(6), 3696-3705.
- Yettram, A.L. and Hussain, M.H. (1965) "A grid framework method for plates in flexure." *ASCE Journal of the Engineering Mechanics Division*, 91(EM1), 53-64.
- Zhao, X., Liew, K.M., Ng, T.Y. (2002). "Vibrations of rotating cross-ply laminated circular cylindrical shells with stringer and rings stiffeners." *Journal of Solids and Structures*, 39, 529–545.

VITA

Liecheng (Charlie) Sun was born on September 21, 1957 in Zhenjiang, Jiangsu, China. After graduating from high school, he worked as a farmer for two-and-a-half years and as a blacksmith for another six months. He earned his bachelor and master's degrees in Engineering Mechanics and Experimental Mechanics, at Zhejiang University in Hangzhou China. After graduation, he worked as a lecturer and laboratory instructor at Zhejiang University.

Beginning in August 1992, he began pursuing a doctoral degree in Structural Engineering, at the University of Kentucky. During this time, he passed his qualifying examination, earned a master's degree in Structural Engineering, obtained a structural design job, and left the Ph. D. program. After three years of structural design work, he obtained a position as a research engineer at the Kentucky Transportation Center, University of Kentucky, beginning in November 1998.

In addition to his many positions and much experience, Sun is a registered professional engineer in the state of Kentucky. He has worked on a variety of Geotechnical Engineering projects, such as reinforced and unreinforced highway embankments, foundations, bridges, culverts, coupled analysis between soils and structures, as well as many others. He is one of the principal investigators in developing information systems with client/server frames and web enabled aspects, in topics related to transportation research.

Liecheng Sun is a co-author of the following publications and research reports:

1. Liecheng Sun and Issam E. Harik, "*ASM Solution to Antisymmetric Laminated Plates*", (to be submitted to ASCE Journal of the Engineering Mechanics)
2. Liecheng Sun and Issam E. Harik, "*ASM Solution to Stiffened and Continuous Antisymmetric Laminated Plates*", (in preparation)
3. Liecheng Sun and Issam E. Harik, "*ASM Solution to Free Vibration of Stiffened and Continuous Antisymmetric Laminated Plates*", (in preparation)
4. Liecheng Sun and Issam E. Harik, "*ASM Solution to Buckling of Stiffened and Continuous Antisymmetric Laminated Plates*", (in preparation)
5. Liecheng Sun, Tommy C. Hopkins, Tony L. Beckham, "*Load Reduction by Geof foam for Culvert Extension: Numerical Analysis*", GeoCongress 2006, Atlanta, GA (February 26 - March 1, 2006)
6. Liecheng Sun, Tommy C. Hopkins, Tony L. Beckham, "*Use of Ultra-lightweight Geof foam to Reduce Stresses in Highway Culvert Extensions*", Research Report, KTC-05-34/SPR-297-05-1I (October 2005)
7. Tony L. Beckham, Liecheng Sun, Tommy C. Hopkins, "*Corrosion Evaluation of Mechanically Reinforced Earth Walls*", Research Report, KTC-05-28/SPR 239-02-1F. (September 2005)
8. Tommy C. Hopkins, Liecheng Sun, M.E. Slepak, "*Bearing Capacity Analysis and Design of Highway Base Material Reinforced with Geofabrics*", Research Report, KTC-05-21/SPR 238-02-1F (June 2005)

9. Liecheng Sun, Tommy C. Hopkins, Tony L. Beckham, “*Stress Reduction by Ultra-Lightweight Geofam for High Fill Culvert: Numerical Analysis*”. The Proceedings of the 13th Annual Great Lakes Geotechnical and Geoenvironmental Engineering Conference (GLGGC), Milwaukee, Wisconsin, May 13, 2005.
10. Liecheng Sun, Tommy C. Hopkins, Tony L. Beckham, “*Reduction of Stresses on Buried Rigid Highway Structures Using the Imperfect Ditch Method and Expanded Polysterene (Geofam)*”, Research Report, KTC-05-05/SPR 228-01-II (April 2005)
11. Liecheng Sun, Tommy C. Hopkins, Tony L. Beckham, B. Ni, “*Examination of Economical Methods for Repairing Highway Landslides*”, Research Report, KTC-05-04/SPR 180-98-1F (April 2005)
12. Tommy C. Hopkins, Tony L. Beckham, Liecheng Sun, “*Kentucky Geotechnical Database*”, Research Report, KTC-05-03/SPR 227-01-1F (March 2005)
13. Tommy C. Hopkins, Tony L. Beckham, Liecheng Sun, B. Butcher, “*Highway Rock Slope Management Program*”, Research Report, KTC-03-06/SPR 177-98-1F (February 2003)
14. Tommy C. Hopkins, Tony L. Beckham, Liecheng Sun, B. Ni, B. Butcher, “*Long-Term Benefits of Stabilizing Soil Subgrades*”, Research Report, KTC-02-19/SPR 196-99-1F (June 2002)
15. Tommy C. Hopkins, Tony L. Beckham, Liecheng Sun, “*Resilient Modulus of Kentucky Soils*”, Research Report, KTC-01-07/SPR 163-95-1F (June 2001)
16. Tommy Hopkins, Tony Beckham, Liecheng Sun, etc. “*Development of Geotechnical Database*”, Transportation Research Board 80th Annual Meeting, (Washington, D. C., January 7-11, 2001)
17. Hongsheng Cao, Liecheng Sun, “*A New Combined Sandwich Method of Image Holographic and Speckle Interferometry for 3-D Displacement Measurement*”, Journal of Experimental Mechanics, 4(1989), No.3, 262-273 (Chinese). Adapted from Master Degree thesis.
18. Liecheng Sun, Zhenlin Wang, “*Six-Coordinate Fine Tuning Instrument for Sandwich Holographic Plates and Its Uses*”, Proceedings of the Fifth National Conference on, Experimental Mechanics (Nanjing, China, 1987)
19. Liecheng Sun, Hongsheng Cao, “*Tele-Controlled Air Gun*”, Proceedings of the National Conference on Dynamic Photomechanics, (Hangzhou, China, 1986)
20. Huaitang Yang, Liecheng Sun, etc. “*Photoelastic Stress Analysis of an Underground Buried Pipe*”, Proceedings of the International Conference on Experimental Mechanics (Beijing, China, 1985), 205-211